Evelyn Friesenbichler, BSc

# Sedimentological Investigations on Lower Triassic Microbialites from Armenia

## MASTER'S THESIS

to achieve the university degree of
Master of Science
Master's degree programm: Earth Sciences

submitted to

## Graz University of Technology

Supervisor

Priv.-Doz. Dr. Sylvain Richoz

Institute of Earth Sciences
University of Graz

# AFFIDAVIT

I declare that I have authored this thesis independently, that I have not used other than the declared sources/resources, and that I have explicitly indicated all material which has been quoted either literally or by content from the sources used. The text document uploaded to TUGRAZonline is identical to the present master's thesis dissertation.

_____          _____
Date                                              Signature

… to everybody who helped
me coming this far…

# Acknowledgements

# Zusammenfassung

Nach dem endpermischen Massenaussterben, welches das größte Massenaussterben der Erdgeschichte war, nahmen Mikrobengemeinschaften den Platz von skelettbildenden Metazoen ein und bildeten so genannte Permian-Triassic Boundary Microbialites (PTBMs). Diese PTBMs formten sich während vier Phasen in der Untertrias und waren in äquatornahen, seichtmarinen Karbonatschelfen weit verbreitet. Die Ziele dieser Masterarbeit waren es herauszufinden, ob sich die PTBMs im oder auf dem Sediment bildeten und ob es einen Zusammenhang zwischen den PTBMs und den sie umgebenden Schwämmen gibt. Dafür wurden drei Aufschlüsse in Südarmenien beschrieben, sowie Proben dieser drei Aufschlüsse mikroskopisch und geochemisch analysiert. Die armenischen PTBMs wurden während zwei mikrobieller Wachstumsphasen im Griesbachium (Unteres Induium, Untertrias) auf einer Karbonatrampe gebildet. Die PTBMs formten sowohl thrombolitische als auch dendrolitische Bänke und Hügel, die eine Mächtigkeit zwischen 5 cm und 1.5 m aufweisen. Der größte Thrombolith ist 12 m hoch und 8 m breit. Die PTBMs, welche sich während der ersten mikrobiellen Wachstumsphase bildeten, kommen zusammen mit so genannten Calcium Carbonate Crystal Fans (CCFs) vor. Mikrofaziesanalysen haben gezeigt, dass die PTBMs eine Reihe von verschiedenen Wachstumsformen und internen Strukturen besitzen. Des Weiteren sind sie in einem bioklastischen Wackestone eingebettet, der neben Schwämmen, Ostracoden und Foraminiferen auch Gastropoden, Bivalven und Ammoniten enthält. Es konnte festgestellt werden, dass die PTBMs auf dem Sediment wuchsen und dass ihr Wachstum unabhängig von den sie umgebenden Schwämmen war. Die Analysen der Kohlenstoffisotope haben gezeigt, dass der Unterschied zwischen den $\delta^{13}C_{Sediment}$- und den $\delta^{13}C_{Mikrobialith}$-Werten der PTBMs, welche sich während der zweiten mikrobiellen Wachstumsphase bildeten, beinahe identisch sind. Im Gegensatz dazu beträgt der Unterschied zwischen den $\delta^{13}C_{Sediment}$- und den $\delta^{13}C_{Mikrobialith}$-Werten der PTBMs, die sich während der ersten mikrobiellen Wachstumsphase bildeten, bis zu 2,3‰. Dieser Unterschied könnte das Resultat mikrobieller Aktivität sein.

# Abstract

The End-Permian mass extinction (EPE) was the most severe biotic crisis in earth's history and microbial communities colonised the space left vacant after the extinction of skeletonized metazoans. These so called Permian-Triassic boundary microbialites (PTBMs) flourished during at least four events in the Lower Triassic and were abundant in low-latitude shallow-marine carbonate shelves in central Tethyan continents. The aims of this master thesis were to find out whether the PTBMs grew in or on the sediment and whether there is a connection between the PTBMs and the surrounding sponges. Therefore three outcrops in southern Armenia were described and samples from these three outcrops were microscopically and geochemically analysed. The PTBMs from Armenia were formed in a distally open marine setting on a pelagic carbonate ramp during two microbial growth phases in Griesbachian (Lower Induan, Lower Triassic) times. The PTBMs formed predominantly thrombolitic but also dendrolitic banks and mounds that vary in size between 5 cm to 1.5 m. The biggest thrombolite has a total height of up to 12 m and a top head diameter of 8 m. The PTBMs from the first microbial growth phase co-occur with Calcium Carbonate Crystal Fans (CCFs). Microfacies analyses revealed that the PTBMs show a number of different growth forms and internal structures and that they are embedded in a bioclastic wackestone that mainly contains sponges, ostracods and foraminifers but also gastropods, bivalves and ammonoids. Furthermore it was found out that the formation of the PTBMs happened above the sediment surface and was independent from the surrounding sponges. Carbon isotope studies from the PTBMs as well as from the surrounding sediment revealed that the difference between the $\delta^{13}C_{sediment}$ and $\delta^{13}C_{microbialite}$ values are nearly the same in the PTBMs that formed during the second microbial growth face. In contrast, the $\delta^{13}C_{sediment}$ and $\delta^{13}C_{microbialite}$ values from the microbialites and CCFs that formed during the first microbial growth phase show a difference of up to 2.3‰, which could be due to microbial activity.

# Table of Content

# 1. Introduction

About 252 Ma ago the End-Permian mass extinction (EPE) extinguished nearly 90% of marine invertebrates and 80% of terrestrial vertebrates (Erwin et al. 2002, Irmis and Whiteside 2011, Payne and Clapham 2012) and lasted around 60.000 a (Burgess et al. 2014). A first and major extinction pulse happened in the latest Permian whereas a second one of lower intensity occurred after a short recovery interval in the earliest Triassic (Song et al. 2013). Several overlapping mechanisms are proposed as causes for the EPE such as widespread Siberian trap volcanism, eventually in association with volcanism in South China (Campbell et al. 1992, Renne et al. 1995, Kozur 1998, 2005, 2007, Morgan et al. 2004, Payne and Kump 2007, Galfetti et al. 2007), oceanic anoxia (Wignall and Hallam 1992, Isozaki 1994, 1997, Knoll et al. 1996, Wignall and Twitchett 1996, 2002, Zhang et al. 2001), euxinia (Grice et al. 2005), global warming (Sun et al. 2012), ocean acidification (Payne et al. 2010, Clarkson et al. 2015), methane release (Erwin 1993, Erwin et al. 2002, Krull and Retallack 2000, Berner 2002, de Wit et al. 2002, Krull et al. 2004) as well as a meteorite impact (Erwin 1993, Rampino et al. 2000, Becker et al. 2001, 2004, Kaiho et al. 2001, Basu et al. 2003). The EPE caused the replacement of the Upper Paleozoic skeletal carbonate factory by a non-skeletal carbonate factory (Baud 1998, Baud and Richoz 2004, Baud et al. 2007). These two types of carbonates are separated in the field by the so-called Boundary Shale of latest Permian age (Baud et al. 2007). The disappearance of frame-building organisms, such as corals and other metazoans, resulted in the proposition of a "reef gap" that should have lasted through the whole Early Triassic (Flügel 2002, Pruss and Bottjer 2005, Algeo et al. 2011). Although corals and reefs with complex ecosystems reappeared effectively only in the Anisian (Middle Triassic; Chen et al. 2010, Chen and Benton 2012) reefs comprising sponges, sponge-bivalve consortia and sponge-microbe-bivalve-serpulid consortia already occurred during the Smithian (Olenekian, Lower Triassic; Brayard et al. 2011). In this master thesis I will show that microbial-sponge-small invertebrates associations already occurred during the Griesbachian and that therefore the "reef gap" actually does not exist.

After the EPE Permian-Triassic boundary microbialites (PTBMs) were abundant in low-latitude shallow-marine carbonate shelves (Kershaw et al. 2012) in the Palaeotethys and Neotethys (Kershaw et al. 2007, Baud et al. 1997, 2005b, 2007, Forel 2013). They were once interpreted as disaster biotas that increase dramatically in range and abundance after several mass extinction events (Schubert and Bottjer 1992) but Kershaw et al. (2007) showed that microbialites did not occur after all mass extinctions. Other authors interpreted PTBMs as anachronistic facies because microbialites were not seen in such abundance since Precambrian to Early Paleozoic times (Sepkoski et al. 1991, Baud et al. 2007, Kershaw et al. 2012, Forel 2013). They were also often considered as a return to environmental conditions that were typical of Neoproterozoic and Cambro-Ordovician times (Kershaw et al. 2009). Some authors say that $CaCO_3$ supersaturation of the oceans must have been important to stimulate microbialites calcification (Riding 2005, Kershaw et al. 2012). Nevertheless, PTBMs show geographical variations and were probably influences by global as well as local control factors (Kershaw et al. 2012). They flourished during four phases in the Early Triassic (base of Griesbachian, Dienerian, early Smithian and mid-Spathian) whereas the first phase, which occurred during latest Permian and earliest Triassic times, was the most extensive one and happened simultaneously with a very rapid and large-scale transgression on the large carbonate platforms around the Tethys Ocean (Baud et al. 2007). These PTBMs formed directly over latest Permian pre-extinction open shelf carbonates (e.g. south China; Kershaw et al. 2007) or on oolitic-bioclastic grainstones to wackestones (e.g. south Turkey; Baud et al. 2005b). These oolitic-bioclastic grainstones formed shortly after the EPE (Baud et al. 2005b) and in some sites they occur again above the PTBMs (Baud et al. 2005b, Hips

and Haas 2006, Kershaw et al. 2011) but they were not found intermixed with PTBMs (Kershaw et al. 2012). The micritic matrix between layers, branches and patches of PTBMs usually contains organisms like ostracods, microgastropods, crinoids, bivalves (Richoz 2006, Kershaw et al. 2007, Forel et al. 2013), foraminifera and conodonts (Kershaw et al. 2012).

In a few sites PTBMs co-occur with Calcium Carbonate Crystal Fans (CCFs; Heydari et al. 2003, Richoz et al. 2010, Kershaw et al. 2012). Such CCFs are also typical features for carbonate platforms of Archean and upper Palaeoproterozoic age as well as for peritidal environments of Mesoproterozoic age. After the Palaeoproterozoic the reoccurrences of CCFs in subtidal environments coincide with C cycle perturbations (Grotzinger and Knoll 1995, Knoll et al. 1996, Hoffman and Schrag 2002, Heindel et al. 2013). Heindel et al. (2013) report that CCFs are also associated with environmental change such as in Neoproterozoic cap carbonates that were deposited after the Marinoan glaciation (Hegenberger 1993, Saylor et al. 1998, Clough and Goldhammer 2000, James et al. 2001, Font et al. 2006, Hoffman et al. 2007, Macdonald et al. 2009a, 2009b), after the EPE (Grotzinger and Knoll 1995, Heydari et al. 2003, Pruss et al. 2006, Baud et al. 2007, Payne and Kump 2007) as well as after the end-Triassic mass extinction (Greene et al. 2012). Algeo and Twitchett (2010) suggested that the CCFs formed due to enhanced chemical weathering on continents that led to an increased bicarbonate supply in the oceans, whereas Baud et al. (2007) suggested an organomineralization due to microbial activity. Although intense research was performed during the last years the exact formation mechanisms that led to the precipitation of such CCFs are still unknown (Heindel et al. 2013).

The $\delta^{13}$C curve spanning the Permian-Triassic boundary (PTB) and the earliest Triassic is characterised by a global negative excursion that is followed by numerous second-order variations (Richoz et al. 2010, Korte and Kozur 2010, Clarkson et al. 2013). According to Korte and Kozur (2010) the global negative excursion, with a gradual decline of 4-7‰, began at the stratigraphic level of the *C. bachmanni* zone (Changhsingian, Upper Permian) and was interrupted by a short-term positive event. After this short-term positive event the $\delta^{13}$C values decreased again and reached a second (occasionally two-peaked) minimum in the lower and middle *I. isarcica* zone (Griesbachian, Lower Triassic). A positive excursion of around 2‰, which is reported from several sections in the world (Baud et al. 1996, Atudorei 1999, Krystyn et al. 2003, Richoz 2004, Krull et al. 2004, Payne et al. 2004, Zuo et al. 2006, Horacek et al. 2007a, 2007c, Tong et al. 2007, Richoz et al. 2010) starts within the *I. isarcica* zone and reaches its maximum in the Upper Griesbachian. The causes as well as the chronology of the end-Permian negative $\delta^{13}$C excursion are still in question (Richoz et al. 2010). At some localities the base of the PTBMs coincides with the negative $\delta^{13}$C excursion but in many sites the base of the PTBMs postdates this isotope excursion (Kershaw et al. 2012).

This study is the first one that has a special focus on the connection between the PTBMs and the co-occurring sponges. Another aim of this study was to find out whether the CCFs and microbialites grew in or on the sediment. Therefore three outcrops in southern Armenia, namely Zangakatun, Vedi and Ogbin (Fig. 1), were described and microscopically characterized. Because the main focus was on Zangakatun cathodoluminescence, fluorescence microscopy, Raman spectroscopy as well as biomarker analyses were performed on some samples from this outcrop. Another aim of this study was to compare the $\delta^{13}$C values of the PTBMs and CCFs with the surrounding sediment. Therefore a high-resolution $\delta^{13}C_{sediment}$ and $\delta^{13}C_{microbialite}$ curve from Zangakatun was created.
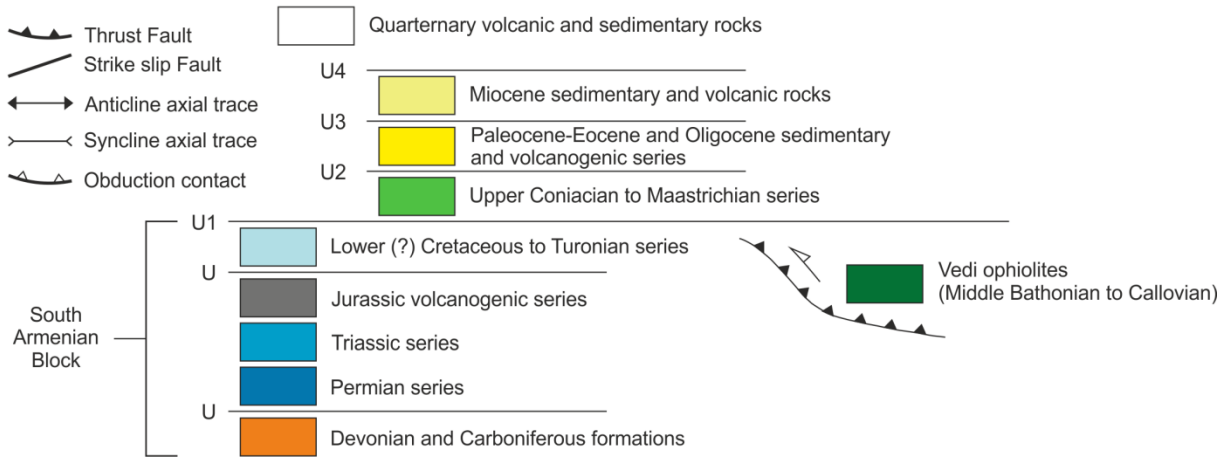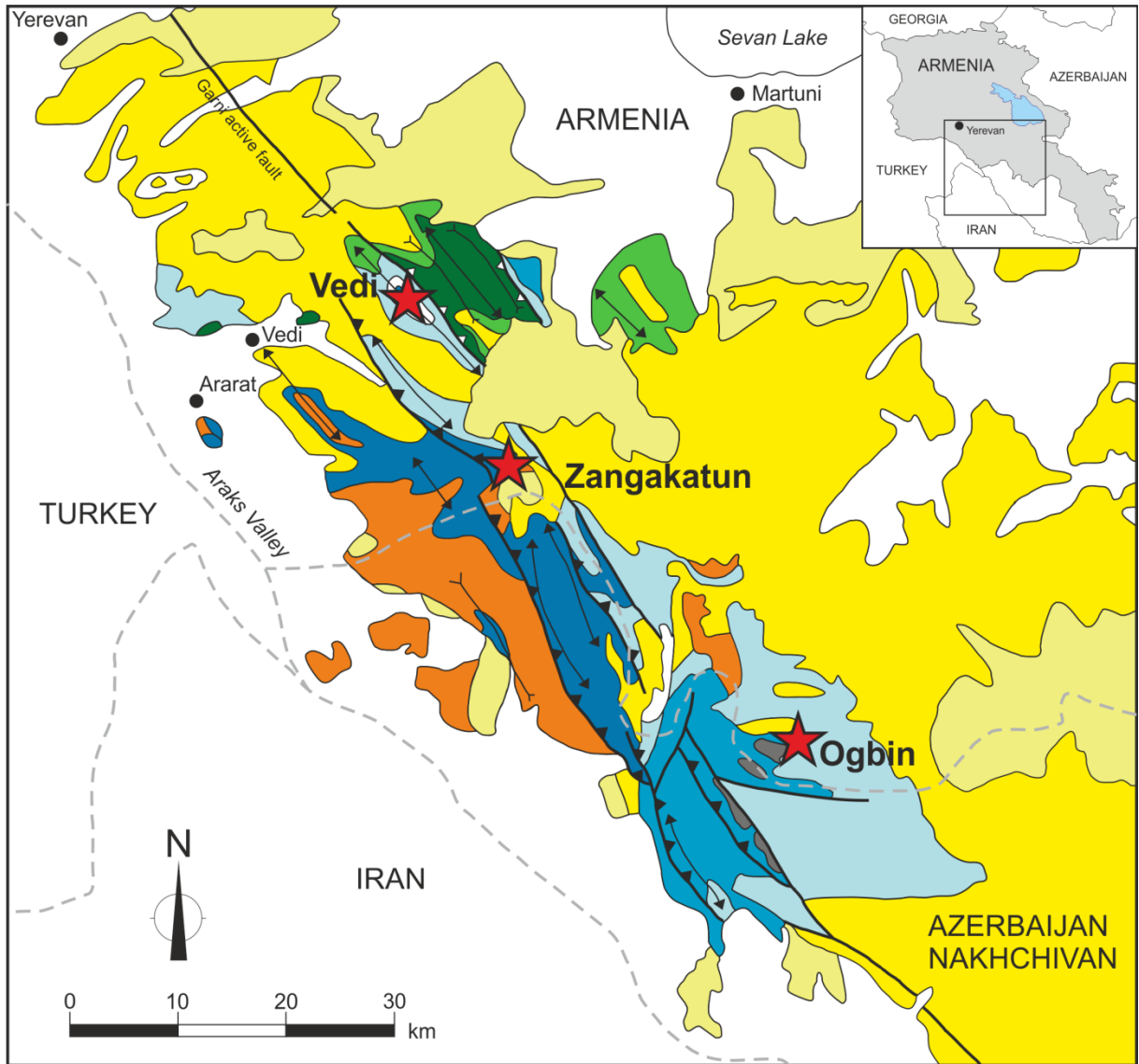
**Fig. 1:** Structural map of the Vedi area. The red stars mark the positions of the three investigated outcrops. Modified after Sosson et al. (2010).

# 2. Methods

To achieve the aims described above the following methods were applied.

## 2.1. Field Work

Three PTB sections in southern Armenia, namely Zangakatun (N 39°50'29.67'', E 45°03'04.40''), Vedi (N 39°56'59.97'', E 44°54'24.29'') and Ogbin (N 39°35'0.45'', E 45°21'42.33''; Fig. 1, Fig. 2 and Fig. 3), were measured. The thicknesses of the investigated sections are almost 30 m in Zangakatun, nearly 22 m in Ogbin and 11.5 m in Vedi. In Zangakatun 86 samples were especially taken from the PTBMs and CCFs but also from sediment without microbialites. The samples were taken at a distance of a few centimeters at the PTB, within the PTBMs and CCFs and up to 1 m in the sediment without microbialites. In Vedi 26 samples were mainly taken from single banks of the PTBMs and CCFs. In Ogbin 52 samples were collected. The samples from the PTB and PTBMs were taken at a distance from several cm. Samples from the overlaying Lower Triassic limestones as well as the underlying Upper Permian limestones were collected at distances varying between 0.5 m up to several meters.

## 2.2. Thin Sections

To solve the question whether the microbialites and CCFs grew in or on the sediment and to find out whether there is a connection between the microbialites and sponges more than 100 thin sections (mostly 5 x 5 cm but also 15 x 10 cm) were observed and characterized with a Zeiss SteREO Discovery.V8 stereomicroscope. In most cases the samples were cut parallel to the growing direction of the crystals. The sediment surrounding the microbialites was characterized after the classification of Dunham (1962) with expansion of Embry and Klovan (1971). Photographs of the thin sections were taken with a SteREO Discovery.V20 stereomicroscope, a Zeiss AxioCam HRc and the program AxioVision SE64 Rel. 4.9.1. The organisms were counted per thin section and were not normalized.

## 2.3. Cathodoluminescence

Cathodoluminescence (CL) microscopy was performed on samples from Zangakatun with a HC5-LM cathodoluminescence microscope at the Institute of Earth Sciences at the University of Graz. Luminescence, in general, is the emission of electromagnetic radiation, ranging from the ultraviolet (UV) to the visible (VIS) and the infrared (IR) spectral range, resulting from a preceding excitation due to the adsorption of energy (Marfunin 1979, Götze 2002). Based on the type of excitation different types of luminescence can be distinguished. Excitation caused by an electron beam is called cathodoluminescence (Götze 2002). In carbonates CL found special application to evaluate the zoning in carbonate cements and its interpretation with regard to the burial history of carbonate sediments and the nature of diagenetic pore waters. Furthermore, it is also used for cement stratigraphy. Luminescence characteristics of carbonate minerals are primarily controlled by the relative abundances of Mn, REE and Fe (Boggs and Krinsley 2006) and there spatial distribution, whereas $Mn^{2+}$ and $REE^{2+/3+}$ are the most important activators in carbonate minerals (Richter et al. 2003, Götze 2012). The most important quencher ion preventing emission in rock-forming minerals is $Fe^{2+}$

**Fig. 2:** Google Earth images showing the locations of the investigated outcrops in Zangakatun and Vedi. **(a)** Position of the investigated outcrop in Zangakatun (N 39°50'29.67'', E 45°03'04.40''). Scale bar = 452 m. **(b)** Position of the investigated outcrop in Vedi (Vedi 1; N 39°56'59.97'', E 44°54'24.29''). The outcrop at Vedi 2 (N 39°57'11.6'', E 44°55'12.43'') is described in Baud et al. (1989). In Vedi 3 (N 39°57'09.92'', E 44°55'07.19'') a 1.5-2 m high microbialite was found (see chapter 4.2.). Scale bar = 434 m.
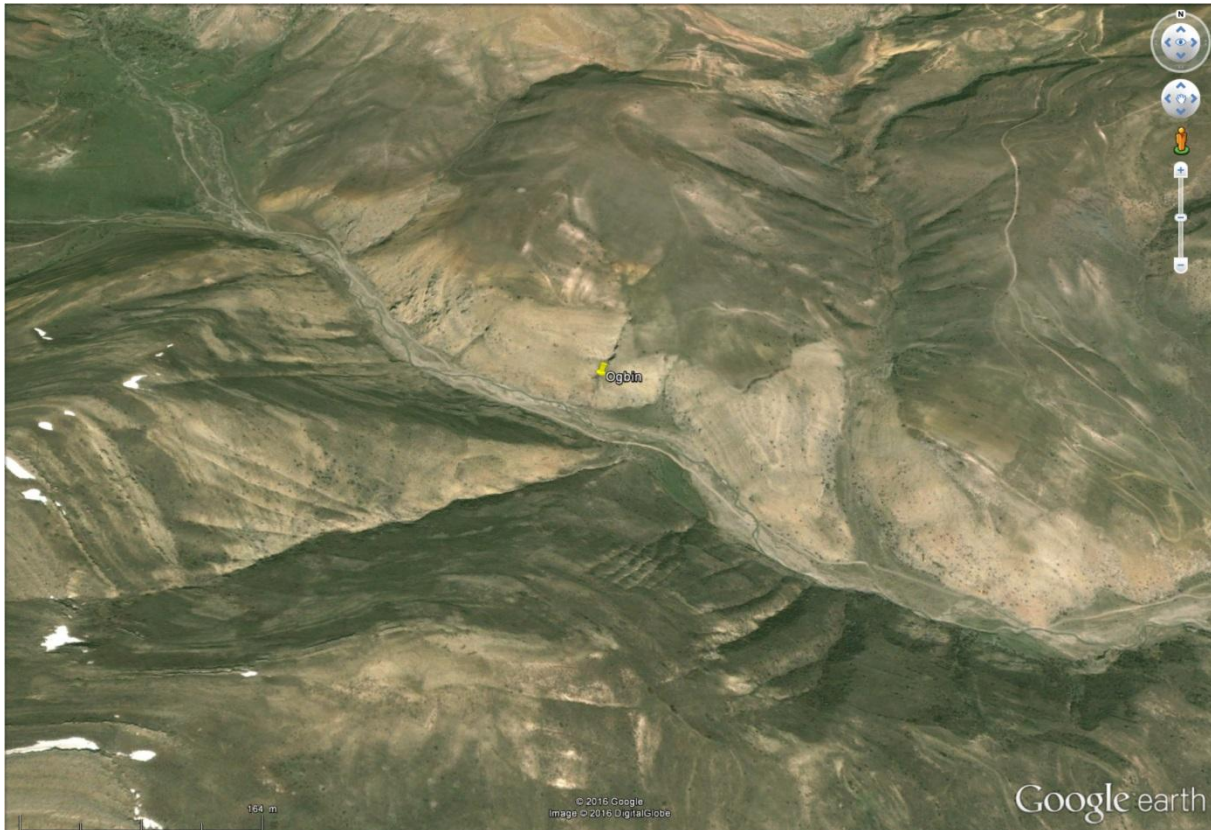
**Fig. 3:** Google Earth image showing the position of the investigated outcrop in Ogbin (N 39°35'0.45'', E 45°21'42.33''). Scale bar = 164 m.

(Marshall 1988, Mason and Mariano 1990). For the relation of CL intensity to $Mn^{2+}$ and $Fe^{2+}$ concentration in calcite and dolomite see Fig. 4. Although $Mn^{2+}$ and $Fe^{2+}$ are the main ions that affect CL emissions, numerous factors influence the partitioning of these ions into carbonates, e.g. processes including activity coefficients, activity of Ca, various chemical species in solution, temperature, crystal surface structures, crystal growth rates, pH and redox reactions (Boggs and Krinsley 2006, for a more complete listing and explanation of these factors see Machel and Burton 1991 and Machel 2000). CL colours from dolomite are red or yellow but the CL colours from aragonite vary from yellow-green to green. The CL colours from calcite vary between orange-yellow, yellow-orange and orange (Table 1). Blue and, less abundant, green are also possible and may be related to intrinsic (structural) defects (Boggs and Krinsley 2006). Zoning in calcite reflects either changing conditions or variations in growth mechanisms and can be divided into two types:

1) Concentric zoning: The compositional interface of the zoning pattern coincides with or is parallel to the growth interface existing at the time of growth. It is generally considered to reflect changing bulk-fluid properties and in turn reflect fluid chemistry, temperature, pressure and possibly redox conditions.

2) Sectoral zoning: the compositional interface does not coincide with and is not parallel to the growth interface (Reeder 1991, Boggs and Krinsley 2006).

Zoning in calcite may also be caused by variations in rates of trace-elements such as $Mn^{2+}$ and $Fe^{2+}$ (Boogs and Krinsley 2006).
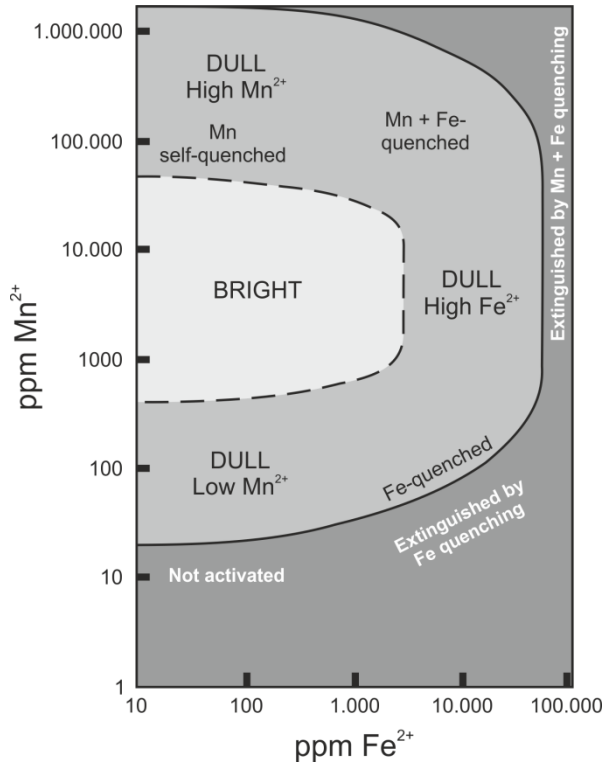
**Fig. 4:** Relation of CL intensity to $Mn^{2+}$ and $Fe^{2+}$ concentrations in calcite and dolomite. Modified after Boggs and Krinsley (2006).

**Table 1:** Peak positions in the CL spectrum and CL colours of calcite, aragonite and dolomite. Modified after Boggs and Krinsley (2006).

| Mineral | Wavelength [nm] | Activator ion(s) | CL colours | References |
|---|---|---|---|---|
| **Calcite** | 590, (605-620) | $Mn^{2+}$ | Orange-yellow, yellow-orange, orange, violet (?) | Habermann et al. (2000), Richter et al. (2003), Marshall (1988) |
| | ~500, 545, 580, 600, 650, 680, 710, 760 | REE (particularly $Sm^{3+}$, $Dy^{3+}$, $Tb^{3+}$) | $Sm^{3+}$-activated CL may be same as $Mn^{2+}$-activated CL; $Tb^{3+}$ activates green CL and $Dy^{3+}$ activates cream-white CL | Machel (2000), Habermann et al. (1996) |
| | ~(400-700) | intrinsic | Blue (weak) | Habermann et al. (2000) |
| **Aragonite** | 540, 560 | $Mn^{2+}$ | Yellow-green, green | Marshall (1988), Richter et al. (2003) |
| **Dolomite** | Two main peaks (570-583), (649-659) | $Mn^{2+}$ | Yellow, red | Richter et al. (2003) |
| Note: REE-activated CL is outshone by much stronger $Mn^{2+}$-activated CL, if $Mn^{2+}$ is present at >10ppm (Habermann et al. (1996)) | | | | |

## 2.4.  Fluorescence Microscopy

To check the distribution of still existing organic matter in the microbialites fluorescence microscopy was performed on thin sections from Zangakatun at the Department for Geodynamics and Sedimentology at the University of Vienna. A Nikon SMZ 1500 stereomicroscope with a Plan Apo 1.0x objective as well as excitation filters with wavelengths of 480/40nm and 337/50nm and a Lumen 200 fluorescence illumination were used. Thin sections were examined with a maximum magnification of 11.25x.

Fluorescence caused by the excitation with light is called photoluminescence (PL; Götze 2002). PL microscopy is a standard technique in coal petrography, palaeobotany and the organic petrography of sediments of mainly organic origin or with a high organic content (Flügel 2010). Although it is a rapid, easily used and non-destructive technique that can be applied not only to unpolished thin sections but also to rock slabs (Dravis and Yurewicz 1985) errors can occur in fluorescence microscopy due to apparent nonfluorescence (caused by insufficient excitation or transmission), extraneous fluorescence (caused by sample preparation materials) or internal reflections or refractions of fluorescent light (Cercone and Pedone 1987). The excitation of a carbonate rock with ultraviolet or blue-reflected light can support the detection of obscure sedimentary structures, diagenetic zoning in crystals as well as liquid hydrocarbon inclusions (Cercone and Pedone 1987). PL in calcite can be activated by organic compounds as well as trace elements (Pedone et al. 1990), e.g. $Mn^{2+}$ (Aguliar and Osendi 1982, Walker 1985, Walker et al. 1989, Pedone et al. 1990). Pedone et al. (1990) showed that with laser-excited luminescence spectroscopy it is possible to distinguish whether the PL is caused by organic matter or trace elements. Weak luminescence is characterized by a slightly green colour whereas strong luminescent areas can have a red colour (Peckmann J., personal communication).

## 2.5.  Carbon and Oxygen Isotopes

To compare the isotopic signals from the PTBMs, the CCFs and the surrounding bioclastic wackestone $\delta^{13}C$ values as well as $\delta^{18}O$ values of more than 150 samples were measured on samples from Zangakatun at the Institute of Earth Sciences at the University of Graz. Except from sample 35 and 50 (see chapter 5.5) only in situ crystals were measured. To make sure to drill at the right spots and to avoid cracks, stylolites, fossils and weathering features the counterparts of the thin sections were drilled. Most samples were drilled manually with a carbonite-tipped drill and yet others with a micro-drill. The resulting powder was reacted in a Kiel II automated reaction system with a 100% phosphoric acid. Because during this reaction a temperature dependent fractionation happens the reaction was proceeded at a temperature of 70 °C. The resulting $CO_2$ was analysed with a Finnigan Delta Plus mass spectrometer and compared with the NBS19 standard. For $\delta^{13}C$ the standard deviation σ was smaller than 0.07‰ and for $\delta^{18}O$ σ was smaller than 0.17‰. All data were corrected to the VPDB standard.

## 2.6.  Biomarker Analyses

Biomarker analyses were performed at the Department of Geodynamic and Sedimentology at the University of Vienna. Therefore the samples were prepared, decalcified and analysed after a method

described by Birgel et al. (2006) and Heindel et al. (2013). First the samples were crushed and cleaned by repeated washing with 10% HCL and acetone. Afterwards doubly distilled water was added to the samples and 10% HCL was slowly poured on the samples to dissolve the carbonate. To avoid transesterifications at low pH no more HCL was added after around 80% of the carbonate matrix has been dissolved. After the remaining carbonate pieces were removed the residual material was centrifuged and washed with water. Afterwards the samples underwent a saponification procedure with 6% KOH in methanol and after this procedure the samples were extracted with a microwave extraction system (CEM discovery) at 80 °C and 250 W with a dichloromethane:methanol (3:1) mixture. The extracts were precleaned by separation into a dichloromethane-soluble (asphaltenes) fraction and an *n*-hexane soluble (maltenes) fraction. Through column chromatography the *n*-hexane fraction was further separated into four fractions of increased polarity (cf. Birgel et al. 2008). The hydrocarbons were analysed with a coupled gas chromatography-mass spectrometer (GC-MS) with an Agilent 7890 A GC system coupled to on Agilent 5975C inert MSD mass spectrometer. The compounds were quantified by gas chromatography-flame ionization detection (GC-FID) with an Agilent 7820 A GC system. The GC-MS as well as the GC-FID were equipped with a 30 m HP-5 MS UI fused silica capillary column (0.25 mm i.d., 0.25 µm film thickness). The carrier gas was helium. The GC temperature program was used at 60 °C (1 min), from 60 °C to 150 °C at 10 °C/min., from 150 °C to 320 °C at 4 °C/min and 15 min isothermal. Unfortunately biomarker analyses failed probably because the organic matter was oxidised.

## 2.7. Raman Spectroscopy

To check whether the microbialites contain organic particles Raman spectroscopy was performed on samples from Zangakatun with a HR-800 Raman microspectrometer from HORIBA Jobin Yvon at the Institute of Earth Sciences at the University of Graz.

This method is based on the interactions between molecules and incident monochromatic radiation. There are two possibilities how a molecule can interact with monochromatic light:

1) The molecule takes up energy (Stokes Raman scattering).
2) The molecule gives up energy (anti-Stokes Raman scattering).

However, the radiation gets scattered and dispersed and does not only contain the original frequency (Rayleigh scattering) but also new frequencies. These new frequencies are referred to as Raman lines or bands and are characterized by a frequency shift that is characteristic of the scattering molecule. The Raman lines and bands constitute a Raman spectrum (Long 1977). The intensity of a Raman line is not only dependent on the power of the incident monochromatic light but also on the frequency of scattered radiation. Also the absorptivity of the materials can influence the Raman lines' intensity (Kontoyannis and Vagenas 2000).

## 3. Geological Overview

The three investigated PTB sections are situated on the so called South Armenian Block (SAB). The SAB, also called Daragalez continental terrane, is a continental terrane of Gondwanian origin (Knipper and Khain 1980, Monin and Zonenshain 1987, Sosson et al. 2010), which is separated by the Sevan-Akera suture zone from the former southern Eurasian margin (Meijers et al. 2015). The SAB, the Sevan-Akera suture zone and the Eurasian margin form the Lesser Caucasus (Fig. 5; Sosson et al. 2010). The SAB is bounded by the Iranian terranes in the east, the Bitlis-Zagros suture zone in the south and the Turkish Anatolide-Tauride Block (ATB) in the west (Meijers et al. 2015). The SAB is the eastern continuation of the ATB and represents the continental part of the Anatolide-Tauride South Armenian Microplate (Fig. 6; Barrier and Vrielynck 2008, Okay and Tüysüz 1999, Rolland et al. 2012, Meijer et al. 2015). There is no clear geological evidence for the timing of rifting of the SAB from the African margin (Meijers et al. 2015). A palaeomagnetic study from Bazhenov et al. (1996) on Jurassic volcanic rocks from the SAB shows that the SAB was positioned at the African margin in the Early Jurassic. Therefore Bazhenov et al. (1996) assumed that the rifting's onset started during or after the Early Jurassic (Meijers et al. 2015). However, the lithology and facies of the SAB's Triassic rocks are very similar to those of the Sanandaj-Sirjan Zone in Central Iran (Richoz S., personal communication), which started its drifting from Gondwana during the Late Permian (Stampfli et al. 1991, Seyed-Emami 2003). Moreover, some palaeogeographic maps show that the ATB and the SAB were already separated from Gondwana during the Permian-Triassic transition (Fig. 7; Stampfli et al. 1991, Stampfli and Borel 2002, 2004, Torsvik et al. 2012). According to Gealey (1988), Kazmin (1991) and Mart (1987) the rifting of the Taurides-Anatolides from Gondwana, including the SAB, initiated during Triassic times (Hässig et al. 2015). The obduction of oceanic lithosphere on the SAB (Knipper 1975, Knipper and Khain 1980, Monin and Zonenshain 1987, Sosson et al. 2010) occurred during the Late Coniacian-Santonian (Upper Cretaceous), around 20 Ma before the collision of the SAB with Eurasia during the Paleocene. The widespread Eocene magmatic activity, which is still ongoing, started after the onset of the collision (Sosson et al. 2010).

The Proterozoic metamorphic basement of the SAB is characterised by gneisses, micaschists and leucogranite intrusions (Sosson et al. 2010). The Palaeozoic rocks are mainly localised in the southwestern part of Armenia (Fig. 1). They include an Upper Devonian series of Frasnian-Famennian age composed of at least 1000 m thick detrital rocks including quarzites, sandstones and argillites and Carboniferous reef limestones with a variable thickness of 500-700 m. The Permian platform disconformably overlies the Devonian and Carboniferous formations and is composed of 500-1500 m thick black limestones and marls with occurrences of bitumen (Sosson et al. 2010).

The thickness of the Triassic formations varies between 700-900 m (Sosson et al. 2010) and, as already mentioned, they are very similar to Triassic rocks of the Sanandaj-Sirjan Zone in Central Iran. Zaninetti et al. (1972) subdivide the Lower and Middle Triassic in Iran into a lower limestone unit, a middle dolomitic unit and an upper limestone unit. The lower limestone unit consists of thin to medium-bedded limestones. These grey, yellow-grey and pink limestones, that often show bioturbation, occur with intercalations of calcareous marls and dolomitic and oolitic beds (Seyed-Emami 2003, Horacek et al. 2007b). Because the bedding-planes are sometimes crowded with worm traces, bivalves (*Claraia*) and small hematized gastropods these limestones in the Sanandaj-Sirjan Zone are called "*Claraia*-beds" (Stepanov et al. 1969) or "Calcaire vermiculé" (Dellenbach 1964, Seyed-Emami 2003). The middle dolomitic unit mainly consists of ridge-forming, light brown to yellowish-grey, well to thick-bedded, dense to fine-crystalline dolomites and limestones. The upper limestone unit consists of thick-bedded to massive and whitish algal limestones. A hiatus, caused by
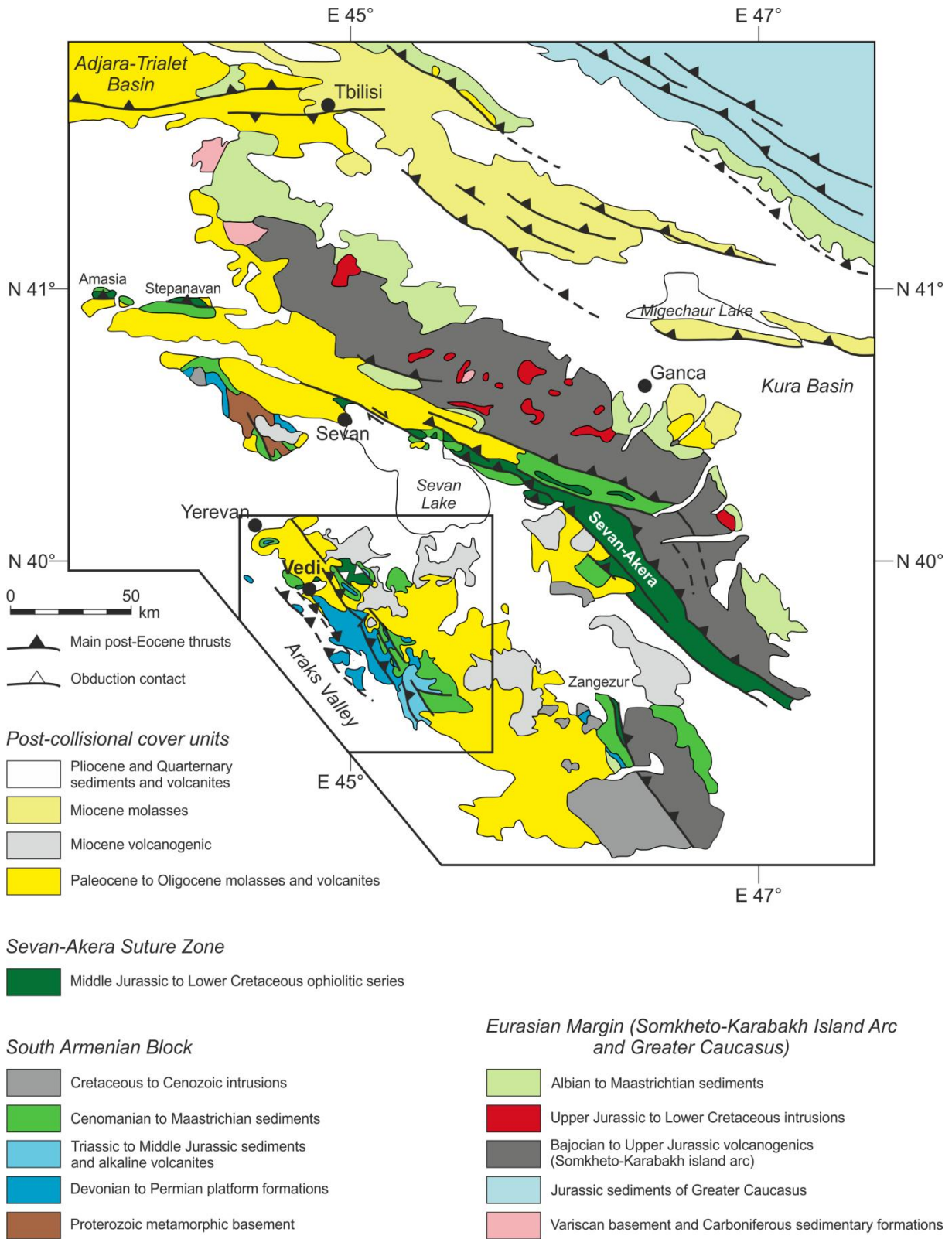
**Fig. 5:** Structural map of the Lesser Caucasus. Location of Fig. 1 is indicated. Modified after Nalivkin (1976) and Sosson et al. (2010).
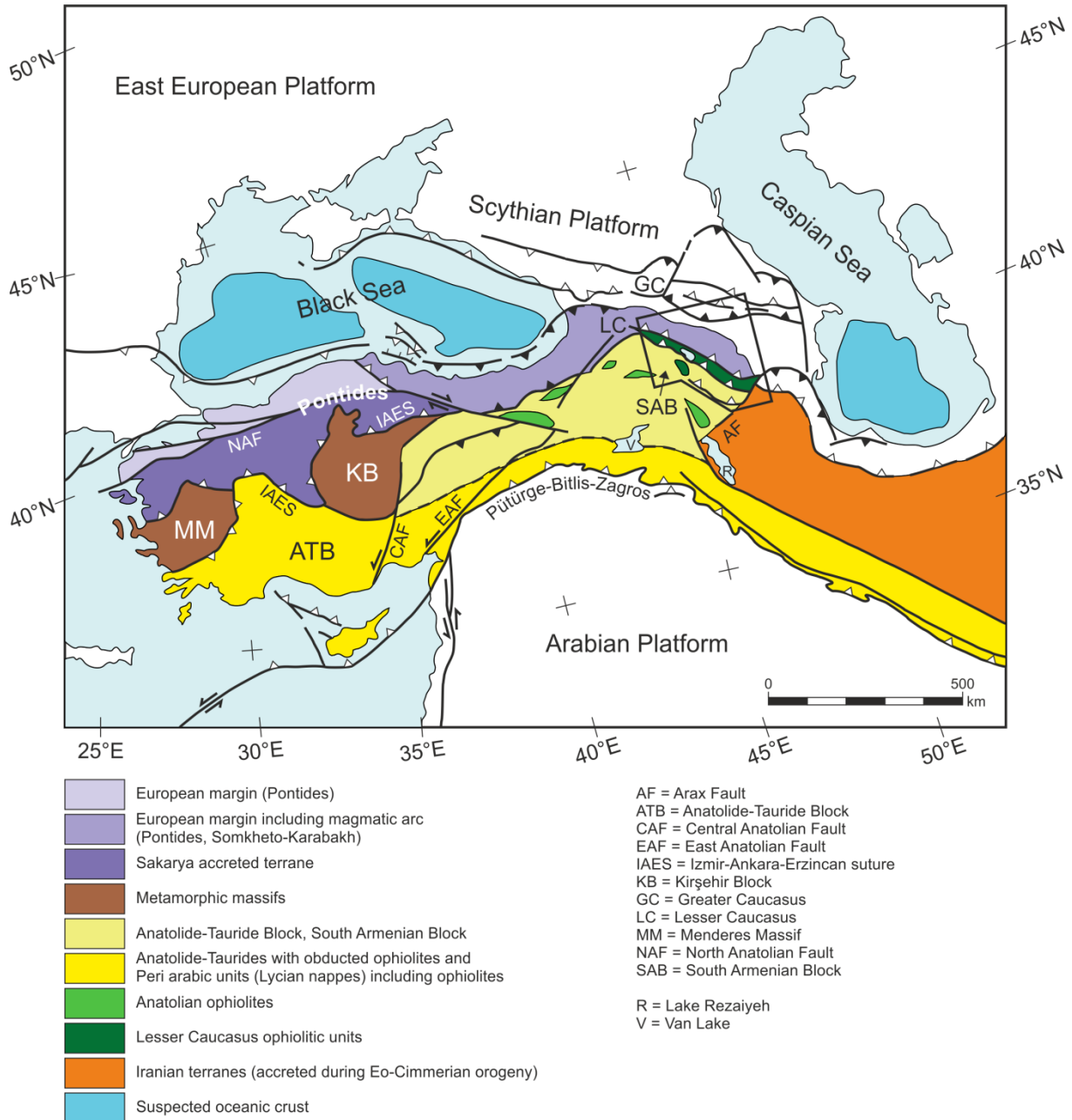
**Fig. 6**: Structural sketch map of the Anatolide-Taurides, Caucasus and Iranian belts. Location of Fig. 5 is indicated. Modified after Sosson et al. (2010).

the pre-Shemshak erosional phase (Early Cimmerian event), separates the upper limestone unit from the overlaying thick, siliciclastic and partly carbonaceous rocks of Upper Triassic age (Seyed-Emami 2003).

Jurassic rocks are unknown in the Armenian part of the SAB but they occur in Nakhijevan (Azerbaijan) and in Iran (south to Araks valley; Sosson et al. 2010). In Armenia, thick reef limestones of Cenomanian and Turonian age unconformably overlie the Triassic series (Eghoyan 1955, Paffenholtz 1959, Sokolov 1977, Hakobyan 1978, Sosson et al. 2010). In Vedi area, these limestones are overlain by an Upper Cenomanian flysch (Sokolov 1977) and an Upper Coniacian-Santonian olistostrome (Eghoyan 1955, Rengarten 1959, Hakobyan 1978) made of ophiolitic blocks contained in a muddy matrix (Sosson et al. 2010). The Vedi ophiolites are mainly Middle Jurassic (Middle to Late
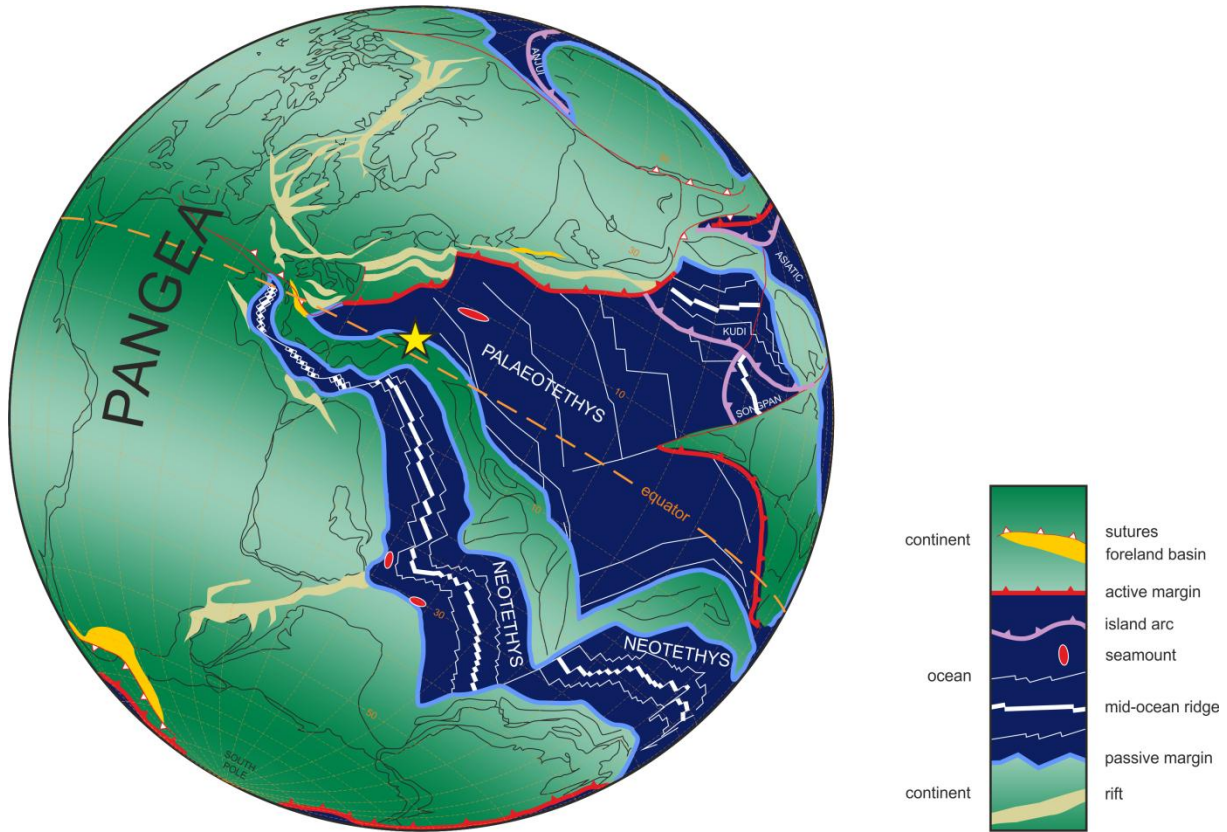
**Fig. 7:** Palaeogeographic map showing the location of the three investigated outcrops. Centered 20°N/20E. Modified after Stampfli and Borel (2002).

Bajocian; Danelian et al. 2008, 2010), Late Jurassic (Danelian et al. 2010) and probably Early Cretaceous in age (Belov et al. 1991, Sosson et al. 2010).

The Permo-Triassic carbonate ramp of southern Armenia is exposed among other places at the Zangakatun (Baud et al. 1989, Zakharov et al. 2005), Vedi (Baud et al. 1989, 2007) and Ogbin localities, which are situated about 45 and 60 km south-east of Yerevan (Fig. 1; Baud et al. 2007). In the Zangakatun section (former Sovetashen) Zakharov et al. (2005) describe the Wuchiapingian rocks as dark-grey to light-grey limestones which are sometimes thin bedded and spotted. The Changhsingian rocks are described as grey, pink and redish-brown limestones with interlayers of mudstone. The total thickness of the Upper Permian sediments is 25.4 m (Zakharov et al. 2005). The Lower Triassic sediments are characterized by red and grey, mostly bedded limestones. At the base, Calcium Carbonate Crystal Fans (CCFs) and microbialites occur. Both, the CCFs and microbialites are surrounded by a bioclastic wackestone. The microbialites are present as isolated mounds characterized by thrombolitic fabrics (Baud et al. 2007) and vary in size between 5 cm to 1.5 m. The biggest microbialite shows an asymmetrical growth and consists of several thrombolite domes (Friesenbichler et al. 2015) with a total height of 12 m. The microbial buildups are overlain by a mostly thin layered and partly laminated or vermiculated limestone, which in some places contains oncoids. The total thickness of the Lower Triassic (Griesbachian to Smithian, the Spathian is tectonically missing) sediments in the Zangakatun Section is around 121 m (Zakharov et al. 2005).

The Vedi section's sedimentation and stratigraphy are similar to those at Zangakatun (Baud et al. 1989). The Wuchiapingian nodular limestones are of grey colour with a total thickness of 17 m. After a hiatus the Upper Changhsingian limestones follow (Baud et al. 1989). They are grey and nodular too but only 6 m thick. The Permian-Triassic boundary is characterized by a few cm of red marl (Baud et

al. 1989). The Lower Triassic limestones are, as in Zangakatun, characterized by microbialites and CCFs, overlain by thin-bedded grey limestones. According to Baud et al. (1989) these thin-bedded limestones are of Late Griesbachian age.

In the Ogbin section, red nodular limestones of Upper Permian age are overlain by a 20 cm thick shale bed. The following Lower Triassic microbialites vary in size between 5 cm to at least 1.7 m. These microbialites are overlain by yellowish and grey platy limestones, containing ammonoids, *Claraia* and oncoids.

# 4. Outcrop Descriptions

In general microbialites are observed in four scales (Grey 1989, Shapiro and Awramik 2000, Shapiro 2000):

1)    Megastructure: Large-scale features of microbilite beds, e.g. biostromal or biohermal build-ups.

2)    Macrostructure: the forms of microbialites at a scale of tens of decimeters to meters, e.g. domes and (branching) columns.

3)    Mesostructure: Internal structures of macrostructural elements that are visible to the naked eye. At this scale the three most important groups of microbialites are defined, namely stromatolites (laminated mesostructure), thrombolites (clotted mesostructure) and dendrolites (dentritic mesostructure; Shapiro 2000). There is also a fourth type, namely leiolites, which are structureless masses (Riding 2000).

4)    Microstructure: Microscopic fabrics observed under the microscope, e.g. microbial constituents, crystals forms and cements (Shapiro 2000).

## 4.1.  Zangakatun

At Zangakatun a 30 m long outcrop was investigated where the layers dip steep (Fig. 8 and 9). All along the section observation gaps occur that vary in thickness between 6 cm and 20 cm. The investigated section starts with red, nodular limestone and marly limestone. Ammonoids as well as conodonts show that these limestones are of Upper Changhsingian age (Zakharov et al. 2005). These limestones are overlain by a red and 5 cm thick Boundary Shale, which represents the extinction level. Above this shale there is a 14 cm thick layer of red and platy limestone, which comprises the latest Permian, post-extinction *C. meishanensis – H. praeparvus* conodont zone (Zakharov et al. 2005). This limestone is overlain by four beds of CCFs that vary in size between 5 and 10 cm. The base of the first CCF bed coincides with the base of the *H. parvus* zone (Zakharov et al. 2005), which marks the beginning of the Triassic. The CCFs are embedded in a red micritic matrix. After an overlaying 15 cm thick layer of red limestone another CCF occurs. It forms a mound with a thickness of 55 cm that changes into a 13 cm thick bed of limestone (Fig. 10a and b). The following 20 cm thick thrombolitic bed is overlain by a 5 cm thick microbialite, followed by a 12 cm thick limestone bed that is overlain by another microbialite with a total thickness of 120 cm. This microbialite starts with a 45 cm thick bedded part followed by a 75 cm thick thrombolitic hill that ends abruptly. The thrombolitic hill is surrounded by a red and partly nodular limestone. The onlap between the microbialite and the surrounding limestone is well visible (Fig. 10c).

A 40 cm thick observation gap separates the thrombolitic hill and the surrounding limestone from two red and massive limestone beds that still lie within the *H. parvus* zone (Zakharov et al. 2005). The following red and marly limestone already lies within the *I. isarcica* zone (Zakharov et al. 2005) and is overlain by 2 m of limestone. This red, grey and partly platy limestone consists of 2 to 6 cm thick beds. The overlaying 5 cm thick limestone layer is followed by a 40 cm thick grey limestone that is in turn overlain by a red and more clayey limestone.

The hereinafter described succession was observed in a parallel profile 5 m above the previous one. A 120 cm thick interval consists of 1 to 7 cm thick red limestone beds. Above this bedded limestone a 6 cm thick layer of pink and marly limestone occurs. The overlaying bedded limestone is of red colour and exhibits features of bioturbation. This bioturbated limestone is overlain by a 40 cm

**Fig. 8:** Photograph from the investigated outcrop in Zangakatun, which was taken from the opposite hillside. The white lines mark the position of the measured section, which starts on the right side of the lower line and ends on the left side of the upper line. Photograph was taken by Lilit Sahakyan.

thick layer of badly exposed limestone that exhibits several small observation gaps. The exposed parts show a red colour and bioturbation features too, just like the overlaying 65 cm thick limestone. On top of this limestone is a microbialite that coincides with the boundary between the *I. isarcica* and the *H. postparvus* zone (Zakharov et al. 2005). The following 100 cm are two layers of grey and massive limestone, overlain by a 35 cm thick nodular limestone. The overlaying 17 cm thick, bioturbated limestone is in turn overlain by a 45 cm thick layer of badly exposed, platy and in some parts nodular limestone with a reddish colour at the base and a grey one on top.

The following layer is a 10 cm thick thrombolitic bed, which is overlain by an 87 cm thick marl layer that contains small ammonoids as well as the bivalve *Claraia*. The overlaying red and thin platy limestone is 80 cm thick. The following layer has a total thickness of 2 m and consists of a red, bedded and thin platy limestone. This limestone layer not only contains some small thrombolitic mounds but also a thrombolitic bed at its base (Fig. 10d). The overlaying red and platy limestone has a total thickness of 155 cm and consists of 3 to 6 cm thick beds. The following limestone layer is 6 cm thick. Above this limestone occurs a red and platy limestone layer of 10 cm thickness that is overlain by a slightly nodular limestone that possesses a rough surface. It is overlain by four thrombolitic beds with a total thickness of 70 cm. On top of these beds starts the *C. planata* zone (Zakharov et al. 2005). The following limestone layer is 11 cm thick and is overlain by a thrombolitic hill of 120 cm in thickness. Above this thrombolitic hill occurs a 20 cm thick layer of limestone, which is in turn overlain by a red limestone with a total thickness of 70 cm that contains at least three thrombolite and dendrolite levels. The following grey and platy limestone is 40 cm thick and is overlain by a 15 cm thick layer of thin platy limestone that is in turn overlain by a 20 cm thick thrombolite. The following
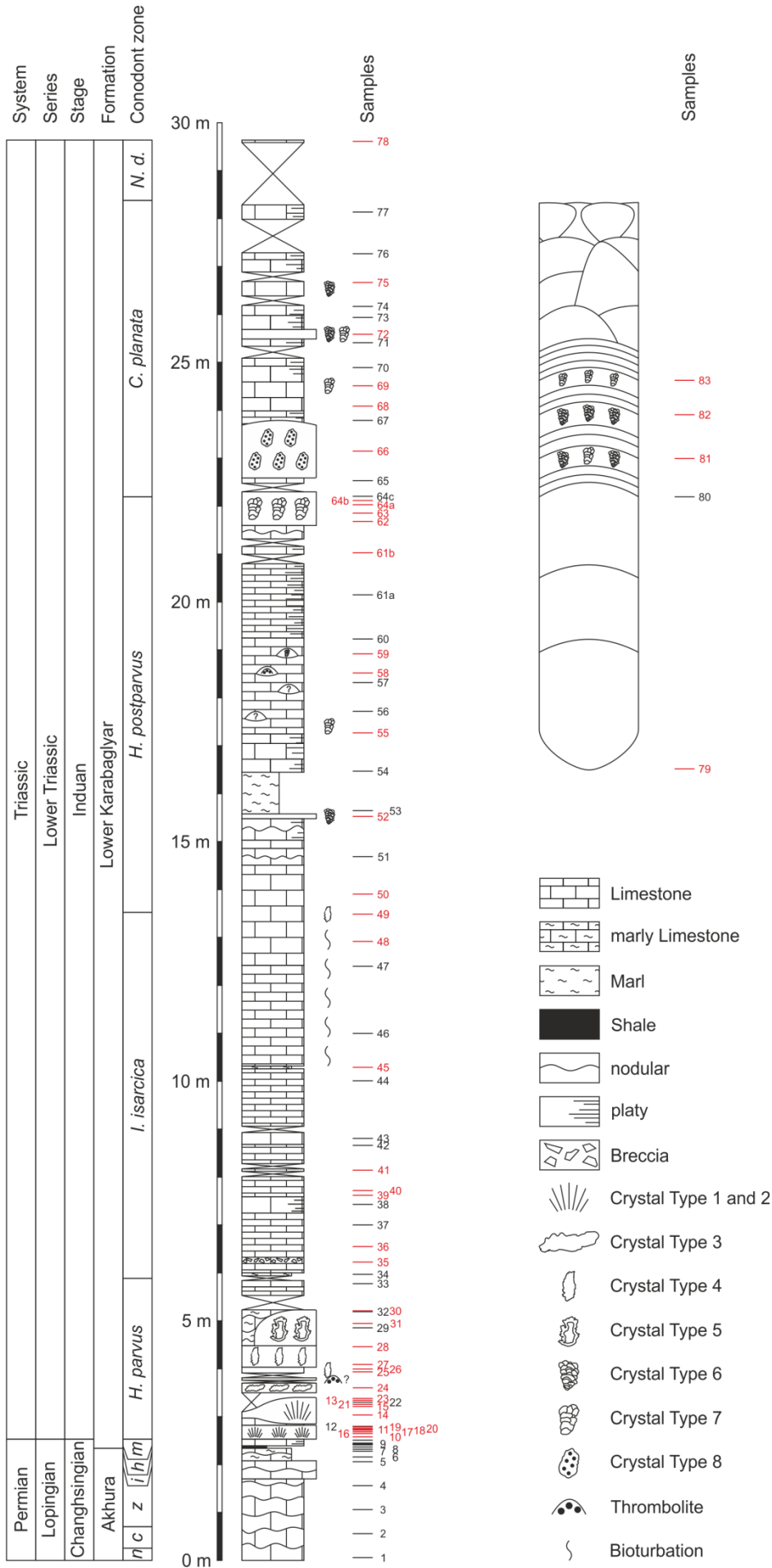
**Fig. 9:** Lithostratigraphy and Biostratigraphy of the investigated outcrop at Zangakatun. From the red samples at least one thin section was made of. Abbreviations for the conodont zones:

N. = *Neospathodus*
d. = *dieneri*
C. = *Clarkina*
H. = *Hindeodus*
I. = *Isarcicella*
m = *C. meishanensis – H. praeparvus*
h = *C. hauschkei*
I = *C. iranica*
z = *C. zhangi*
c = *C. changxingensis – C. deflecta*
n = *C. nodosa*

Lithostratigraphy and conodont zones modified after Zakharov et al. (2005).
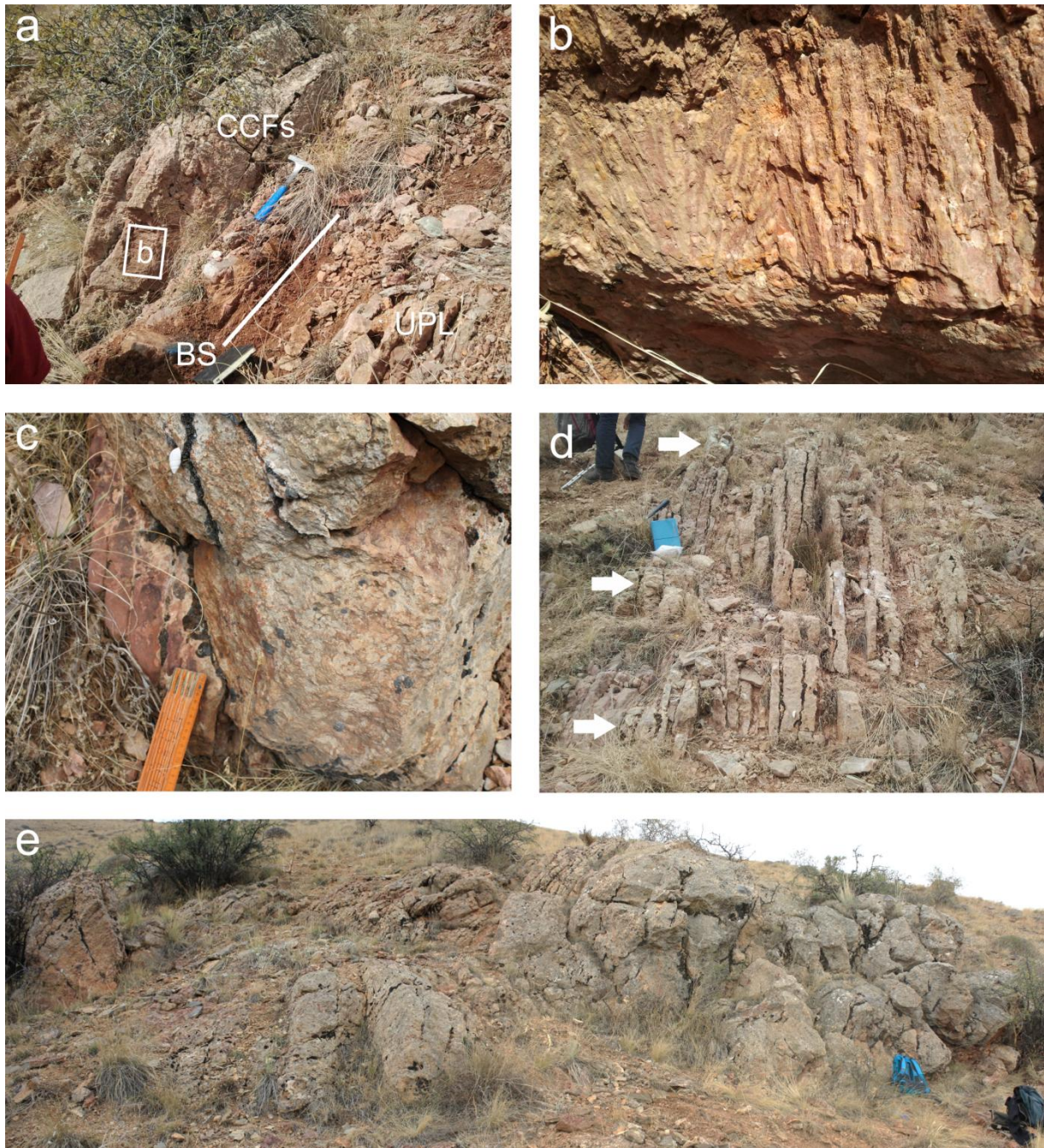
**Fig. 10:** Field photographs from the investigated outcrop at Zangakatun. **(a)** The Permian-Triassic boundary. The picture shows upper Permian limestone (UPL) overlain by Boundary Shale (BS, white line) that is in turn overlain by CCFs. The white rectangle marks the position of (b). **(b)** Detail view of CCFs. The crystal's fan-like arrangement is well visible. **(c)** Onlap between a thrombolitic hill and the surrounding limestone. **(d)** Thrombolitic hills (white arrows) embedded in a bedded limestone. **(e)** Total view of the huge microbialite. Photographs were taken by Evelyn Friesenbichler (a, b and d) and Sylvain Richoz (c and e).

five layers of thin platy limestone vary in size between 5 and 50 cm and are separated by several larger observation gaps. The last limestone layer belongs to the *N. dieneri* conodont zone (Zakharov et al. 2005).

Zakharov et al. (2005) describe the overlaying limestones of Lower Olenekian age (Lower Triassic) as grey and brownish-grey fucoid limestones with calcareous clay and microbialite layers. The

overlaying grey and pink, thin and medium bedded fucoid limestones with thin interbeds of conglomerate in the lower and upper parts is also of Olenekian age.

Microbialites do not only occur in the just described section but also laterally. The biggest one was next to the upper half of the investigated section. It is up to 8 m wide and has a total thickness of 12 m (Fig. 9). The lower half of this microbialite is characterized by a massive appearance. Above this massive part several beds follow and on top it consists of numerous thrombolitic domes (Fig. 10e). It shows an asymmetrical growth.

## 4.2.  Vedi

In Vedi 1 a nearly 11.5 m long outcrop was investigated (Fig. 11 and 12). As in Zangakatun limestones, microbialites and CCFs are present that also dip with a steep angle, but in contrast to Zangakatun the limestones and microbialites in Vedi are often separated by shale layers. These shale layers are predominantly yellow but also black and, especially in the upper part, red and vary in thickness between 3 and 35 cm.

The section begins with a black, cherty limestone of Midian (Middle Permian) age. The overlaying grey and nodular limestones of Wuchiapingian (Upper Permian) age have a thickness of 17 m. A hiatus is separating these limestones from the overlaying limestones of Upper Changhsingian (Upper Permian) age. These grey and nodular limestones of the *Shevyrevites* and *Paratirolites* ammonoid zone have a thickness of 6 m. The PTB is marked by a few cm thick red marl (Baud et al. 1989). A thrust fault led to a doubling of the PTB.

The shale layer underlying the first microbialite belongs to the Boundary Shale. The following three microbialites have a thickness of 23, 25 and 10 cm, respectively. The next microbialite has a thickness of 8 cm and is directly overlain by 50 cm thick CCFs. In contrast to the CCFs in Zangakatun they do not occur as a mound and are more weathered and therefore more brittle. The transitions between single CCFs are well visible (Fig. 13a). The CCFs are overlain by an 18 cm thick layer of marl that is in turn overlain by three thrombolitic beds with a total thickness of 45 cm. After a 10 cm thick limestone layer and a 14 cm thick marl layer another microbialite, which has a thickness of 16 cm, occurs. The next microbialite has a thickness of 27 cm and occurs after three layers of yellow and black shales. The following 2.5 m thick limestone layer if overlain by an 11 cm thick microbialite. After another microbialite with a thickness of 8 cm occurs a 16 cm thick marl layer, which is in turn overlain by three microbialites with a total thickness of 28 cm (Fig. 13b). After these microbialites follows an 8 cm thick limestone layer, which is in turn followed by the last microbialites of this investigated outcrop (Fig. 13c). These microbialites have a total thickness of 35 cm and occur 8 m above the base of this profile.

The last part of this outcrop consists of eight limestone layers that vary in thickness between 6 and 55 cm. Two of these limestone layers contain remains of the bivalve *Claraia* and can therefore be denoted as *Claraia* limestone. The limestone layers are separated from each other by yellow, black and red shale layers.

Baud et al. (1989) describe the rocks that overlie the microbialites as thin-bedded, grey limestones that contain not only the bivalve *Claraia* but also the ammonoid *Ophiceras*. These two fossils indicate a late Griesbachian age.

Microbialites are not restricted to the just described section but also occur laterally. Vedi 1 is located on one side of an anticline, whereas Vedi 2 and 3 (Fig. 2b), which are around 1.2 km to the east-north-east, are on the other side. Vedi 2 is the section described in Baud et al. (1989). All around

**Fig. 11:** Field photograph showing the investigated outcrop in Vedi 1. The white line marks the position of the measured section, which starts on the right side and ends on the left side. Photograph was taken by Evelyn Friesenbichler.

this side of the anticline, microbialitic mounds occurs in several locations, but the surrounding beds are not well exposed and sections are thus difficult to measure. In Vedi 3 (Fig. 2b) a 1.5-2 m high microbialite was found (Fig. 14). It has an asymmetrical growth like the huge microbialite from Zangakatun. Another similarity to the huge microbialite from Zangakatun is that this microbialite also starts with a massive appearance that changes into a bedded one.

## 4.3. Ogbin

At Ogbin a 21.5 m long outcrop was investigated, which is located on the right side of a trench (Fig. 15 and Fig. 16a). As in Zangakatun and Vedi limestones, CCFs and microbialites are present. As in Zangakatun shale layers are rare.

The investigated section starts with around 5 m of Permian limestone. The first two massive red limestone beds, with a total thickness of 45 cm, are overlain by a 20 cm thick, red, nodular and thin platy limestone. The overlaying nodular and thin platy marly limestone is 20 cm thick and is in turn overlain by an 80 cm thick nodular limestone. This nodular limestone can be divided into 4 beds and contains pieces of crinoids. After a 5 cm thick marl layer follows a 30 cm thick layer consisting of nodular limestone, which can be divided into three beds. The overlaying nodular limestone has a total thickness of 120 cm and is in turn overlain by a 15 cm thick marly limestone. The following 70
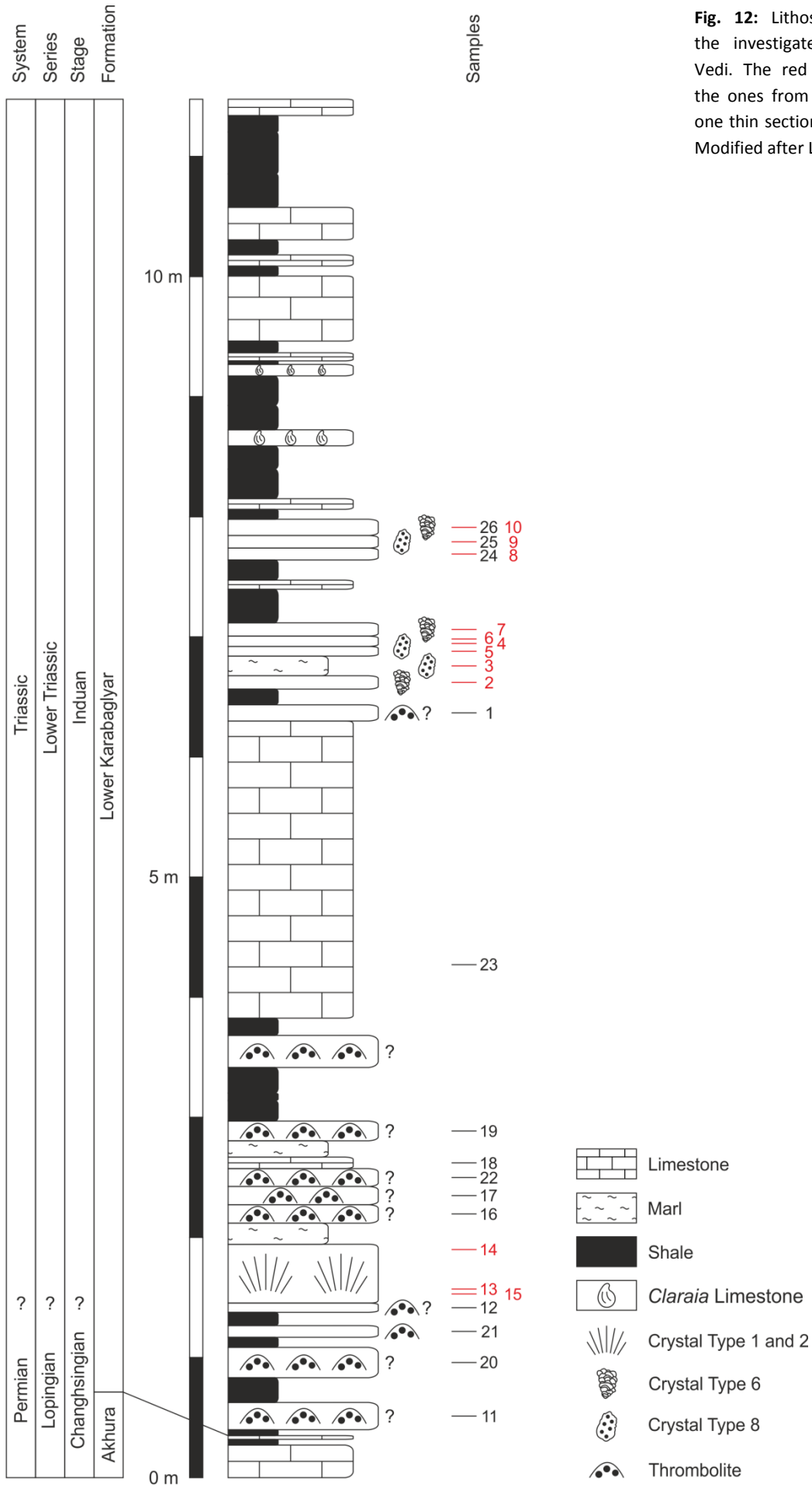
**Fig. 12:** Lithostratigraphy of the investigated outcrop at Vedi. The red samples mark the ones from which at least one thin section was made of. Modified after Lilit Sahakyan.
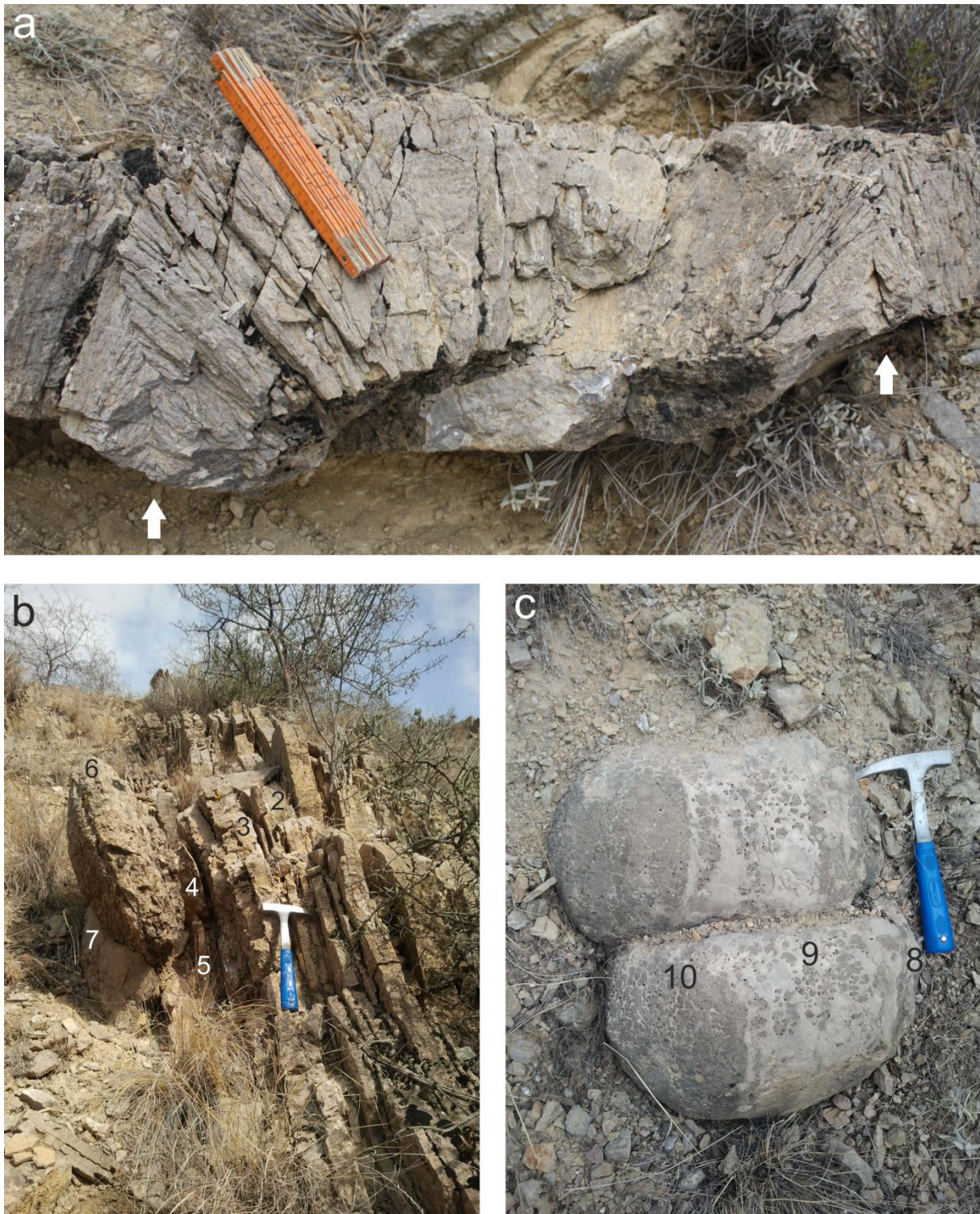
**Fig. 13:** Field photographs from the investigated outcrop at Vedi 1 showing the units from which thin sections were analysed. The numbers represent the sample numbers. **(a)** CCFs. In contrast to the ones from Zangakatun these CCFs are more weathered and more brittle. The white arrows mark the well visible transitions between neighbouring CCFs. **(b)** Limestones and microbialites from around 6 m above the base of the investigated section. **(c)** Thrombolite from the last microbialite layers of the investigated section with its base on the right side (sample 8) and its top on the left side (sample 10). Note the for microbialites unusual appearance. Photographs were taken by Sylvain Richoz (a) and Evelyn Friesenbichler (b and c).

**Fig. 14:** Field photograph showing a huge microbialite at Vedi 3. It starts with a massive part and continues on the left side with beds. Photograph was taken by Sylvain Richoz.

cm consist of red nodular limestone that is in turn overlain by a 35 cm thick massive limestone layer. The following marly limestone is 18 cm thick and is partly red and green. The overlaying limestone shows a grey-green and violet colour. It has a total thickness of 38 cm but only the first 15 cm are nodular. This limestone layer is overlain by another limestone layer with a thickness of 12 cm. The following 3 cm thick shale is overlain by a 2 cm thick limestone layer. The overlaying 20 cm thick shale shows a grey colour in the first 15 cm and a red one in the last 5 cm. The upper shale layer is the Boundary Shale but whether the lower shale layer also belongs to the Boundary Shale is not clear.

After a 5 cm thick marly limestone and a 1 cm thick marl layer occur the first microbialites. These two thrombolitic beds have a thickness of 4 and 6 cm, respectively. After a 6 cm thick marly limestone follows the next thrombolite with a thickness of 26 cm. The following 7 cm thick limestone layer is overlain by a thrombolitic hill with a thickness of 55 cm. This thrombolitic hill is surrounded by a platy limestone that shows a yellow and red colour (Fig. 16b and c). Further to the right the microbialites reach a total thickness of around 1.7 m. These microbialites are thrombolites as well as dendrolites (Fig. 16d) and laterally interfinger with marl. The microbialites are overlain by two platy and massive limestone layers, which are in turn overlain by another limestone layer. This limestone has a thickness of 60 cm and contains ammonoids of the genus *Ophiceras*. The overlaying marly limestone shows a yellow colour and contains bivalves of the genus *Claraia*. After a 4 cm thick shale follows an 80 cm thick yellow limestone layer. This limestone contains not only oncoids at its base but also *Claraia* and is overlain by a 10 cm thick marly limestone. The following two limestone layers are yellow and 26 cm thick, respectively. Both layers contain oncoids but only in the lower layer occur *Claraia* whereas in the upper one ammonoids, mostly *Ophiceras*, are very abundant. The
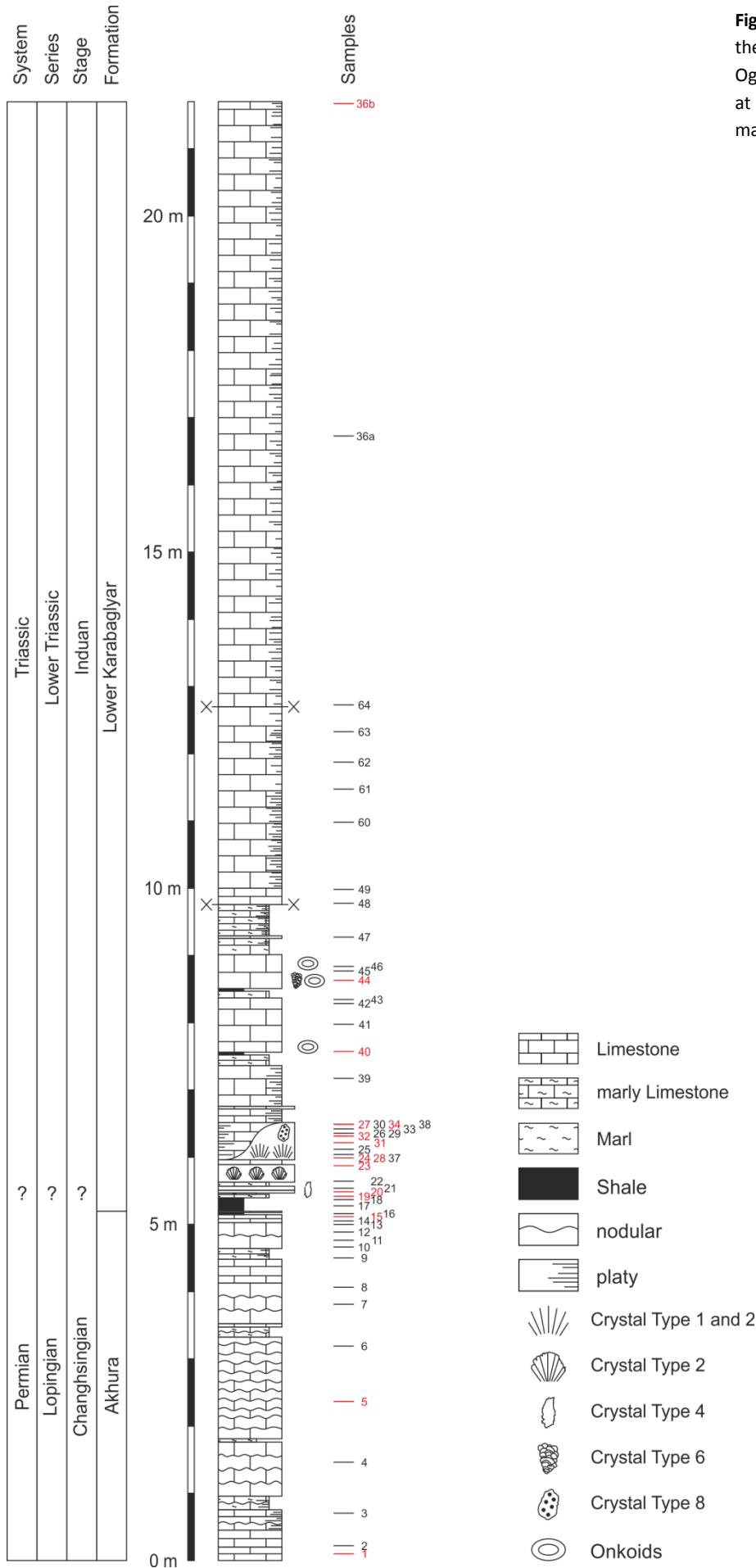
**Fig. 15:** Lithostratigraphy of the investigated outcrop at Ogbin. From the red samples at least one thin section was made of.
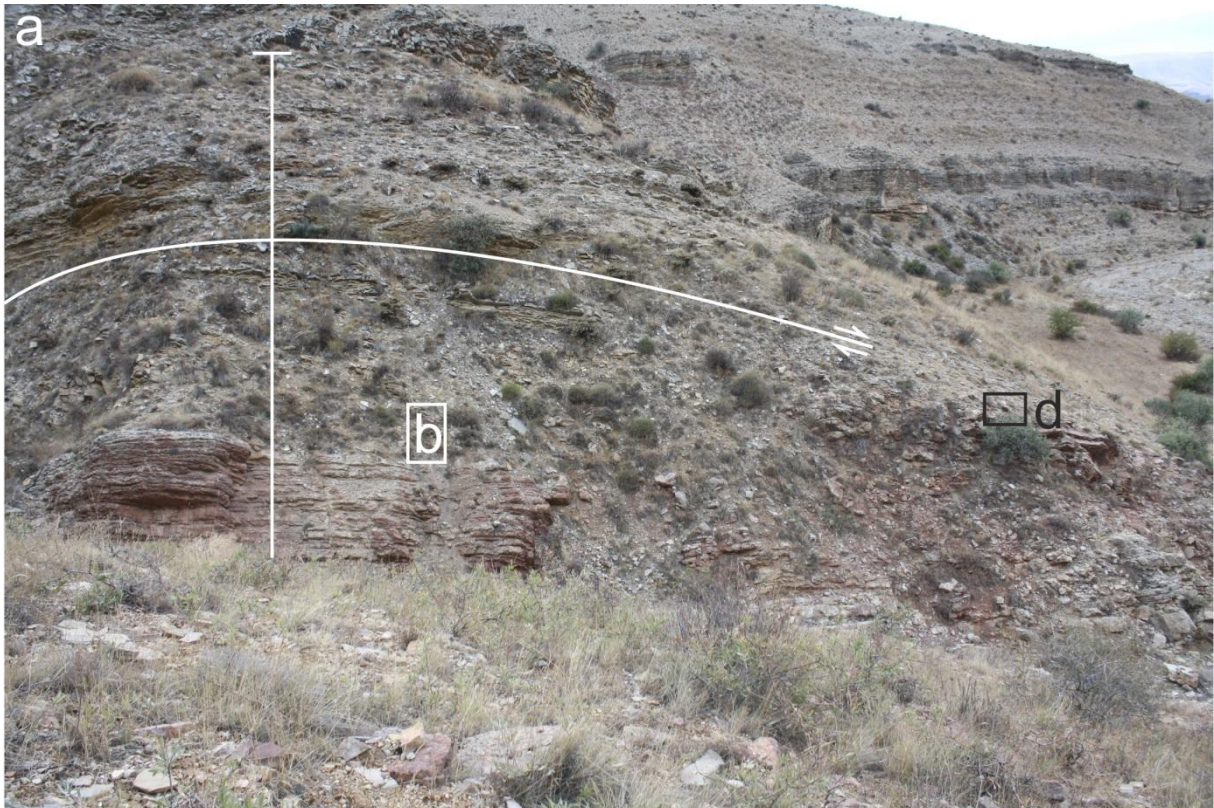
← **Fig. 16:** Field photographs from the investigated outcrop at Ogbin. **(a)** Photograph from the investigated outcrop that was taken from the opposite hillside. The positions of the measured section and the uppermost fault are indicated. The base of the investigated section is not visible on this picture. The rectangles mark the positions of picture (b) and (d). **(b)** Lower Triassic microbialites located above the Boundary Shale (BS). The white rectangle marks the position of picture (c). The well visible thrombolitic **(c)** and dendrolitic fabric **(d)** of the microbialites. Photographs taken by Sylvain Richoz (a and b) and Evelyn Friesenbichler (c and d).

following yellow marly limestone layers have a total thickness of 24 cm and are overlain by a 4 cm thick grey limestone. This limestone is in turn overlain by another marly limestone with a thickness of 46 cm. In contrast to the previous marly limestone this one has a platy appearance. A fault separates the marly limestone from the overlaying grey limestone, which is in turn overlain by thin and thick platy limestones with a total thickness of 1.9 m. The following thin platy and marly limestone is overlain by a thick platy limestone. Both intervals have a thickness of 40 cm, respectively. After another fault occurs a 9 m thick interval of platy limestone. This fault is almost parallel to the bedding plane and could therefore be of local importance because it could be responsible for a hiatus in the section.

Going west from the trench, several microbialitic mounds occur in a straight on a distance of 250 m. They can reach a thickness of up to 1 m. Because the trench is the only place where a continuous section and the surrounding beds can be described, it is difficult to place these mounds in the section. However, their position regarding the top of the Permian beds is higher than the one of the microbialitic mounds in the trench and could rather correspond to the height of the fault.

# 5. Results

## 5.1. Microfacies Analyses

### 5.1.1. Zangakatun

The sample positions, the distribution of the different crystal types and the distribution of the organisms are illustrated in Fig. 9 and Fig. 17. The numbers of organisms found in each thin section are shown in Table 2.

***The Calcium Carbonate Crystal Fans***

Within the CCFs two different types of crystals, all of them made of calcite, can be distinguished. Crystals of type 1 are long crystals with straight margins. They initiate with a mottled fabric that change into a fine, regular and slightly wavy lamination. This lamination can be followed between neighbouring crystals (Fig. 18a). After the termination of crystal growth the next crystals started to grow on top of the previous ones. Again these crystals started with a mottled fabric changing into a laminated one (Fig. 19a). Crystals of type 2 started to grow on top and on the sides of the laminated crystals (Fig. 19b and c). These elongated and sometimes botryoidal, upward-branching crystals often show flattened terminations indicating that they were originally precipitated as aragonite (Fig. 19d). Crystals of type 2 seem to be more common on top of the CCFs mound and beds, where the laminated crystals of type 1 can be entirely absent. Some of the crystals are slightly tilted and not upright.

The fan-like arrangement of the crystals was well visible in the field but this feature is not visible in the thin sections anymore. Crystals that were cut parallel to their growth direction stand more or less straight to each other (Fig. 20a). Thin sections from samples that were cut perpendicular to the crystals growth direction do not show that there are only single crystals standing next to each other, as someone could expect. These thin sections show a wall-like arrangement of the crystals (Fig. 20b). That is because almost all crystals of type 1 are at least partly overgrown by crystals of type 2. With the ongoing growth of the type 2 crystals they finally started to coalesce, resulting in the wall-like arrangement of the crystals.

The crystals are embedded in a homogenous red micritic matrix that contains some microspar and bioclasts, which are mostly ostracods and *Earlandia* (foraminifer). Gastropods, ammonoids and *Rectocornuspira* (foraminifer) are less common (Fig. 21b-f). In almost all samples from CCFs the crystals are partly or completely surrounded by sponges (Fig. 19b and c). Occasionally organisms, mainly Ostracods and *Earlandia*, can be found within the crystals. They are mainly enclosed in crystals of type 2 but they also occur to a smaller extent in crystals of type 1. The majority of these enclosed organisms can be found in the middle of the crystals and less common at the crystal margins (Fig. 19e and Fig. 21f). One ostracod was enclosed between two crystals (Fig. 19f). Fig. 17 shows that the fauna associated with the CCFs is the most diverse one. The CCFs also contain the highest number of organisms (Table 2).

In sample 19, which was taken from the top of the first CCF bed the crystals of type 1 and 2 seem to form groups of branching crystals that stand next to each other (Fig. 20c). Between these groups of crystals occur accumulations of organisms that are sometimes strongly recrystallized (Fig. 21a).
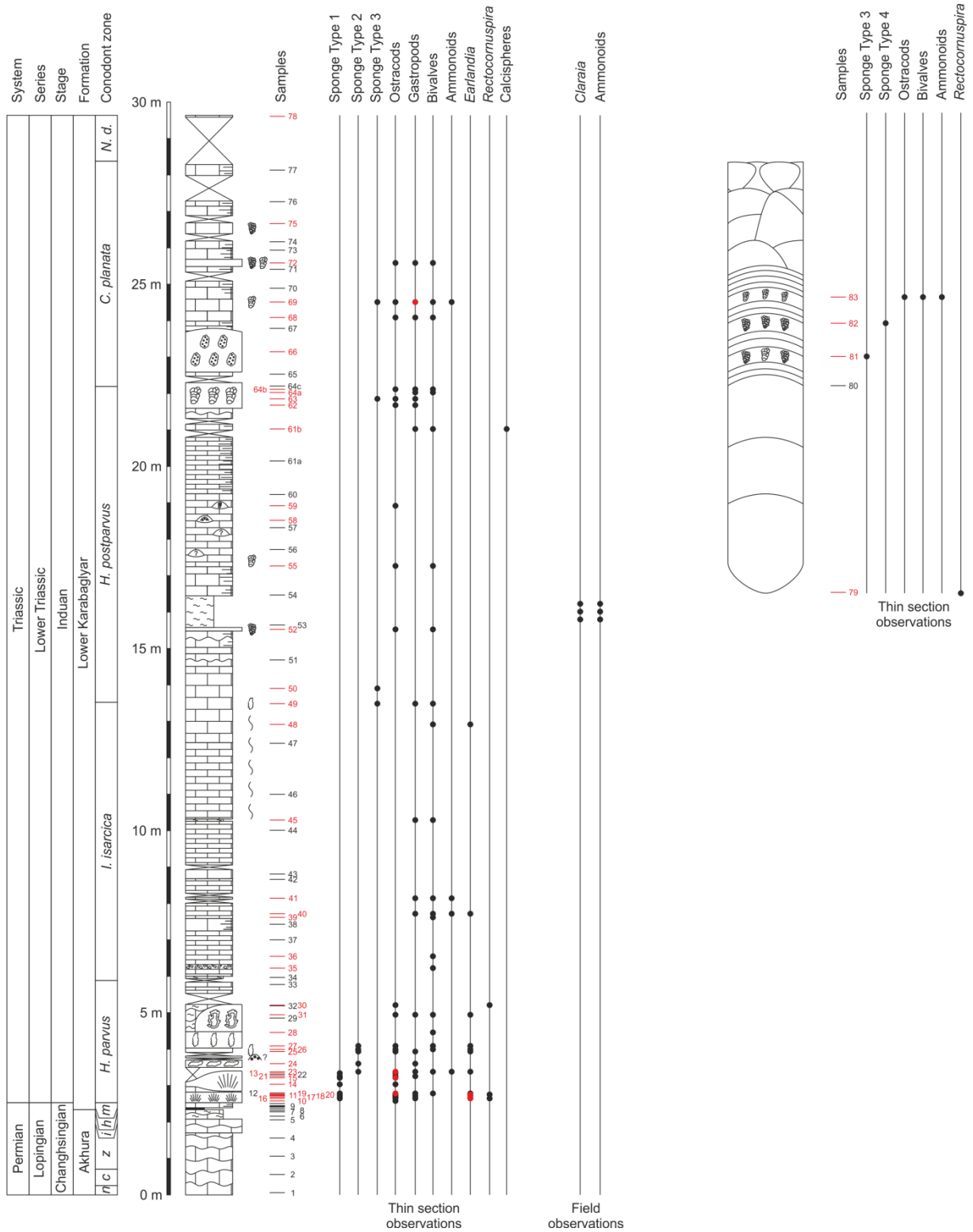
**Fig. 17:** Fossil distribution in Zangakatun. The picture shows the fossils observed in thin sections as well as in the field. The fossil distribution from the thin sections shows that the fauna associated with the CCFs and microbialites is more diverse. For legend see Fig. 9.

Above these accumulations occur sponges, which are covered by sediment. The sediment does not only cover the sponges but also partly the crystals. The next crystals started to grow on top of the previous ones or on the sediment. This succession of crystals, accumulations of organisms, sponges

**Table 2:** The fossil distribution in the thin sections from Zangakatun. The table shows how many of the organisms are in the sediment (sed.), the sponges (sp.) or the crystals (cr.). It also shows whether the samples were taken from CCFs (dark grey background), microbialites (light grey background) or the bioclastic wackestone without CCFs or microbialites (white background). For explanation see text.

| Sample | Ostracods | | | Gastropods | | | Bivalves | | | *Earlandia* | | | *Rectocornuspira* | | | Ammonites | | | Size | Notes |
|---|---|---|---|---|---|---|---|---|---|---|---|---|---|---|---|---|---|---|---|---|
| | sed. | sp. | cr. | sed. | sp. | cr. | sed. | sp. | cr. | sed. | sp. | cr. | sed. | sp. | cr. | sed. | sp. | cr. | [cm] | |
| 72 | 5 | | | 4 | | | 5 | | | | | | | | | | | | 5 x 5 | no sponges |
| 83 | 48 | | | | | | 12 | | | | | | | | | | | | 5 x 5 | no sponges, maybe 1 *Rectocornuspira* in the sediment |
| 81 | | | | | | | | | | | | | | | | | | | 5 x 5 | |
| 79 | | | | | | | | | | | | | | | 1 | | | | 5 x 5 | the whole thin section is one crystal |
| 69 | 1 | 2 | | 83 | 29 | | 1 | | | | | | | | | | | | 5 x 5 | |
| 69k | 7 | | | 28 | 22 | | 2 | | | | | | | | | 1 | | | 4,6 x 2,7 | |
| 68 | 1 | | | 4 | | | 2 | | | | | | | | | | | | 5 x 5 | only sediment |
| 66 | | | | 1 | | | | | | | | | | | | | | | 5 x 5 | |
| 64b | 71 | | | 4 | | | 1 | | | | | | | | | | | | 5 x 5 | no sponges |
| 64a | | | | 2 | | | 2 | | | | | | | | | | | | 5 x 5 | no sponges |
| 63W | 45 | 29 | | 11 | 6 | | | | | | | | | | | | | | 10 x 15 | |
| 62 | 7 | | | 3 | | | | | | | | | | | | | | | 5 x 5 | no sponges |
| 62k | 15 | | | | | | | | | | | | | | | | | | 4,6 x 2,7 | |
| 61b | | | | 3 | | | 7 | | | | | | | | | | | | 5 x 5 | only sediment |
| 55 | 15 | | | | | | | | 1 | | | | | | | | | | 5 x 5 | no sponges |
| 55k | 12 | | 1 | | | | | | | | | | | | | | | | 4,6 x 2,7 | |
| 52 | 1 | | | | | | 3 | | | | | | | | | | | | 5 x 5 | only loose spicules |
| 49 | | | | 1 | | | 1 | | | | | | | | | | | | 5 x 5 | |
| 48 | | | | | | | 12 | | | | | | | | | | | | 5 x 5 | only sediment |
| 48k | | | | | | | 12 | | | 2 | | | | | | | | | 4,6 x 2,7 | only sediment |
| 45 | | | | 1 | | | 7 | | | | | | | | | | | | 5 x 5 | only sediment |
| 41 | | | | 2 | | | 1 | | | | | | | | | 1 | | | 5 x 5 | only sediment |

| Sample | Ostracods | | | Gastropods | | | Bivalves | | | *Earlandia* | | | *Rectocornuspira* | | | Ammonites | | | Size | Notes |
|---|---|---|---|---|---|---|---|---|---|---|---|---|---|---|---|---|---|---|---|---|
| | sed. | sp. | cr. | sed. | sp. | cr. | sed. | sp. | cr. | sed. | sp. | cr. | sed. | sp. | cr. | sed. | sp. | cr. | [cm] | |
| 40 | | | | 3 | | | 5 | | | 14 | | | | | | 1 | | | 5 x 5 | only sediment, maybe 2 *Rectocornuspira* |
| 39 | | | | | | | 48 | | | | | | | | | | | | 5 x 5 | only sediment |
| 36 | | | | | | | 4 | | | | | | | | | | | | 5 x 5 | only sediment |
| 35 | | | | | | | 5 | | | | | | | | | | | | 5 x 5 | only sediment |
| 30 | 1 | | 2 | | | | | | | | | | 1 | | 6 | | | | 5 x 5 | no sponges |
| 30k | 1 | | | | | | | | | | | | | | | | | | 4,6 x 2,7 | no sponges |
| 31 | 3 | | | 4 | | | 34 | | | 19 | | | | | | | | | 5 x 5 | only sediment |
| 28 | | | | | | | 2 | | 1 | | | | | | | | | | 5 x 5 | no sponges |
| 27_1 | 1 | 1 | | | | | | 4 | | | | | | | | | | | 5 x 5 | |
| 27_2 | 3 | 4 | 1 | | | | 2 | | 1 | 1 | | 1 | | | | | | | 5 x 5 | |
| 26 | 2 | | | | | | 1 | | | | | | | | | | | | 5 x 5 | organisms in the strongly recrystallized/dolomitized areas are not included |
| 26k | 17 | | 1 | | | | 1 | | | 1 | | | | | | | | | 4,6 x 2,7 | no sponges, organisms in the strongly recrystallized areas are not included |
| 25 | 13 | 19 | | 3 | 2 | | | | | 3 | 1 | 2 | | | | | | | 5 x 5 | |
| 24 | | | | | 1 | | | | | | | | | | | | | | 5 x 5 | |
| 23_1 | 18 | 9 | | | | | 6 | 4 | | 2 | 1 | | | | | | | | 5 x 5 | maybe 1 *Rectocornuspira* in a crystal |
| 23_2 | 9 | 10 | | 4 | | | 1 | | | 2 | | | | | | 1 | | | 5 x 5 | organisms in the strongly recrystallized areas are not included |
| 23_2k | 15 | | | 1 | | | | | | 1 | | | | | | | | | 4,6 x 2,7 | |
| 23W | 113 | 40 | | 25 | 4 | 1 | | | 1 | 3 | | 1 | | | | 8 | | | 10 x 15 | organisms in the strongly recrystallized areas are not included |
| 13 | | 1 | | | | | | | | | | | | | | | | | 5 x 5 | |
| 21 | | 2 | | | 2 | | | | | | | | | | | | | | 5 x 5 | |
| 15_1 | 8 | 4 | | | | | | | | | | | | | | | | | 5 x 5 | |

| Sample | Ostracods | | | Gastropods | | | Bivalves | | | *Earlandia* | | | *Rectocornuspira* | | | Ammonites | | | Size | Notes |
|---|---|---|---|---|---|---|---|---|---|---|---|---|---|---|---|---|---|---|---|---|
| | sed. | sp. | cr. | sed. | sp. | cr. | sed. | sp. | cr. | sed. | sp. | cr. | sed. | sp. | cr. | sed. | sp. | cr. | [cm] | |
| 15_1k | | 2 | 1 | | | | | | | | | | | | | | | | 4,6 x 2,7 | |
| 15_2 | 10 | 12 | | | | | | | | | | | | | | | | | 5 x 5 | |
| 15W | 59 | 52 | | | | | | | | | | | | | | | | | 10 x 15 | |
| 14 | 12 | 7 | | | | | | | | | | | | | | | | | 5 x 5 | |
| 19W | 322 | 272 | 15 | 2 | 3 | | | | 1 | 2 | 2 | | | | | | | | 10 x 15 | organisms in the strongly recrystallized areas are not included |
| 20W | 51 | 18 | | | | | | | | 66 | 31 | 4 | 1 | | | | | | 10 x 15 | |
| 11 | 10 | 26 | 1 | | | | | | | 3 | | | | | | | | | 5 x 5 | |
| 11k | | 23 | | | | | | | | | | | | | | | | | 4,6 x 2,7 | |
| 18 | 10 | | | 1 | | | | | | | | | | | | | | | 5 x 5 | |
| 17_1 | | 9 | | | | | | | | 2 | 10 | | | | | | | | 5 x 5 | |
| 17_2 | 2 | 7 | | | | | | | | 5 | 11 | 2 | | | | | | | 5 x 5 | |
| 17_2k | 4 | 6 | | | | | | | | 1 | 1 | | | | | | | | 4,6 x 2,7 | |
| 17W | 22 | 41 | | | | | | | | 48 | 116 | 7 | | | | | | | 10 x 15 | |
| 16a_1 | | 1 | | | | | | | | 14 | 30 | 13 | | | | | | | 5 x 5 | |
| 16a_2 | 1 | 1 | | | | | | | | 4 | 5 | 1 | | | | | | | 5 x 5 | |
| 16aW | 5 | 16 | | | | 1 | | | | 12 | 85 | 12 | | 1 | | | | | 10 x 15 | |
| 16b | | | | | | | | | | 5 | 20 | 3 | | 1 | | | | | 5 x 5 | |
| 10 | 3 | | | | | | | | | | | | | | | | | | 5 x 5 | |
| 84W | 1560 | | | 264 | | | 37 | | | | | | | | | 5 | | | 10 x 15 | |
| 86 | | 3 | | | 2 | | | 5 | | | | | | 1 | | | | | 5 x 5 | small thrombolite-boulder |
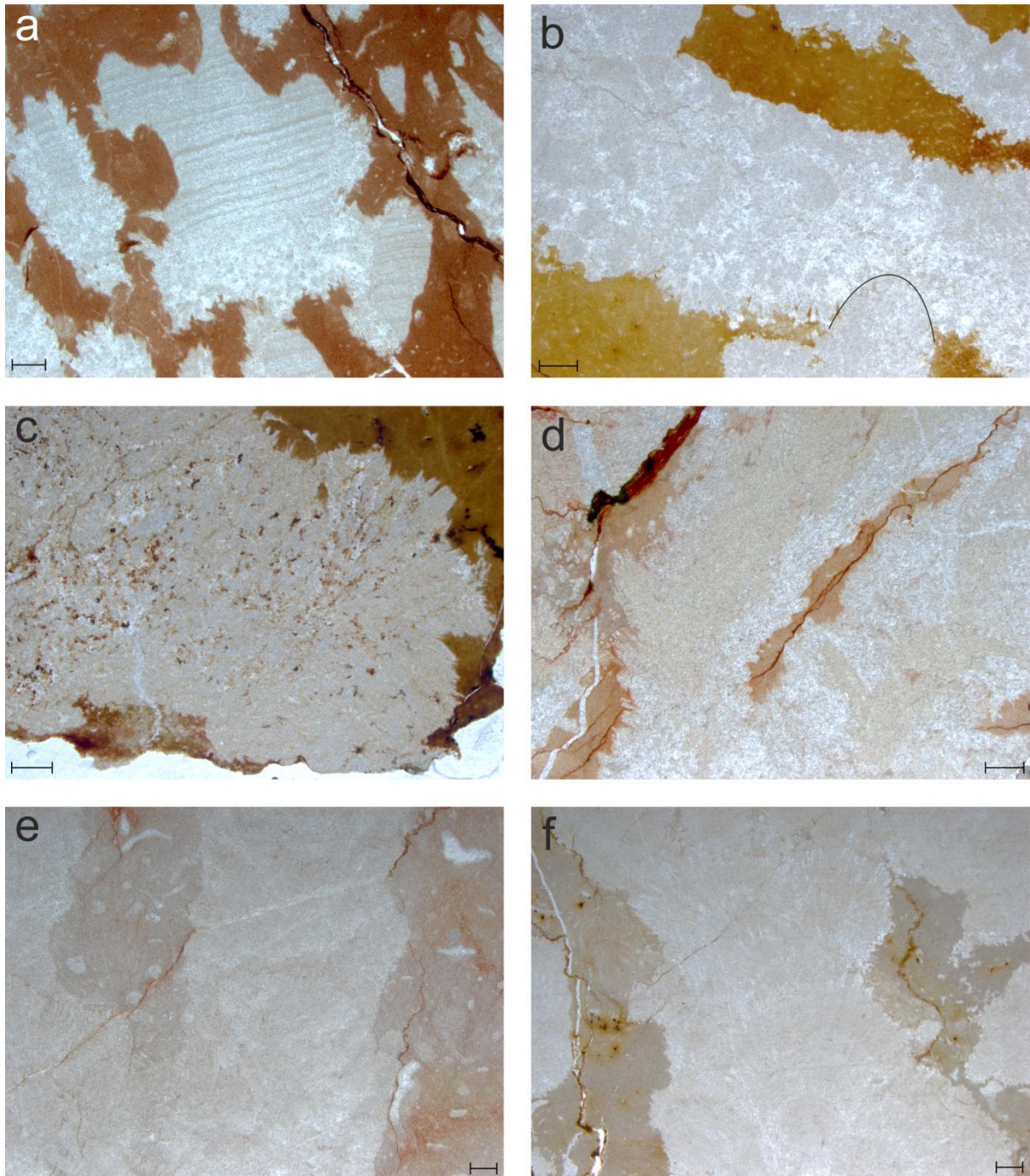
**Fig. 18:** The different types of crystals. For explanation see text. **(a)** Crystals type 1. The lamination can be followed between neighbouring crystals. Sample 15. **(b)** Crystal type 3. The lower crystal extends into the upper one. Sample 24. **(c)** Crystal type 4. Sample 26. **(d)** Crystal type 5. Sample 30. **(e)** Crystal type 6. Sample 55. **(f)** Crystal type 7. Sample 63. Scale bar = 1 mm.

and sediment happened several times (Fig. 20c). Partly strongly recrystallized accumulations of organisms also occur in sample 23. This sample is from the top of the CCF mound but in contrast to sample 19 it does not show the same succession as described above.

Richoz et al. (2010) report about borings on the surface of a calcite crystal from an equivalent facies in the Zal section (northwestern Iran) but none of the crystals from Zangakatun, neither from type 1 nor from type 2, shows any evidence of boring.
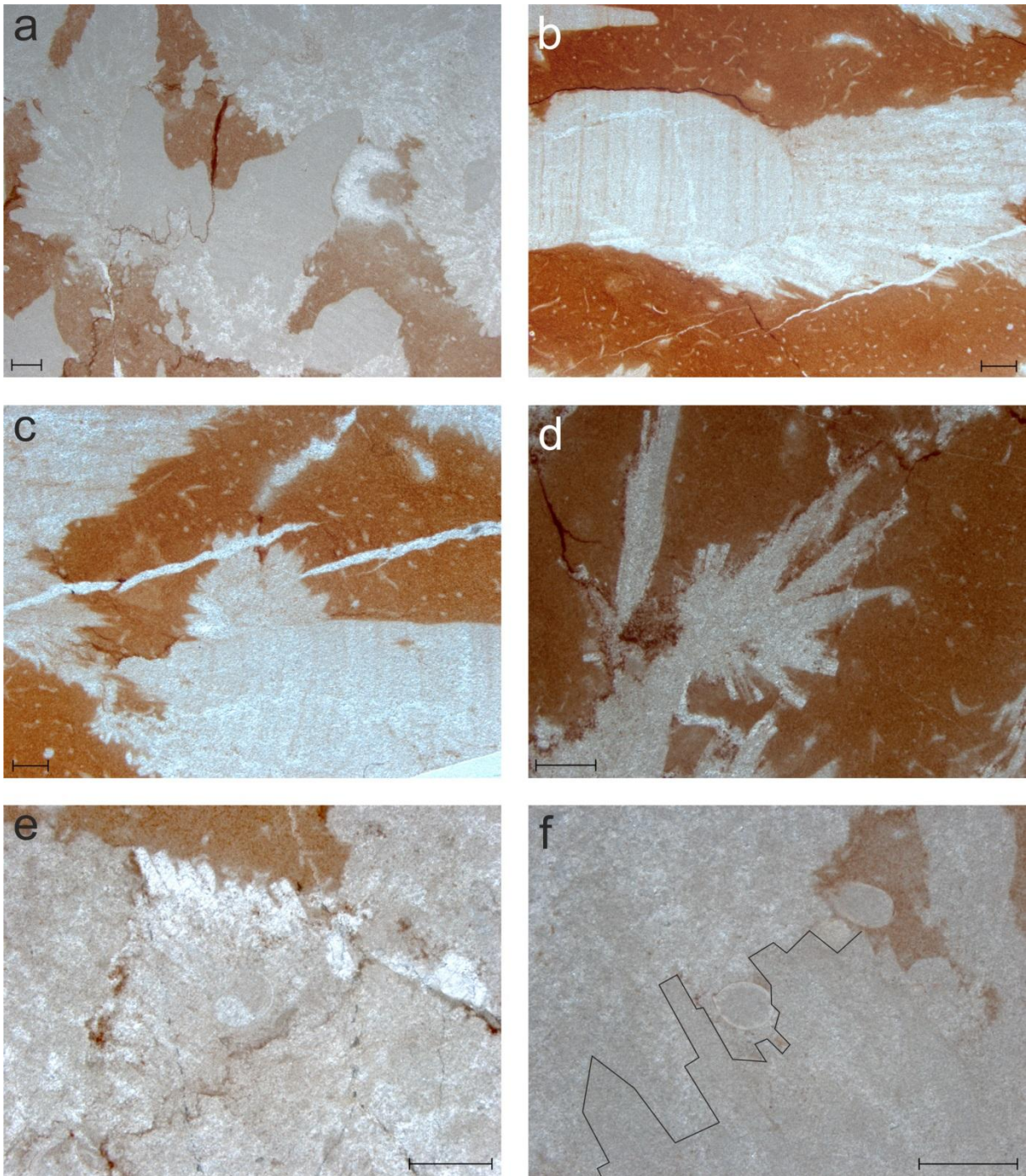
**Fig. 19:** Images from CCFs. **(a)** Crystals of crystal type 1 that initiated with a clotted fabric and changed into the laminated form. On the side crystals of type 2 started to grow. On top of the previous crystals the new ones started to grow again with the clotted fabric. Sample 19. **(b)** Type 2 crystals that grew on the laminated crystals of type 1. All crystals are completely surrounded by sponges of type 1. Sample 11. **(c)** Botryoidal crystals of type 2 growing on the side of a laminated type 1 crystal. All crystals are completely surrounded by sponges. Sample 11. **(d)** Branching calcite crystals with flattened terminations indicating that these crystals were originally precipitated as aragonite. Sample 15. **(e)** Gastropod enclosed in a crystal. Sample 16. **(f)** Ostracod enclosed between two crystals. The black line marks the border between the two crystals. Sample 19. Scale bar = 1 mm.
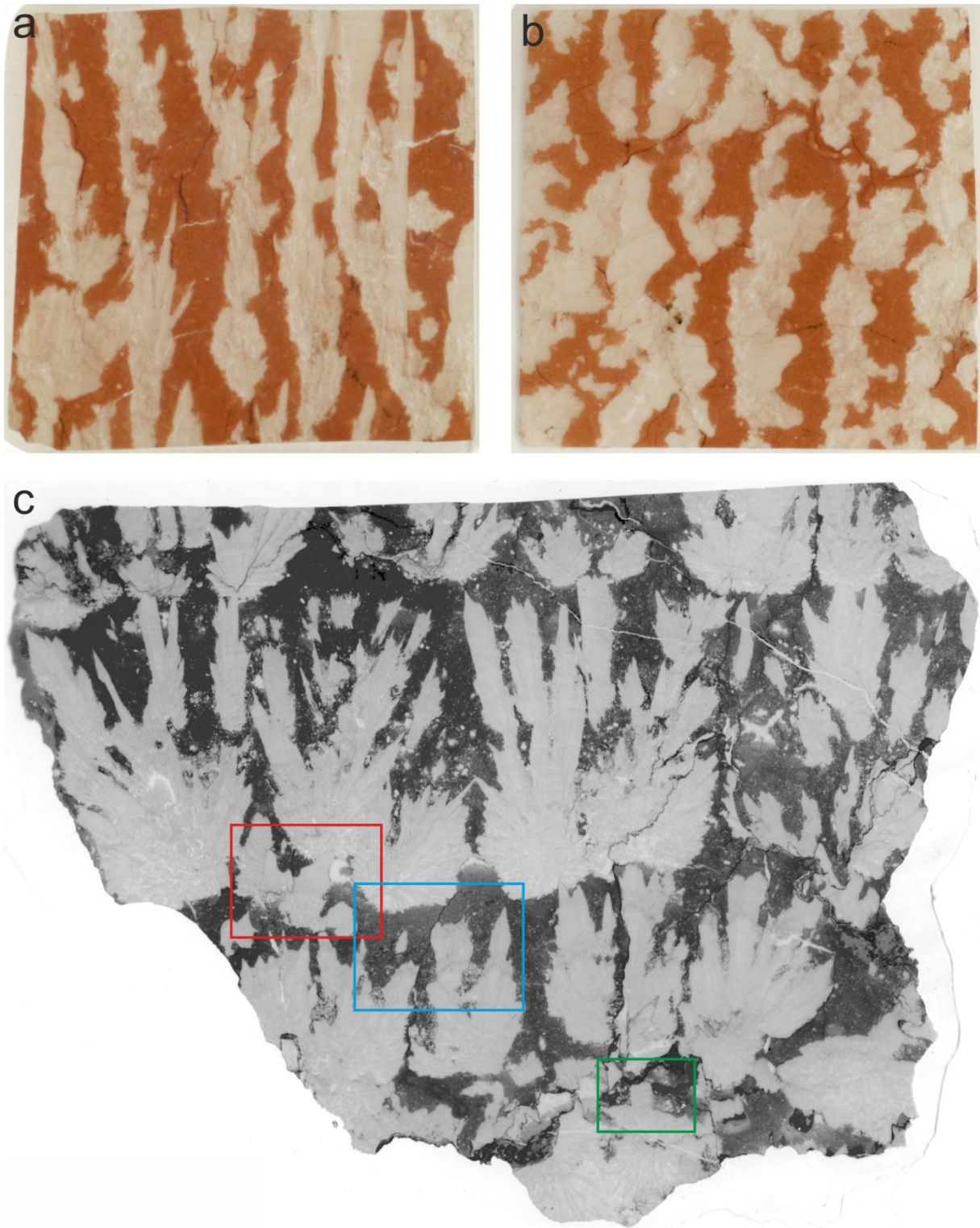
**Fig. 20:** Scans of thin sections. **(a)** Scan from sample 17 showing that the crystals are not fan-like arranged but stand straight next to each other. 3,5 x 3,5 cm. **(b)** Cut perpendicular to the growth direction from sample 17 showing the crystals „wall-like" arrangement. 3,5 x 3,5 cm. **(c)** Scan from sample 19 showing groups of branching crystals next to each other. Between the crystals are accumulations of organisms and sponges. After a small area of only sediment the next crystals started to grow on the sediment or on top of the previous crystals. Rectangles indicate the positions of Fig. 19a (red), Fig. 21a (blue) and Fig. 21b (green). 11 x 9 cm.
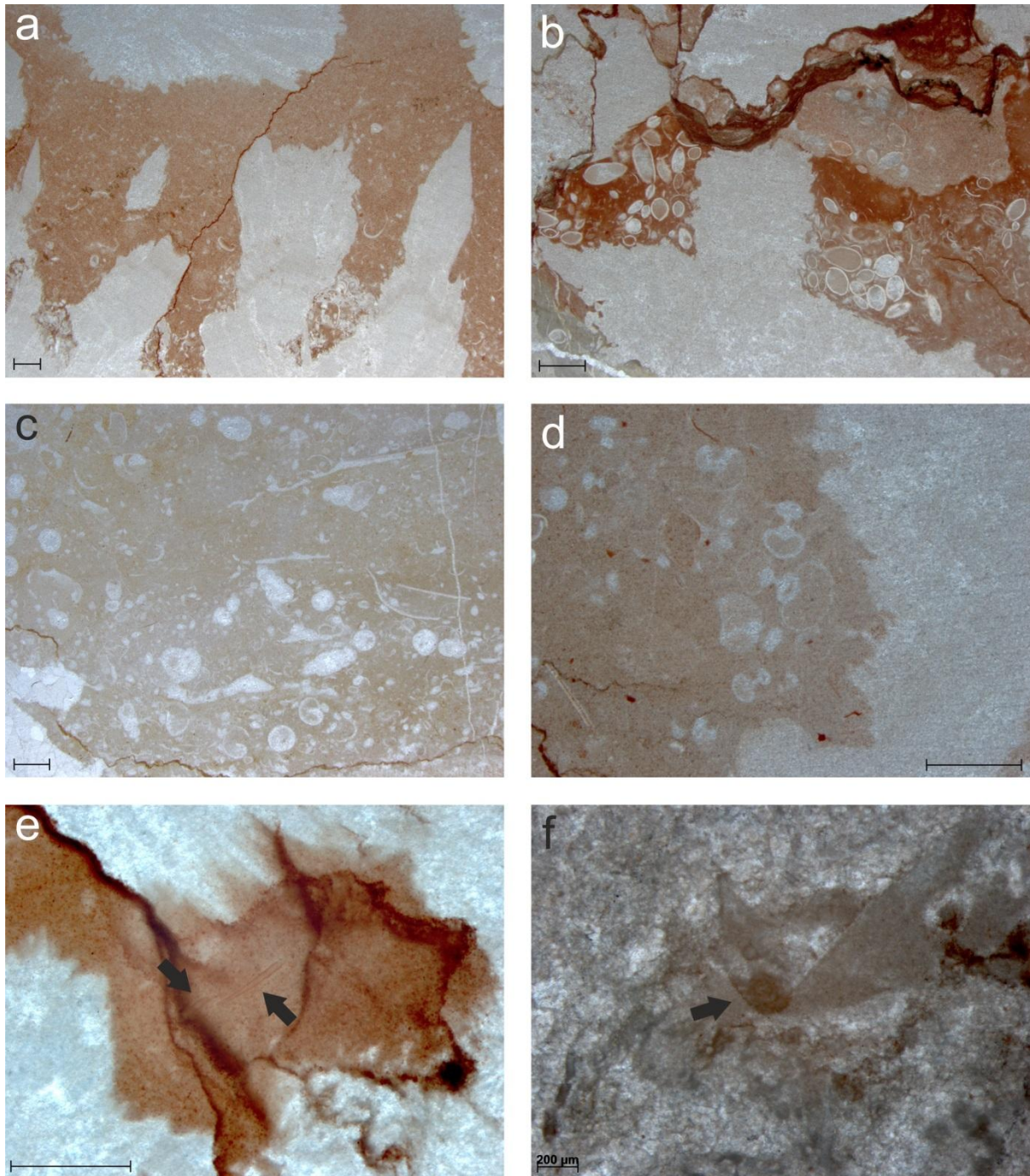
**Fig. 21:** Thin section photographs showing organisms from Zangakatun. **(a)** Accumulations of organisms trapped between crystals. Above these accumulations sponges occur, followed by sediment that is in turn followed by crystals. Sample 19. **(b)** Accumulations of ostracods. Sample 19. **(c)** Bioclastic packstone mostly containing gastropods and bivalves. Sample 84. **(d)** Ammonoids. Sample 23. **(e)** *Earlandia* (arrows). Sample 16. **(f)** *Rectocornuspira* (arrow) trapped in a crystal. Sample 16. Scale bar is 1 mm for (a)-(e) and 200 μm for (f).

### *The Microbialites*

In this work I am using the term "microbialite" with its definition at the mesostructural scale (Shapiro 2000; see also chapter 4). Except the mounds build from CCFs described above, most of the mounds have a clotted mesostructure and are thus described as thrombolites, some others are dendrolites. Stromatolites were not observed. Most of the mounds consist of rather diffuse shaped crystals, which are on the mesostructural level giving a clotted or dendrolititc impression. In Zangakatun only sample 58 shows a microstructure (Fig. 22b) that is approaching, but not completely typical, a thrombolitic clotted microstructure. No organisms are enclosed in this thrombolite.

### *The diffuse shaped Crystals*

In this outcrop numerous crystals were found that neither look like typical microbialites nor have the same appearance as the crystals from type 1 or 2.

Crystals of type 3 occur in sample 16 and 24. They exhibit a mottled structure similar to the initial phase of crystals from type 1 but in contrast to them they are not giving rise to elongated nor fan-like crystals. Their shape is very variable. On closer inspection it seems that a thinner and longer crystal extends into a shorter and broader crystal (Fig. 18b).

The shape of type 4 crystals is similar to the one from type 1 and 2 but they are very fine crystalline, grey and sometimes yellowish (Fig. 18c). The boundaries between neighbouring crystals are often difficult or impossible to recognize.

The central part of crystal type 5 (sample 30) is as finely crystallized and yellowish as crystal type 4 but in contrast to their central part their outside is coarser crystalline and not yellow (Fig. 18d).

Crystals of type 6 are mostly relatively broad, elongated and sometimes branching but also more or less rotund crystals occur. They are characterized by a fine crystalline, diffuse and sort of "cloudy" appearance (Fig. 18e). Crystals from type 7 are also broad, elongated and sometimes branching. They look like botryoidal cements that were growing on each other, resulting in a "bushy" appearance (Fig. 18f). Both type 6 and 7 occur in the upper half of the outcrop as well as in the huge microbialite.

The last crystal type (Fig. 22a) occurs in the thrombolitic hill 22.5 m above the base of the investigated section. In these crystals are fine crystalline as well as coarser crystalline areas. The fine crystalline areas look grey whereas the coarser crystalline areas are translucent. As a result the crystals show a grey and white pattern. These crystals from type 8 look similar to the ones from type 3 but in contrast to them they show a stronger vertical growth and not a wide lateral expansion. Their shape is similar to the one from crystal type 6 and 7.

As well as the crystals from the CCFs these crystals are embedded in a red or grey, homogenous bioclastic wackestone or, much less common, bioclastic packstone. The components are usually ostracods, gastropods and bivalves. The last two are more frequent in the surrounding sediment of the microbialites compared to the matrix of the CCFs. In contrast to the CCFs sponges and *Earlandia* are much less common and *Earlandia* is entirely absent in the upper half of the outcrop. *Rectocornuspira* and ammonoids are still very rare. Some of the organisms are enclosed within the diffuse shaped crystals or lie on their margins and border them (Fig. 23a). The fauna associated with the diffuse shaped crystals is not as diverse as the fauna associated with the CCFs but it is still more diverse than the fauna associated with the bioclastic wackestone. Also the number of organisms is not as high as within the CCFs but it is still higher than the number of organisms within the bioclastic wackestone (Fig. 17 and Table 2).
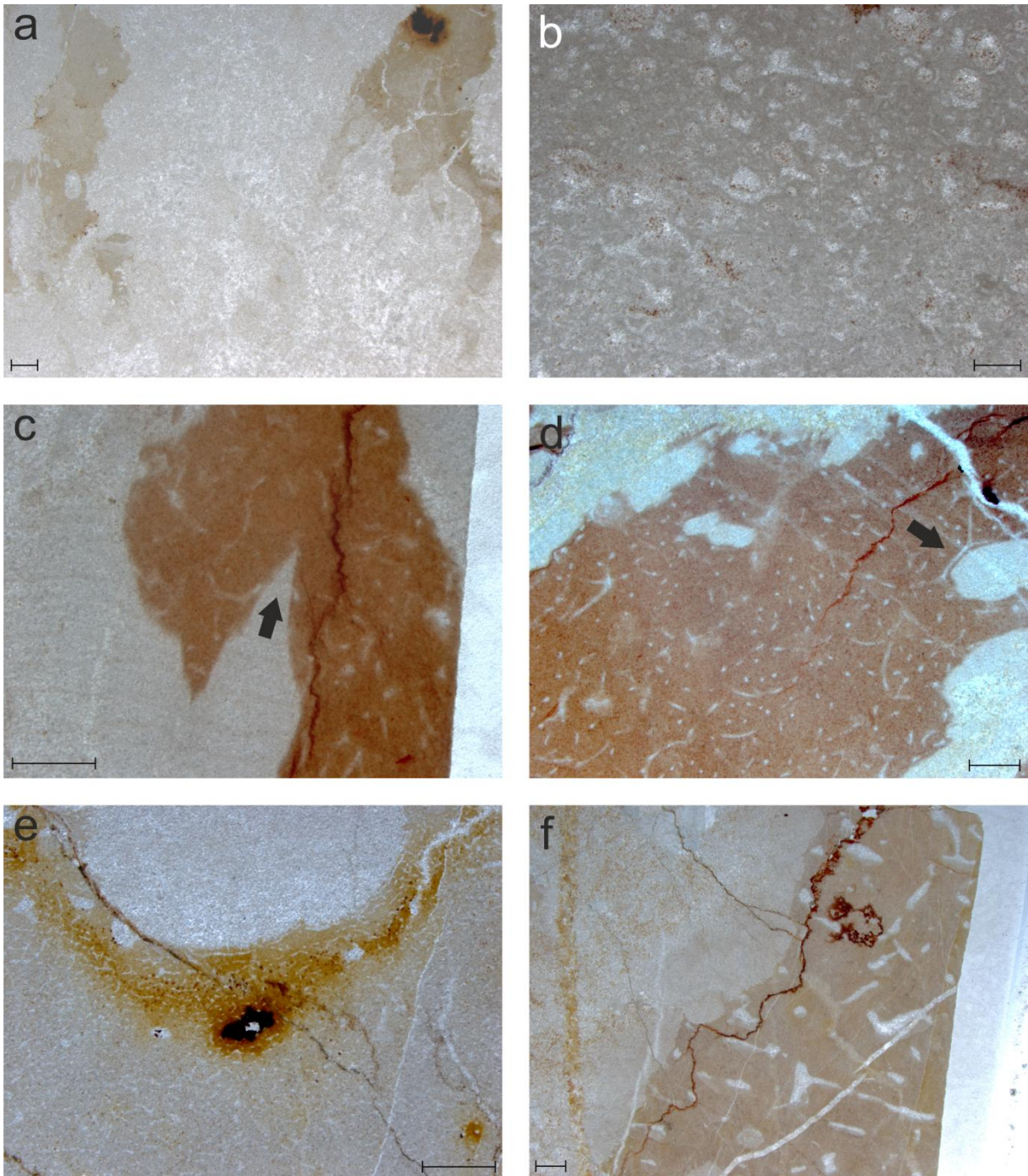
**Fig. 22:** Crystals and sponges. **(a)** Crystal type 8. Sample 66. **(b)** Picture from the microbialite from sample 58. It does not show a microstructure that is typical for microbialites but it looks similar to such a microstructure. **(c)** Sponge spicule pierced by a crystal (arrow). Sample 21. **(d)** Sponge type 1. A sponge spicule fits perfectly to the crystal's margin (arrow). Sample 16. **(e)** Sponge type 3. The spicules arranged in layers fit perfectly to the crystal's margin. Sample 81. **(f)** Sponge type 4 with big and broad spicules. Sample 82. Scale bar = 1 mm.
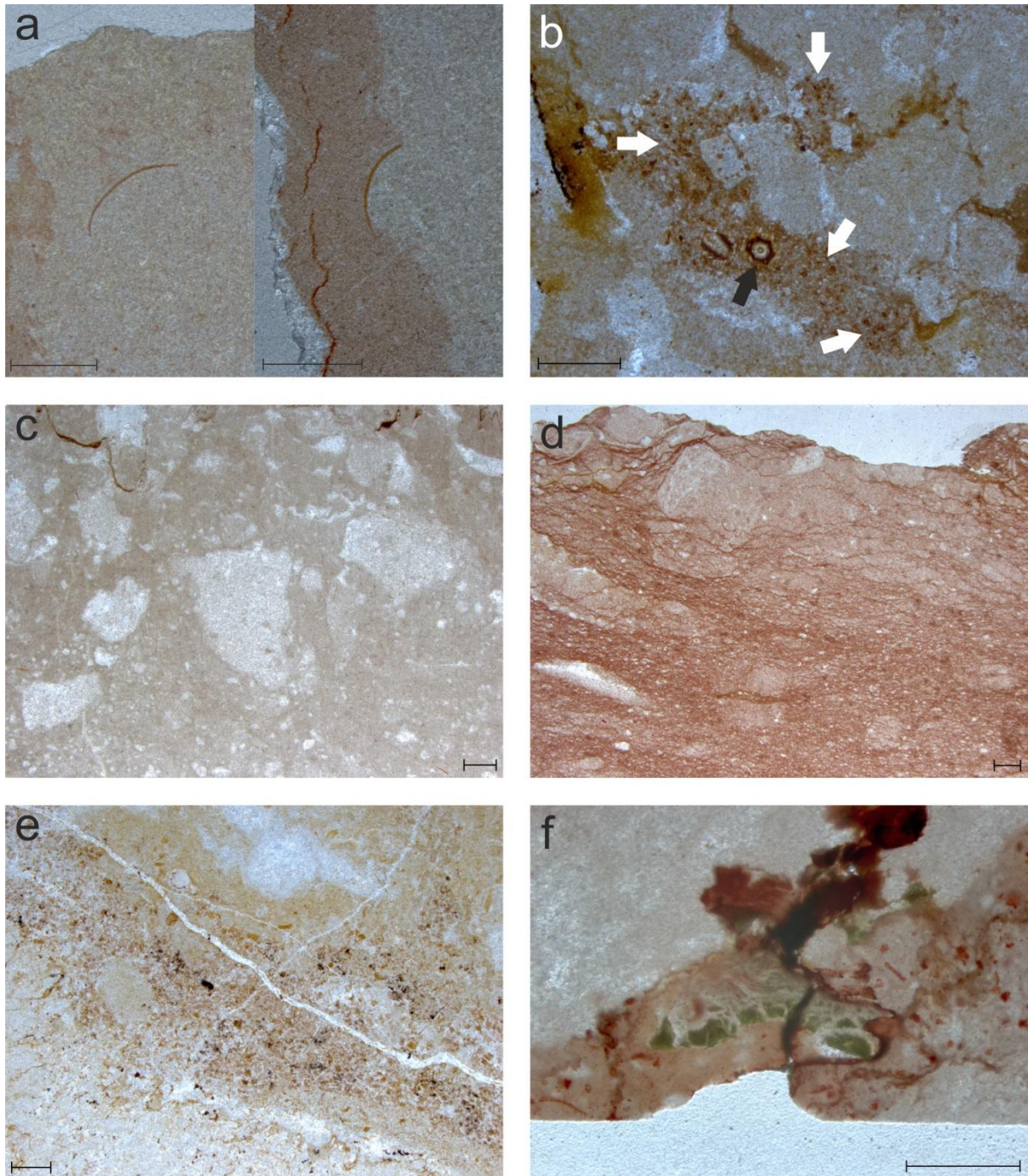
**Fig. 23:** Further features from Zangakatun's thin sections. **(a)** left: Bivalve embedded in a crystal; right: Bivalve laying on the crystal's margin; both pictures are from sample 28. **(b)** Piece of an echinoderm (black arrow) and small dolomite crystals (white arrows). Sample 39. **(c)** Breccia. Sample 35. **(d)** Bioclastic breccia. Sample 45. **(e)** Dolomitization front. Sample 26. **(f)** Glauconite. Sample 23. Scale bar = 1 mm.

### *Sponges*

Sponges occur almost entirely together with CCFs and microbialites. Only in sample 50 sponge spicules occur without CCFs or microbialites but it cannot be said for sure whether these sponge spicules represent an accumulation of sponge spicules or an in situ sponge. In sample 19 the sponges occur above the accumulations of organisms between the crystals but without contact to the crystals (Fig. 20c and Fig 21a). The silicious skeletons were dissolved and replaced by calcite, so that the spicules are now preserved as calcite pseudomorphs embedded in a micritic matrix. It can be observed very often that the sponge spicules fit perfectly to the margins of the neighbouring crystals (Fig. 22d and e). In a few cases sponge spicules were enclosed or pierced by crystals (Fig. 22c). Ostracods are very common within the sponges as well as *Earlandia*. Gastropods are much less frequent.

On the basis of different spicule morphologies four sponge types can be distinguished. The spicules of sponge type 1 (Fig. 22d) strongly vary in size and shape and irregular forms predominate. A preferred orientation of the spicules cannot be seen. This sponge type is restricted to the lower CCFs and diffuse shaped crystals and becomes less common on top of each thrombolitic hill and mound. The shape of spicules from sponge type 2 is very similar to the one of type 1 but the spicules are smaller and denser. Because of the similarity to sponge type 1 I am not sure if it is really an own type or just a variation of type 1. Sponge type 3 is characterized by very small and dense spicules that sometimes seem to be arranged in layers (Fig. 22e). This type occurs in the upper half of the outcrop. Sponge type 4 only occurs in one sample from the bedded part of the huge thrombolite. The spicules are relatively thick compared to the spicules of the other sponge types (Fig. 22f).

### *The bioclastic Wackestone*

The non-microbial red and grey limestone that is rather common in the second quarter of the outcrop is classified as a bioclastic wackestone. The most common bioclasts are bivalves but also *Earlandia* and gastropods occur more frequently compared to the matrix surrounding CCFs and microbialites. Ostracods and ammonoids are very rare. In sample 39 a piece of an echinoderm was found (Fig. 23b). Sample number 61b contains a high number of calcispheres and in sample number 68 fragments of sponges were found.

Sample number 35 can be denoted as a breccia. The components of this breccia are mainly broken pieces of crystals (Fig. 23c).

Sample number 45 contains red sediment with brighter spots (Fig. 23d). It is quite difficult to recognize what these spots actually are. Most of them are elongated or elliptical in shape but the others are more irregular. None of these spots contains any organisms. Their edges are rounded and their margins are relatively sharp. Because of these sharp margins they are probably not traces of bioturbation but rather broken bioclasts (Reuter M., personal communication). In this case this sample can be denoted as a bioclastic breccia.

### *Other Observations*

Stylolites are very common and occur in nearly all thin sections. Interestingly, in thin sections with CCFs or the diffuse shaped crystals the stylolites very often proceed along the crystal margins but

they very rarely pass through the crystals. They do not only show the typically brown colour but are sometimes greenish-grey.

Pyrite and oxides also occur in almost all thin sections. Their amount is very variable as well as their size but very small pyrite and oxides are much more frequent than big ones. They occur in clusters or as single crystals in the sediment, in the crystals from type 1 and 2 from the CCFs as well as in the diffuse shaped crystals. Also in stylolites they are common. They rarely occur in fissures or within shell remnants (e.g. bivalve shells) or surround bioclastic components. In one diffuse shaped crystal from sample number 23 it looks like many pyrite crystals and oxides surround the central part of the crystal.

Dolomite is very rare. Small dolomite rhombohedrons can only be observed in six thin sections and only two of them show a partial dolomitization with a diffuse dolomitization front (Fig. 23e).

Only a few crystals of glauconite were found in sample number 23 (Fig. 23f).

### 5.1.2. Vedi

The sample positions as well as the distribution of the crystals and the organisms are illustrated in Fig. 12 and Fig. 24. The numbers of organisms found in each thin section are shown in Table 3.

### *Comparison to Zangakatun*

In Vedi only samples from the CCFs and the microbialites 6.5 m and 7.5 m above the base of the investigated section were microfacially analysed. A comparison with the thin sections from Zangakatun reveals a range of differences.

The first difference is that in Vedi only crystals from the types 1, 2, 6 and 8 occur. Sponges from type 1 are the only ones found in the investigated thin sections and they are restricted to the CCFs. The sediment is always grey and not reddish. It contains ostracods, gastropods and bivalves but no ammonoids or *Earlandia*. In contrast to Zangakatun, the fauna associated with Vedi's CCFs is the less diverse and numerous one and the fauna associated with the diffuse shaped crystals is the most diverse one and more numerous than in the CCFs. Another difference to Zangakatun is that the bioclastic wackestone contains most organisms (Fig. 24 and Table 3). Although in Zangakatun the crystals contain a rather high number of enclosed organisms in Vedi only one *Rectocornuspira* was found inside a crystal. This *Rectocornuspira* was the only foraminifer found in all thin sections. Another difference is that calcispheres are more common than in Zangakatun. However, neither breccias nor glauconite were found in Vedi.

The already mentioned borings on the surfaces of CCFs from Iran described by Richoz et al. (2010) could not be found in Vedi too.

### *The Calcium Carbonate Crystal Fans*

In the CCFs from Vedi crystals from type 1 and 2 occur. The lamination of the type 1 crystals is well visible and can be followed in neighbouring crystals. The crystals of type 2 started to grow on the sides and on top of the crystals from type 1 and show very often flattened termination, which is an indication of their aragonitic origin. Only few crystals of type 1 are mottled at their base.

Results
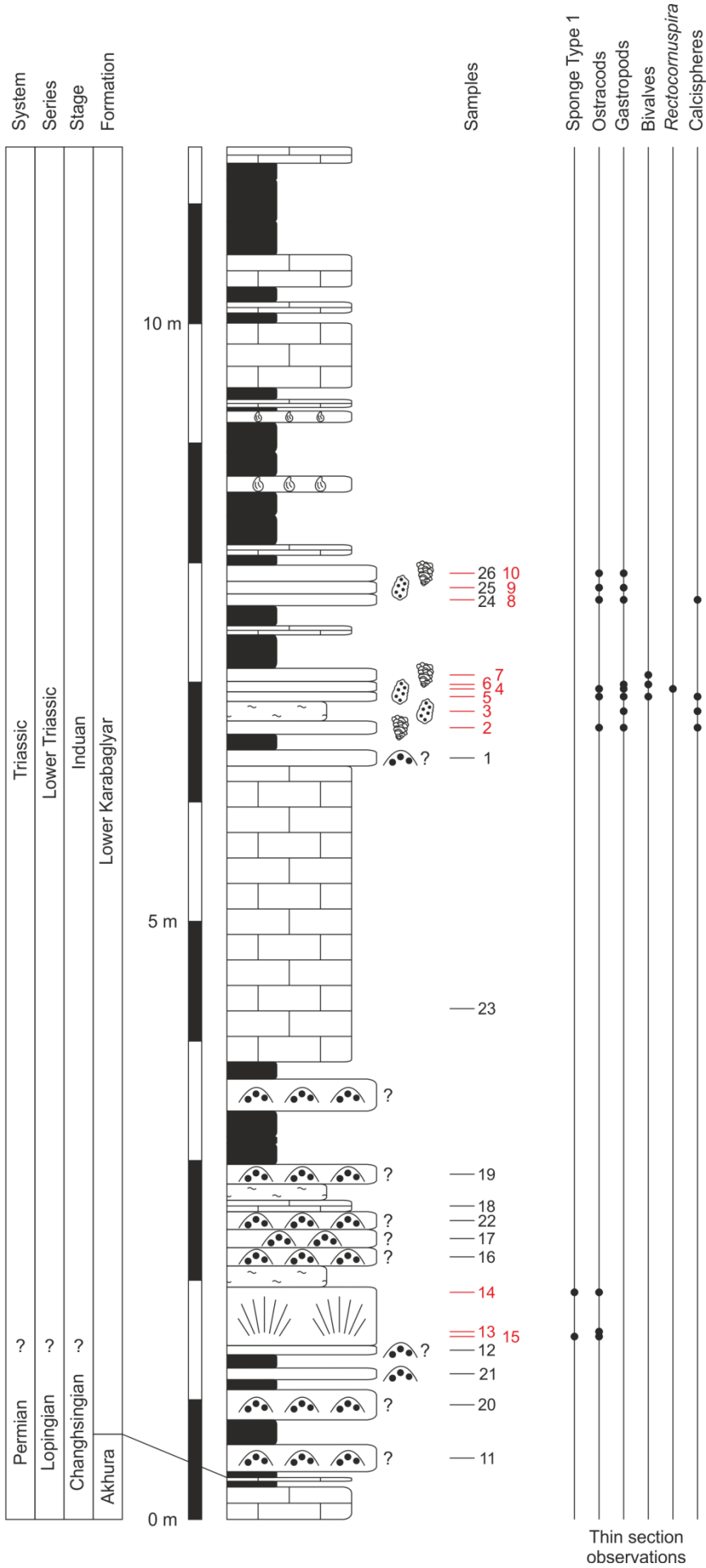


**Fig. 24:** Fossil distribution from Vedi. For legend see Fig. 12.

41

**Table 3:** The fossil distribution in the thin sections from Vedi. The table shows how many of the organisms are in the sediment (sed.), the sponges (sp.) or the crystals (cr.). It also shows whether the samples were taken from CCFs (dark grey background), microbialites (light grey background) or the bioclastic wackestone without CCFs or microbialites (white background). For explanation see text.

| Sample | Ostracods | | | Gastropods | | | Bivalves | | | *Rectocornuspira* | | | Size | Notes |
|---|---|---|---|---|---|---|---|---|---|---|---|---|---|---|
| | sed. | sp. | cr. | sed. | sp. | cr. | sed. | sp. | cr. | sed. | sp. | cr. | [cm] | |
| 2 | 13 | | | 9 | | | | | | | | | 5 x 5 | no sponges |
| 3 | | | | 4 | | | | | | | | | 5 x 5 | no sponges |
| 4 | 6 | | | 1 | | | | | | | | 1 | 5 x 5 | no sponges |
| 5 | 2 | | | 7 | | | 8 | | | | | | 5 x 5 | only sediment |
| 6 | | | | 2 | | | 7 | | | | | | 5 x 5 | no sponges |
| 7 | | | | | | | 2 | | | | | | 5 x 5 | no sponges |
| 8 | 40 | | | 101 | | | | | | | | | 5 x 5 | only sediment |
| 9 | 8 | | | 5 | | | | | | | | | 5 x 5 | no sponges |
| 10 | 4 | | | 5 | | | | | | | | | 5 x 5 | no sponges |
| 13a | 1 | | | | | | | | | | | | 5 x 5 | maybe sponges |
| 13b | 2 | | | | | | | | | | | | 5 x 5 | maybe sponges |
| 14 | | 4 | | | | | | | | | | | 5 x 5 | |
| 15 | 2 | 2 | | | | | | | | | | | 5 x 5 | |
| 27a | 6 | | | 2 | | | 1 | | | | | | 5 x 5 | no sponges |
| 27b | | | 1 | | | | | | | | | | 5 x 5 | no sponges |

In sample 13b occurs a crystal from type 1 that has an unusual appearance. The lower part of this crystal is not parallel to the other laminated crystals and is mottled at its base. However, the upper part of this crystal is parallel to the other ones (Fig. 25a).

Sample 15 shows the transition between two CCFs. The different growing directions of the crystals from the two CCFs can be seen well (Fig. 26). The crystals at the boundary of the two CCFs stopped growing before touching each other. Two neighbouring crystals in the lower part of this thin section are an exception from that. These two crystals are not parallel to each other and seem to coalesce at their tops where crystals from type 2 grew afterwards. The laminations of these two crystals are different and cannot be correlated to each other. Furthermore the laminations tilt in different directions (Fig. 25b). Moreover this thin section contains crystals of type 1 that do not show the typical termination for this kind of crystals. These crystals seem to diverge at their tops (Fig. 25c).

The crystals are embedded in a homogenous grey micritic matrix that only contains few ostracods. Sponges occur partly between the crystals, meaning that there are many places without any sponge spicules. As in Zangakatun the sponge spicules partly surround the crystals (Fig. 25c) but none of the spicules was pierced by a crystal.

### *The Microbialites*

Only one sample with a microstructure that resembles the microstructure from thrombolites was found around 20 m above the base of the profile. Its structure is similar to the one in sample 58 from Zangakatun (Fig. 25d). It contains one ostracod.
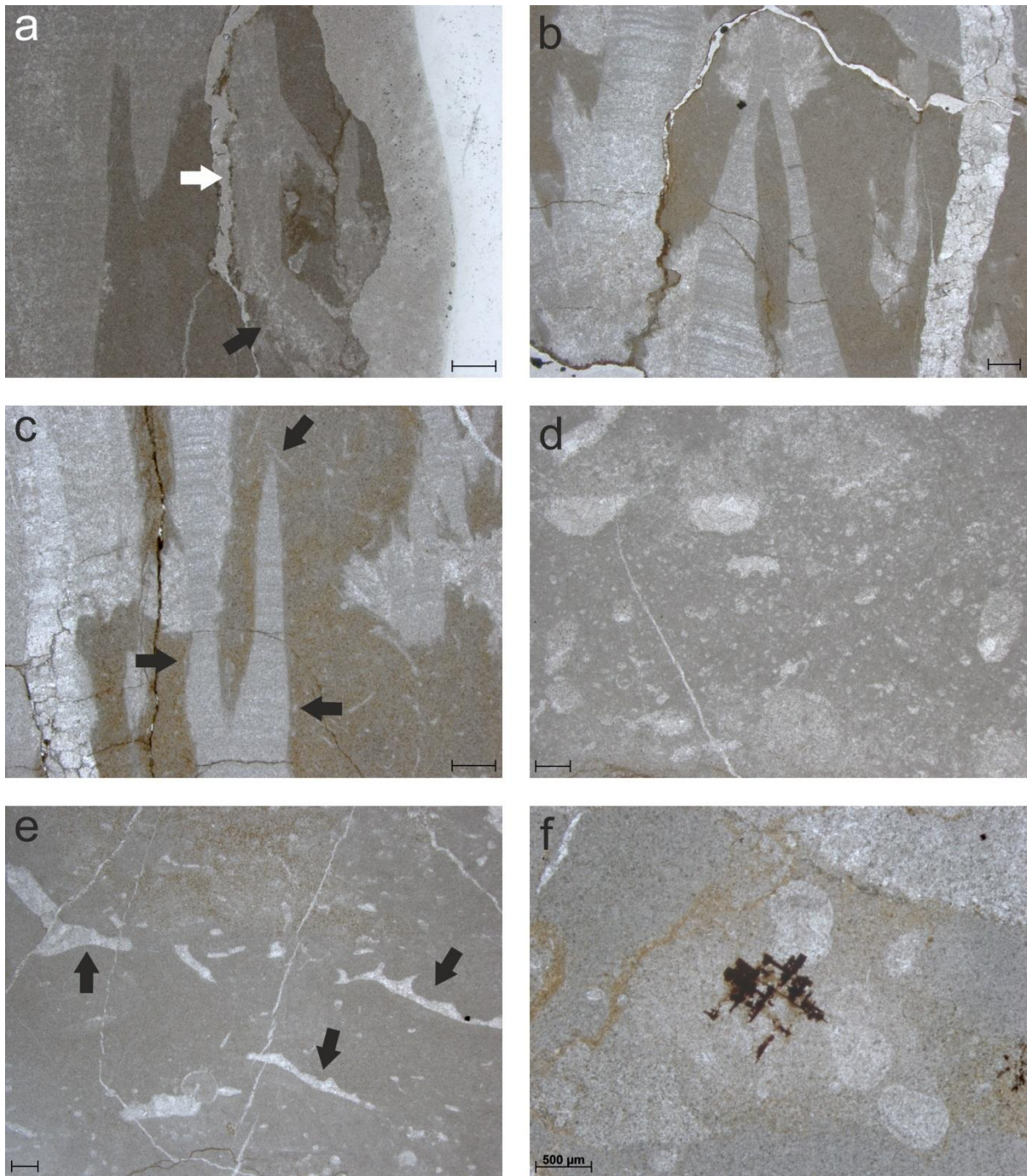
**Fig. 25:** Thin section photographs from Vedi. **(a)** Unusual crystal from a CCF. The lower part of this crystal, which shows a mottled structure at its base, is not parallel to the other laminated crystals (black arrow) but the upper part of this crystal is parallel to the other ones (white arrow). Sample 13b. **(b)** Two crystals from sample 15 that seem to coalesce at their tops. Sample 15. **(c)** Diverging crystal from sample 15. The black arrows mark sponge spicules that fit perfectly to the crystal's margin. **(d)** Microbialite. Sample 27b. **(e)** Sediment next to the thrombolytic hill from Fig. 13b. The black arrows mark the stromatactis structures. The brownish colour on top of the picture is caused by small dolomite rhombohedrons. Sample 5. **(f)** Lattice-like pyrite from the top of the unusual thrombolite shown in Fig. 13c. Sample 10. Scale bar is 1 mm for (a)-(e) and 500 μm for (f).
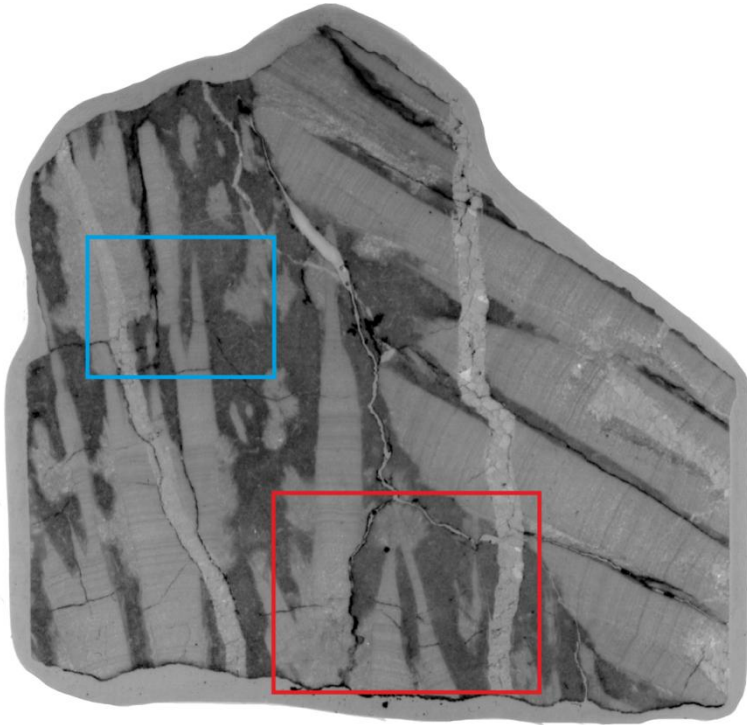
**Fig. 26:** Scan of a thin section showing the transition between two CCFs. Rectangles indicate the positions of Fig. 25b (red) Fig. 25c (blue). Sample 15. 4.5 x 4 cm.

## *The diffuse shaped Crystals*

The diffuse shaped crystals, only from type 6 and 8, were found in the microbialites shown in Fig. 13b and c.

The diffuse shaped crystals from the thrombolitic hill shown in Fig. 13b belong to crystal type 8. This thrombolitic hill (sample 4) is microscopically very similar to the underlying limestone layers (sample 2 and 3). The underlying layers contain diffuse shaped crystals both from type 6 and 8. The crystals from the thrombolitic hill as well as from the underlying layers are embedded in a grey bioclastic packstone and wackestone, which contains mainly gastropods and ostracods but also bivalves. One *Rectocornuspira* is embedded in a crystal from this thrombolitic hill. The sediment contains several sites where dolomite occurs more occasionally. Dolomite was also found in crystals from the thrombolitic hill. Only the sample from the sediment laterally next to the thrombolitic hill (sample 5) differs clearly from the others. It is a bioclastic packstone that probably contains stromatactis structures (Fig. 25e).

The unusual looking thrombolite from Fig. 13c starts at its base (right side, sample 8) with a bioclastic packstone that contains gastropods, ostracods and calcispheres. The middle and the top of this thrombolite (sample 9 and 10) macroscopically differ from each other but they are similar microscopically. They contain crystals of type 6 (sample 10) and 8 (sample 9). The crystals are surrounded by a bioclastic wackestone that contains ostracods and gastropods. The top of this microbialite contains many big pyrite crystals with a meshed or lattice-like appearance (Fig. 25f).

## *Sponges*

Sponges from type 1 are the only ones found in Vedi. As in Zangakatun their originally silicious skeletons are preserved as calcite pseudomorphs. They are restricted to the CCFs but unfortunately

sometimes hard to recognize. They occasionally fit perfectly to the margins of the crystals and partly surround them (Fig. 25c).

### *Other Observations*

Stylolites occur in nearly all thin sections and often pass through the sediment. They rarely proceed along the crystal margins and even less commonly they pass through the crystals. All of them show the typical brown colour.

Pyrite and oxides are very common in the sediment and occur as very small sized spheres. They also often occur in fissures and stylolites but are less common in the crystals. They rarely occur in form of bigger clusters. Only on top of the strange looking thrombolite the pyrites have a meshed appearance (Fig. 25f).

Dolomite is relatively common. Some sites in the sediment are full with small dolomite rhombohedrons. Dolomite also occurs in crystals but only in the ones from the thrombolitic hill shown in Fig. 13b.

### 5.1.3. Ogbin

The sample positions, the distribution of the different types of crystals and the distribution of the organisms are illustrated in Fig. 15 and Fig. 27. The numbers of organisms found in each thin section are shown in Table 4.

### *Comparison to Zangakatun and Vedi*

At this outcrop not only samples of Lower Triassic age but also of Upper Permian age were microscopically characterized. A comparison with the thin sections of Zangakatun and Vedi reveals similarities and some differences.

As in Vedi in Ogbin occur crystals of the types 1, 2, 6 and 8 but also crystals from type 4. Another similarity to Vedi is that also in Ogbin only sponges from type 1 occur. The sediment shows a red, yellow or grey colour and contains ostracods, gastropods, bivalves, ammonoids and *Earlandia*. As in Zangakatun the fauna associated with the CCFs is the most diverse one and also shows the highest number of organisms. The fauna associated with the diffuse shaped crystals is as diverse as the fauna associated with the CCFs. Another similarity to Zangakatun is that the number of organisms within the CCFs is also higher than the number of organisms associated with the diffuse shaped crystals and the bioclastic wackestone (Fig. 27 and Table 4). In contrast to the other two outcrops *Rectocornuspira* and calcispheres do not occur. In contrast to Vedi a few more organisms, mainly ostracods, are enclosed in the crystals but by far not so many as in Zangakatun. As in Vedi the investigated thin sections do neither contain breccias nor glauconite.

As in Zangakatun and Vedi the borings reported from Richoz et al. (2010) were not found in Ogbin either. In contrast to the other two outcrops bioturbated sediments were found (Fig. 28a).
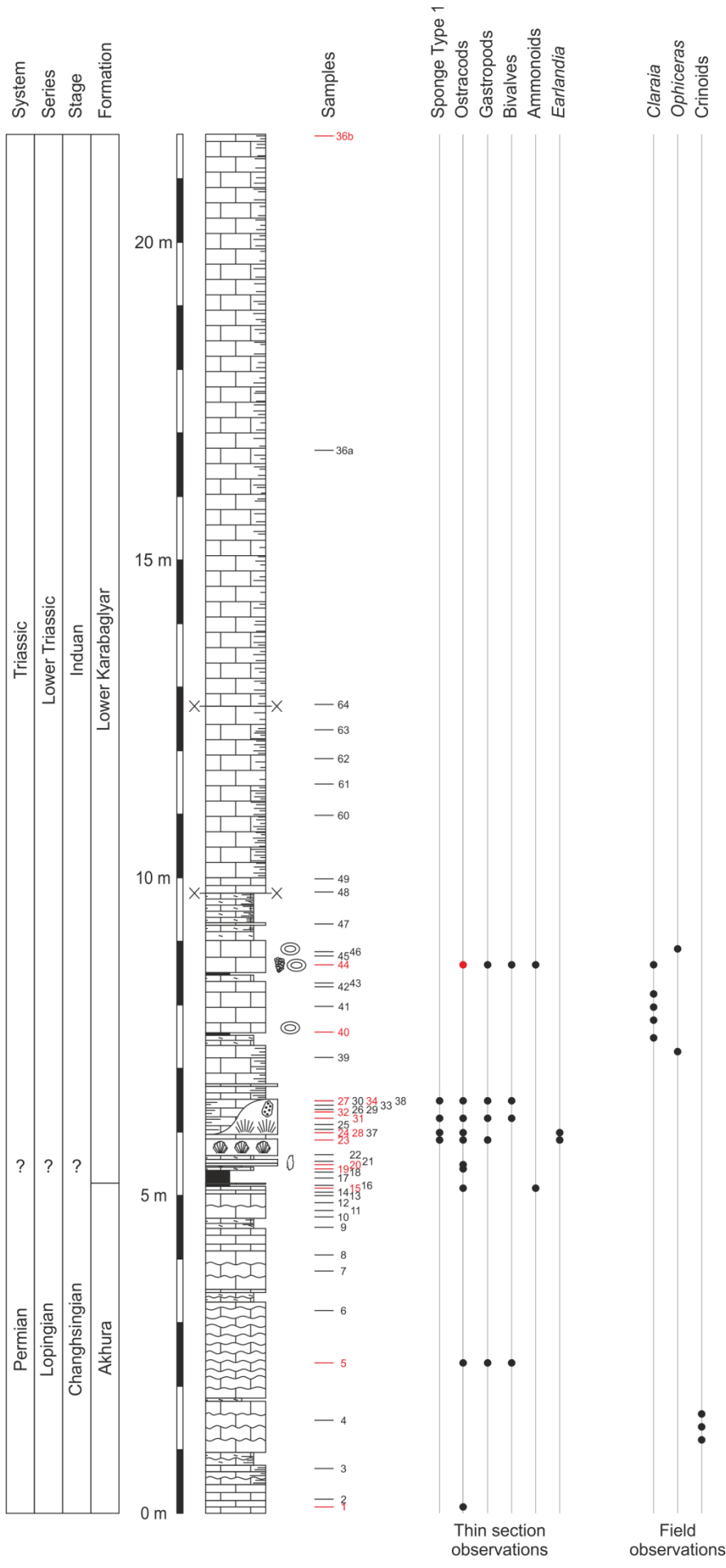
**Fig. 27:** Fossil distribution in Ogbin. The picture shows the fossils observed in thin sections as well as in the field. For the legend see Fig. 15.

**Table 4:** The fossil distribution in the thin sections from Ogbin. The table shows how many of the organisms are in the sediment (sed.), the sponges (sp.) or the crystals (cr.). It also shows whether the samples were taken from CCFs (dark grey background), microbialites (light grey background) or the bioclastic wackestone without CCFs or microbialites (white background). For explanation see text.

| Sample | Ostracods | | | Gastropods | | | Bivalves | | | *Earlandia* | | | *Rectocornuspira* | | | Ammonites | | | Size | Notes |
|---|---|---|---|---|---|---|---|---|---|---|---|---|---|---|---|---|---|---|---|---|
| | sed. | sp. | cr. | sed. | sp. | cr. | sed. | sp. | cr. | sed. | sp. | cr. | sed. | sp. | cr. | sed. | sp. | cr. | [cm] | |
| 36b | | | | | | | | | | | | | | | | | | | 5 x 5 | only sediment |
| 66 | 3 | | | | | | | | | | | | | | | | | | 5 x 5 | only sediment |
| 44 | 126 | | | 12 | | | 17 | | | | | | | | | 2 | | | 5 x 5 | no sponges |
| 40 | | | | | | | | | | | | | | | | | | | 5 x 5 | |
| 34 | 2 | | | | | | | | | | | | | | | | | | 5 x 5 | |
| 27 | | 18 | | | 4 | | | 3 | | | | | | | | | | | 5 x 5 | |
| 31_2 | 14 | | | 3 | | | | | | | | | | | | | | | 5 x 5 | maybe sponges |
| 31_1 | 69 | | 1 | 1 | | | 4 | | 1 | | | | | | | | | | 5 x 5 | |
| 28c_2 | | 2 | | | | | | | | | | | | | | | | | 5 x 5 | |
| 28c_1 | | 1 | | | | | | | | | | | | | | | | | 5 x 5 | |
| 28bW | 9 | 30 | 1 | | | | | | | | | | | | | | | | 10 x 15 | |
| 24 | | 2 | | | | | | | | | | | 1 | | | | | | 5 x 5 | |
| 23 | | 10 | | | 1 | | | | | | 4 | | | | | | | | 5 x 5 | |
| 20 | 66 | | | | | | | | | | | | | | | | | | 5 x 5 | no sponges |
| 19 | 99 | | | | | | | | | | | | | | | | | | 5 x 5 | only sediment |
| 35 | 5 | | | | | | | | | | | | | | | | | | 5 x 5 | no sponges |
| 72 | 3 | 2 | | | | | | 1 | | | | | | | | | | | 5 x 5 | |
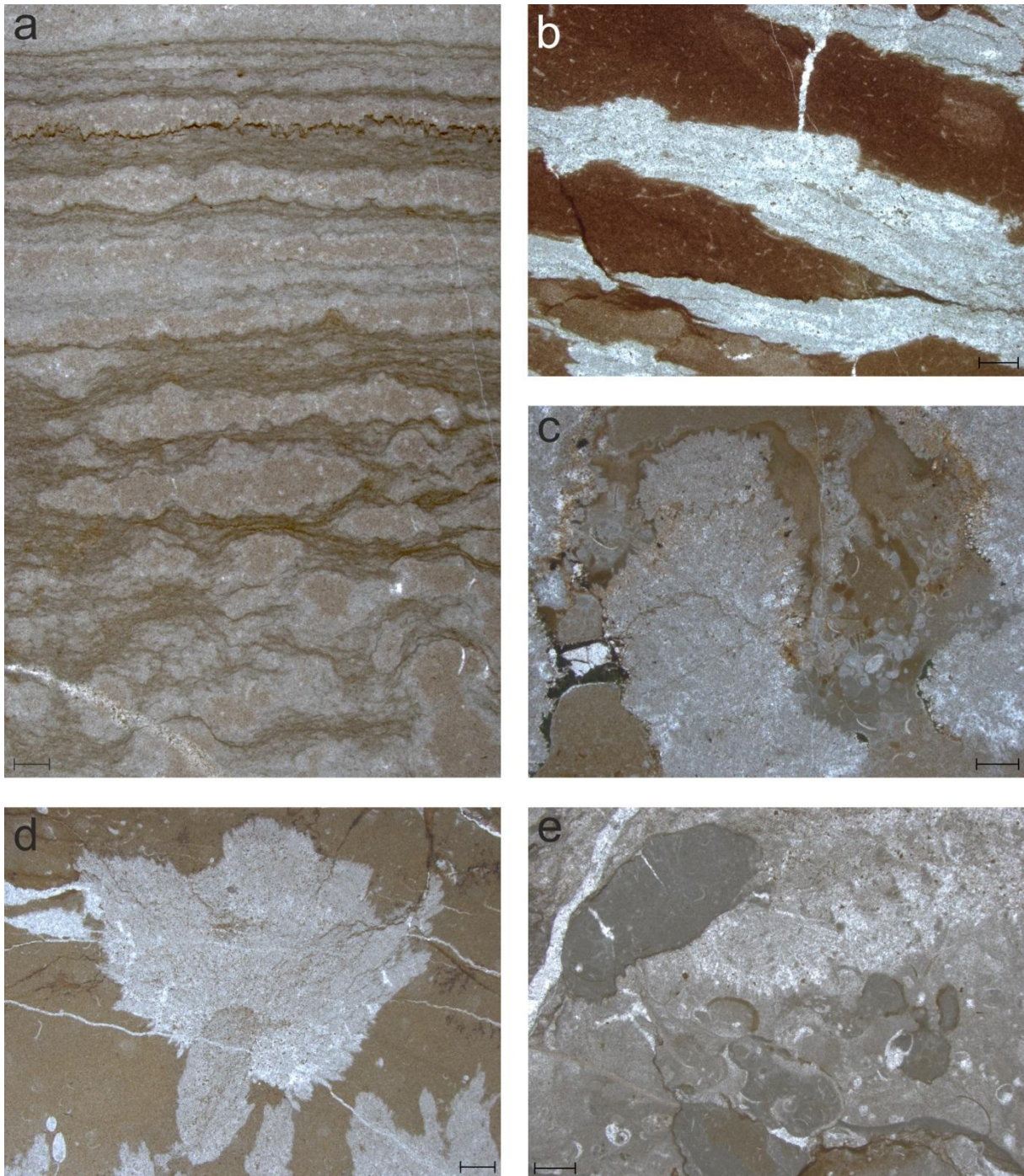
**Fig. 28:** Thin section photographs from Ogbin. **(a)** Laminated (above) and bioturbated (below) mudstone. Sample 36b. **(b)** Crystals and sponges from the base of the thrombolitic hill. Sometimes the sponge spicules fit well to the crystals margins. Sample 24. **(c)** Accumulations of organisms, mainly ostracods, between crystals of type 8. Sample 31. **(d)** Crystals of type 4. Their shape resembles the one from crystals of type 1 and 2. Sample 20. **(e)** Crystals growing on an accumulation of organisms and lithoclasts. Sample 44. Scale bar = 1 mm.

### *The Upper Permian Limestone*

The Upper Permian limestone contains ostracods, bivalves and gastropods as well as rugose corals and ammonoids. The other bioclasts are small and very thin and therefore cannot be allocated to a certain group of organisms. Moreover, the limestone contains thick and strongly recrystallized shell remains that could originate from brachiopods. The bioclasts are embedded in red, yellow or grey coloured sediment, which is sometimes strongly recrystallized.

### *The Calcium Carbonate Crystal Fans*

The crystals of type 1, which are typical for the CCFs of Zangakatun and Vedi, occur in Ogbin only at the base of the thrombolitic hill around 80 cm above the base of the Boundary Shale. Compared with the other two outcrops the lamination is not well visible and sometimes seem to be absent. Crystals of type 2 are more common and do not only occur together with the ones from type 1 at the base of the thrombolitic hill but also in the thrombolitic bed below this hill. They often show flattened terminations that are an evidence of their aragonitic origin. On top of the already mentioned thrombolitic hill occur crystals of type 8. They show the typical grey and white pattern but their shape is evocative of the shape of crystals from type 1 and 2. Some crystals are not preserved in their original upright position but are tilted.

Sponges of type 1 occur in the thrombolitic hill and in the thrombolitic bed below. Sometimes the sponge spicules fit perfectly to the crystal margins (Fig. 28b). They are very common at the base of the thrombolitic hill but on its top they are much less common.

The red and yellow sediment is mostly micritic but also contains microspar. The sediment contains ostracods, gastropods, bivalves and *Earlandia* but no *Rectocornuspira* or ammonoids. Accumulations of organisms occur only in sample 23 and 31 and mainly consist of ostracods (Fig. 28c).

### *The Microbialites*

In samples 36b and 66 laminated structures are present that are partly bioturbated (Fig. 28a). These structures might be of microbial origin and could therefore be denoted as stromatolites. None of the investigated thin sections shows microstructures that are similar to the ones from thrombolites found in Vedi or Zangakatun.

### *The diffuse shaped Crystals*

The diffuse shaped crystals occur in the first thrombolitic bed above the Boundary Shale as well as at the base of a limestone bed around 3.5 m above the base of the Boundary Shale. Furthermore, they occur in a sample of the scree from the opposite hillside.

The first thrombolitic bed contains crystals of type 4 (Fig. 28d) that contain a few dolomite rhombohedrons. The surrounding sediment can be denoted as a bioclastic packstone that contains ostracods.

A crystal of type 6 occurs in the already mentioned scree sample from the opposite hillside. The crystal shows a typical dendrolitic shape but is strongly recrystallized. The surrounding sediment is similar to the sediment surrounding a thrombolitic hill in Vedi that probably contains stromatactis

structures. Crystals from type 6 also occur in a sample from the already mentioned limestone bed. The thin section shows that the crystals grew on accumulations of organisms that contain not only ostracods but also bivalves, gastropods and ammonoids. They probably also grew on lithoclasts that look like the surrounding sediment (Fig. 28e). The remaining sediment surrounding the crystal can be denoted as a bioclastic wackestone that contains ostracods.

### *Sponges*

As well as in Vedi only sponges from type 1 occur in Ogbin. Again their originally silicious skeleton was replaced by calcite so that they are now present as calcite pseudomorphs. They are restricted to the thrombolitic hill and the thrombolitic bed below. Sometimes the spicules fit perfectly to the neighbouring crystal margins. On top of the thrombolitic hill spots without sponge spicules are more common than at its base indicating that the sponges' frequency decreases from bottom to top.

Fig. 29 shows the distribution of crystals and sponges from a sample taken at the base of the thrombolitic hill. The crystals are mainly from type 2 and only a few from type 1 occur at the top and on the lower left side of the thin section. It is conspicuous that the crystals do not stand parallel next to each other as they do in all the other samples. Instead they have a rather fan-like appearance. Only the crystals from the left side seem to have grown perpendicular to the sediment surface. Sponges are more common in the lower part of the thin section as well as on the left side where the crystals did not grow perpendicular to the sediment surface but they are not totally absent in the other areas. It seems that the distribution of the sponges does not correlate with the growing directions of the crystals. Furthermore, there are no hints that the sponges influenced the growing direction of the crystals and forced them to grow in a certain direction.

### *The bioturbated Mudstone*

The bioturbated mudstone occurs in samples 36b, 40 and 66. Sample 66 was collected from scree in the last 9 m of the investigated outcrop. These samples show a sometimes more, sometimes less regular lamination as well as bioturbated parts. A microbial origin of the lamination cannot be excluded, therefore these samples could represent stromatolites. However, there is no certitude on its microbial origin. In the bioturbated parts the lithoclasts are recrystallized at their margins and are embedded in a stylolaminated fabric (Fig. 28a).

### *Other Observations*

Stylolites only occur in the Triassic samples and not in the Permian ones. They are common in the weathered areas of the thin sections and also often proceed along the crystal margins. Furthermore, they often pass through the sediment but rarely through the crystals.

Pyrite and oxides occur in the crystals as well as in the sediment. They are usually small and often form small clusters. They are also common in stylolites and fissures. Only in samples 23 and 31 bigger pyrite crystals have a lattice-like appearance.

Dolomite is a very common feature in the Permian sediments. In the Triassic samples dolomite is rare in the sediment but sometimes occurs in the crystals.
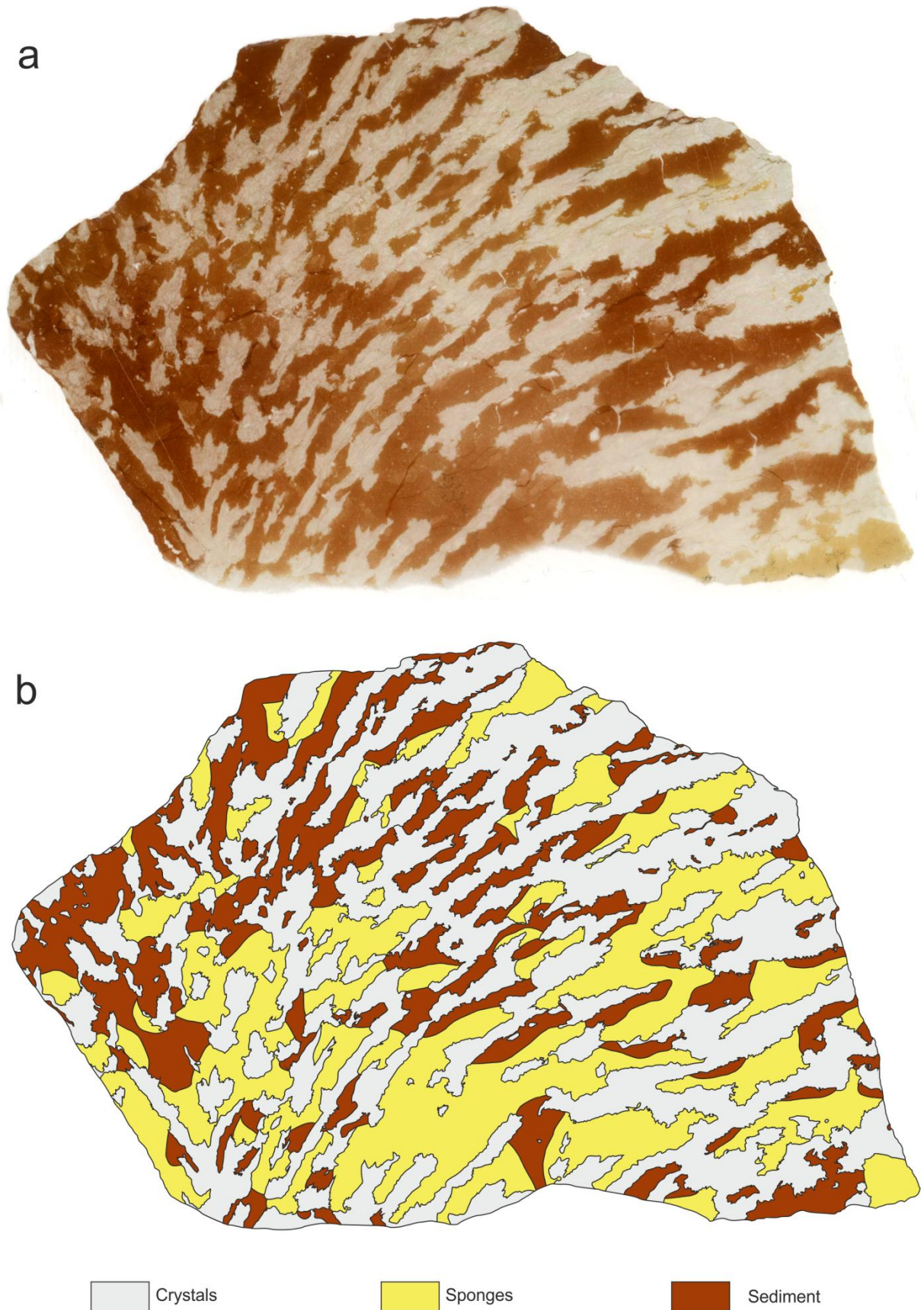
**Fig. 29:** Distribution of crystals and sponges in a thrombolitic hill from Ogbin. Sample 28. **(a)** Scan of a thin section. 12 x 7.5 cm. **(b)** Distribution of crystals, sponges and sediment without sponges. The picture shows that there is no correlation between the sponge distribution and the growing directions of the crystals.

During the thin section preparation of the samples 36b and 66 that belong to the bioturbated mudstone a bituminous smell was noticeable.

## 5.2. Cathodoluminescence

All investigated thin sections show an orange colour with variable brightness. Only in sample 48 a few very small yellow spots are recognizable.

The single sub-crystal grains within the CCFs and the diffused shaped crystals show a zoning. The core is surrounded by a very bright zone, whereby the border between them is in many cases not sharp. After this very bright zone follows another zone that has the same brightness as the core. The outermost zone is very dark and nearly non luminescent and occurs only in the biggest sub-crystals. Because of the small size of the single sub-crystals in most cases only the darker core and the first very bright zone are visible. The zoning is not always parallel and the thickness of the zones is very variable, also within the very same sample (Fig. 30a, b and c). Because of the very bright zone around the core, the CCFs seem to be brighter than the micrite and due to the similar colour of crystals and micrite it is only possible to distinguish them because of their grain size. Therefore it is very difficult to distinguish a very fine grained crystal from the surrounding micrite. The clear lamination of the CCFs, however, that was well visible in the thin sections is not visible with CL (Fig. 30d).

Although the micrite's brightness is more or less always the same the amount of brighter or darker spots within the micrite varies in the samples. Furthermore, micrite that is very dark in the thin sections has also very dark CL colours.

In many cases shells of bivalves and ostracods are only poorly recognisable. Crystals filling the space between the two shells of ostracods also show zoning (Fig. 30b). Sponge spicules are just slightly brighter than the surrounding micrite and therefore not well visible too.

## 5.3. Fluorescence Microscopy

In the investigated thin sections the micrite is always non luminescent. The crystals are weak luminescent with a slightly greenish colour. The dark laminae of the crystals of type 1 are slightly darker and therefore weaker luminescent than the brighter laminae. The outer coarser crystalline parts from crystals of type 5 are the only slightly more luminescent areas in all crystals but they still show a green colour and are therefore again not very luminescent. Only a stylolite from sample 19 shows the same light green colour. Crystal structures were best visible in the mottled part of the crystals from type 1.

## 5.4. Raman Spectroscopy

The Raman spectroscopy showed that the darker laminae from the laminated crystals from type 1 do not contain any organic particles or other important changes in the mineralogical composition. Furthermore, it revealed that the crystals are made of calcite with no important lateral variations in the mineralogical composition.
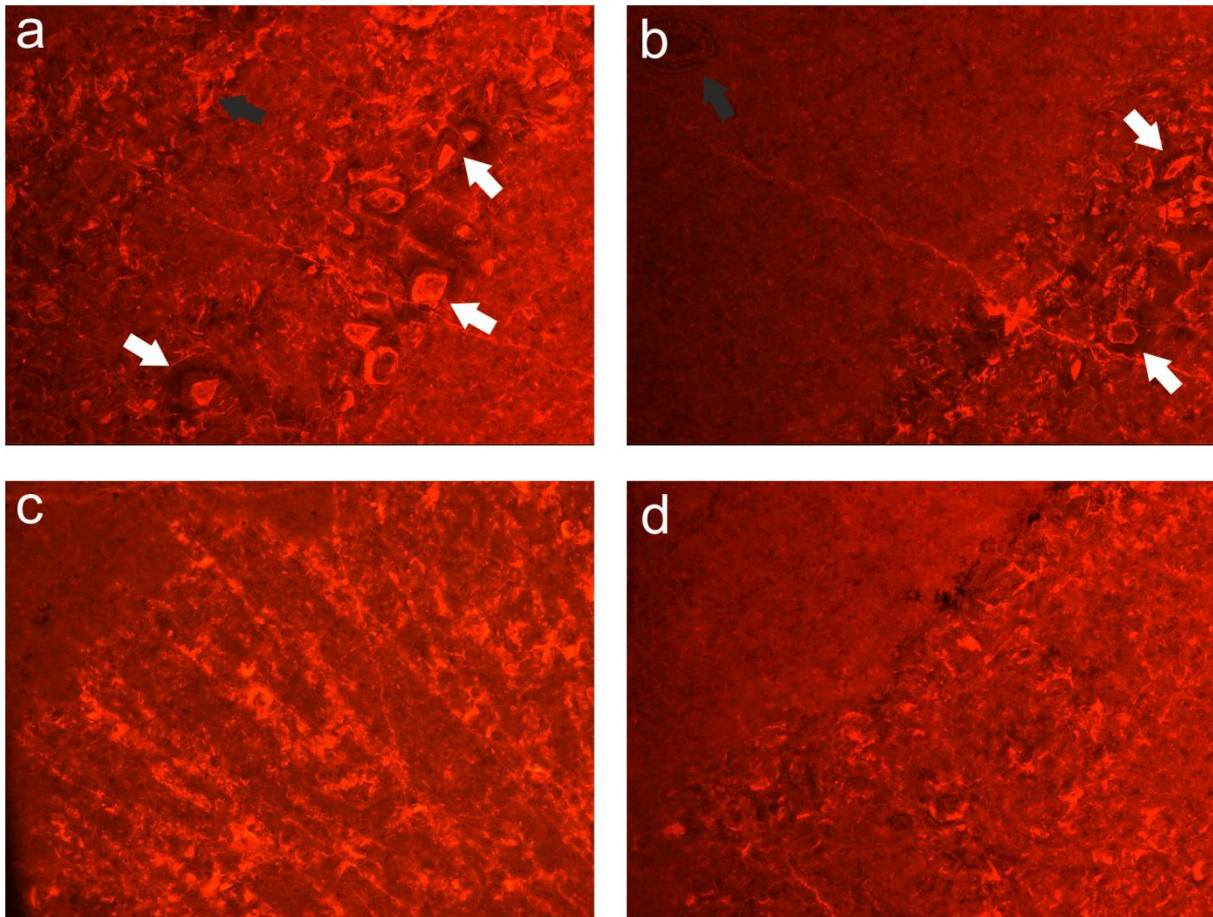
**Fig. 30:** Cathodoluminescence pictures. **(a)** Detailed view of a crystal from type 1. The bigger sub-crystals show an irregular zoning. The dark core is surrounded by a very bright zone, followed by a zone with the same colour of the core. This zone is followed by a nearly non luminescent zone (white arrows). Smaller sub-crystals only show the dark core and the very bright rim (black arrow). In contrast to the thin section this crystal of type 1 shows no lamination. Sample 17. **(b)** Crystal of type 1 (right) and the surrounding sediment (left). Sub-crystals in the crystal show the same zoning as described in (a) (white arrows). Again the lamination that is well visible in the thin section is not visible in the CL picture. The filling of the ostracod shows a zoning too (black arrow). Sample 17. **(c)** Crystal from type 7. Because of the bright, irregular rims the radial form of the crystals is visible. Sample 62. **(d)** Crystal type 1 (right) and the surrounding sediment (left). Due to the very bright rims of some sub-crystals the crystal of type 1 seems to be brighter than the micrite. Again the crystal shows no lamination. Sample 17.

## 5.5.    Carbon Isotope Analyses

### 5.5.1.   The $\delta^{13}C_{sediment}$ Curve

The $\delta^{13}C_{sediment}$ values for the $\delta^{13}C_{sediment}$ curve were measured from the bioclastic wackestone that surrounds the crystals. The curve can be divided into five intervals (Fig. 31).

Interval 1 starts at the red nodular limestone at the base of the investigated outcrop and ends in the middle of the marly limestone below the Boundary Shale. Therefore this interval starts in the *C. nodosa* conodont zone and ends in the *C. hauschkei* zone. During the lower part of this interval the $\delta^{13}C$ values are constant around 2.2‰. At the top they become more negative around 1.6‰ with a small negative peak (N1) at 1‰.
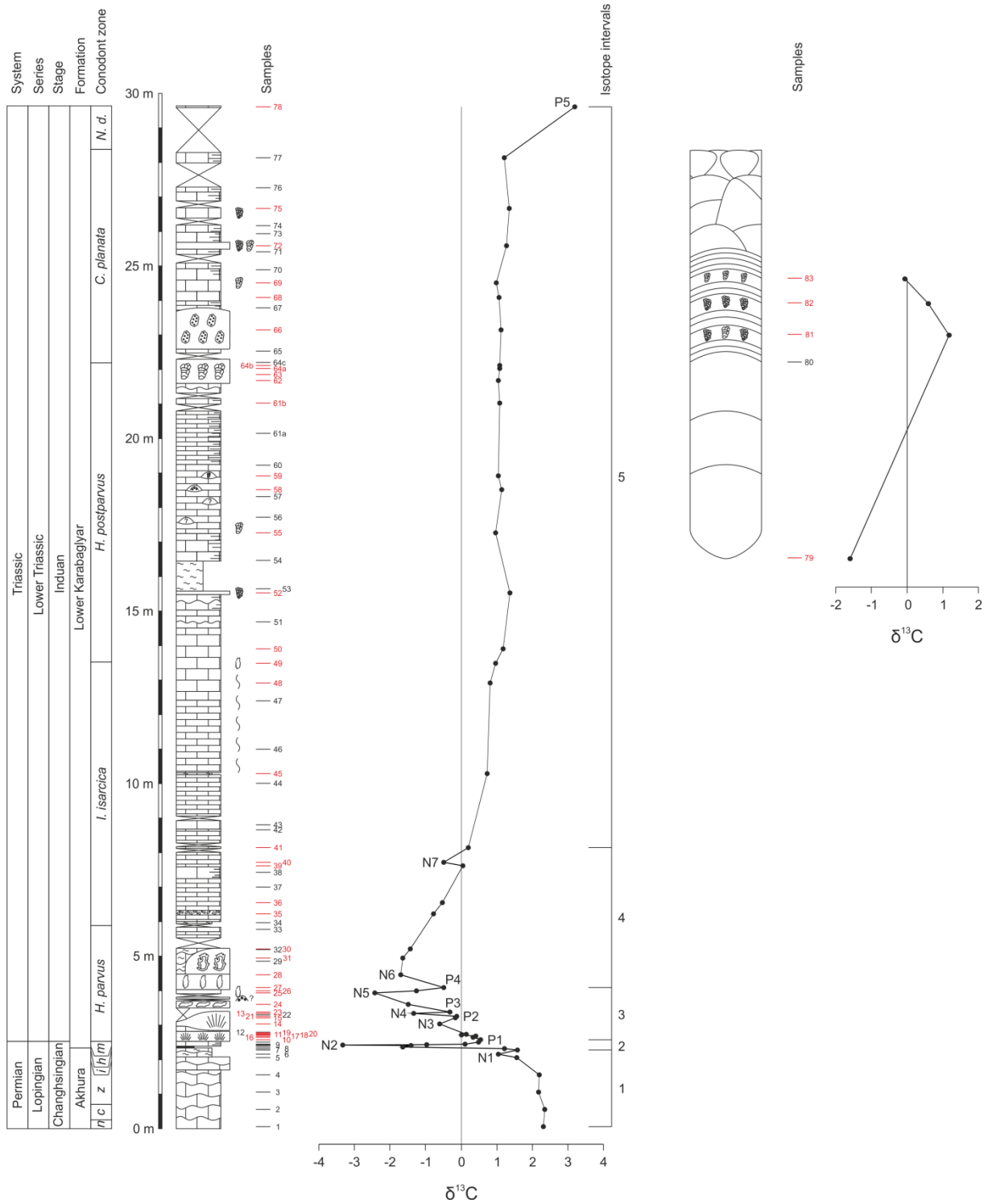
**Fig. 31:** The $\delta^{13}C_{sediment}$ curve from Zangakatun. The $\delta^{13}C_{sediment}$ values were measured on the bioclastic wackestone that surrounds the crystals. For the legend see Fig. 9. For explanation see text.

The following interval 2 comprises the upper half of the marly limestone below the boundary shale as well as the first few centimeters of both the first CCF and the *H. parvus* zone. This interval is characterized by an abrupt decrease of the $\delta^{13}C$ values. In the marly limestone and the Boundary Shale the values decrease and reach an absolute minimum of -3.3‰ (N2) at the bottom of the

overlaying platy limestone. Then the $\delta^{13}$C values increase and reach 0.5‰ (P1) at the top of this interval.

Interval 3 ends after the first few centimeters of the 120 cm high microbialite and comprises the lower half of the *H. parvus* zone. In this interval the $\delta^{13}$C values fluctuate but the isotope record shows a general decrease. Three negative peaks (N3-N5) are recorded that become more negative from bottom to top of this interval. The same is for the recorded positive peaks (P2-P4). The first negative peak N3 (-0.6‰) occurs in the CCF mound. After a slight increase to -0.2‰ (P2) the second negative peak (N4) with -1.4‰ occurs. The following positive peak P3 (-0.3‰) occurs on top of the CCF mound. The third negative peak N5 reaches -2.4‰ and is the second most negative peak in the $\delta^{13}$C$_{sediment}$ record. On top of this interval the $\delta^{13}$C values rise again (P4) and reach -0.5‰.

Interval 4 extends to the 5 cm thick limestone layer that is situated between two observation gaps and comprises the upper half of the *H. parvus* zone and the lower third of the *I. isarcica* zone. It starts with another negative peak of -1.7‰ (N6) that is still within the bedded part of the 120 cm thick thrombolite. Then the $\delta^{13}$C values rise again until they reach 0‰. On top of this interval the last negative peak N7 occurs where the $\delta^{13}$C values decrease to -0.5‰. After N7 all $\delta^{13}$C values are positive. On top of this interval the $\delta^{13}$C values reach 0.2‰.

The following interval 5 comprises the remaining part of the outcrop. After a slight increase in the lower half of this interval the $\delta^{13}$C record reaches a plateau with $\delta^{13}$C values around 1.1‰. At the top of the outcrop the $\delta^{13}$C values increase relatively strongly in the last sample and reach 3.2‰ (P5).

The base of the huge microbialite has negative $\delta^{13}$C values, namely -1.6‰. At the beginning of the bedded part the $\delta^{13}$C values are 2.8‰ higher than at the base of the microbialite. Because of missing samples in the massive part it is not known whether this increase to 1.2‰ is gradual or whether there are fluctuations. After this increase the $\delta^{13}$C values decrease in the bedded part, reaching $\delta^{13}$C values of -0.1‰ on top of it.

### The $\delta^{18}$O$_{sediment}$ curve

The $\delta^{18}$O$_{sediment}$ values were measured on the same samples than the $\delta^{13}$C$_{sediment}$ values and thus from the bioclastic wackestone that surrounds the crystals. In the Upper Permian limestones the $\delta^{18}$O values are stable at around -6‰ but in the *C. zhangi* conodont zone the $\delta^{18}$O values increase to -4.9‰. After this increase the $\delta^{18}$O values decrease again and reach values of about -5.4‰. A rapid decrease to -8.2‰ happens at the base of the *C. meishanensis – H. praeparvus* zone, only a few centimeters below the major decrease of the $\delta^{13}$C values (N2). After this sharp decrease the $\delta^{18}$O values increase again to -6‰. In the lower half of the *H. parvus* zone the $\delta^{18}$O values show fluctuations and vary between -6.8‰ and -5.6‰. After these fluctuations the $\delta^{18}$O values stay relatively stable and vary between -7.2‰ and -5.9‰ (Fig. 32).

### 5.5.2. Comparison between $\delta^{13}$C$_{sediment}$ and $\delta^{13}$C$_{crystal}$

A comparison between the $\delta^{13}$C values of the bioclastic wackestone and crystals shows that the $\delta^{13}$C values exhibit obvious differences, especially in the lower part (Fig. 33).

In interval 3 all $\delta^{13}$C$_{crystal}$ values are all more positive than the corresponding $\delta^{13}$C$_{sediment}$ values. The general negative trend of the $\delta^{13}$C$_{sediment}$ record is also recorded in the crystals but the decrease is not that strong than in the bioclastic wackestone. In contrast to the sediment that records three negative peaks (N3-N5) only one negative peak, namely N4, is also well noticable in the crystals. Sediment and
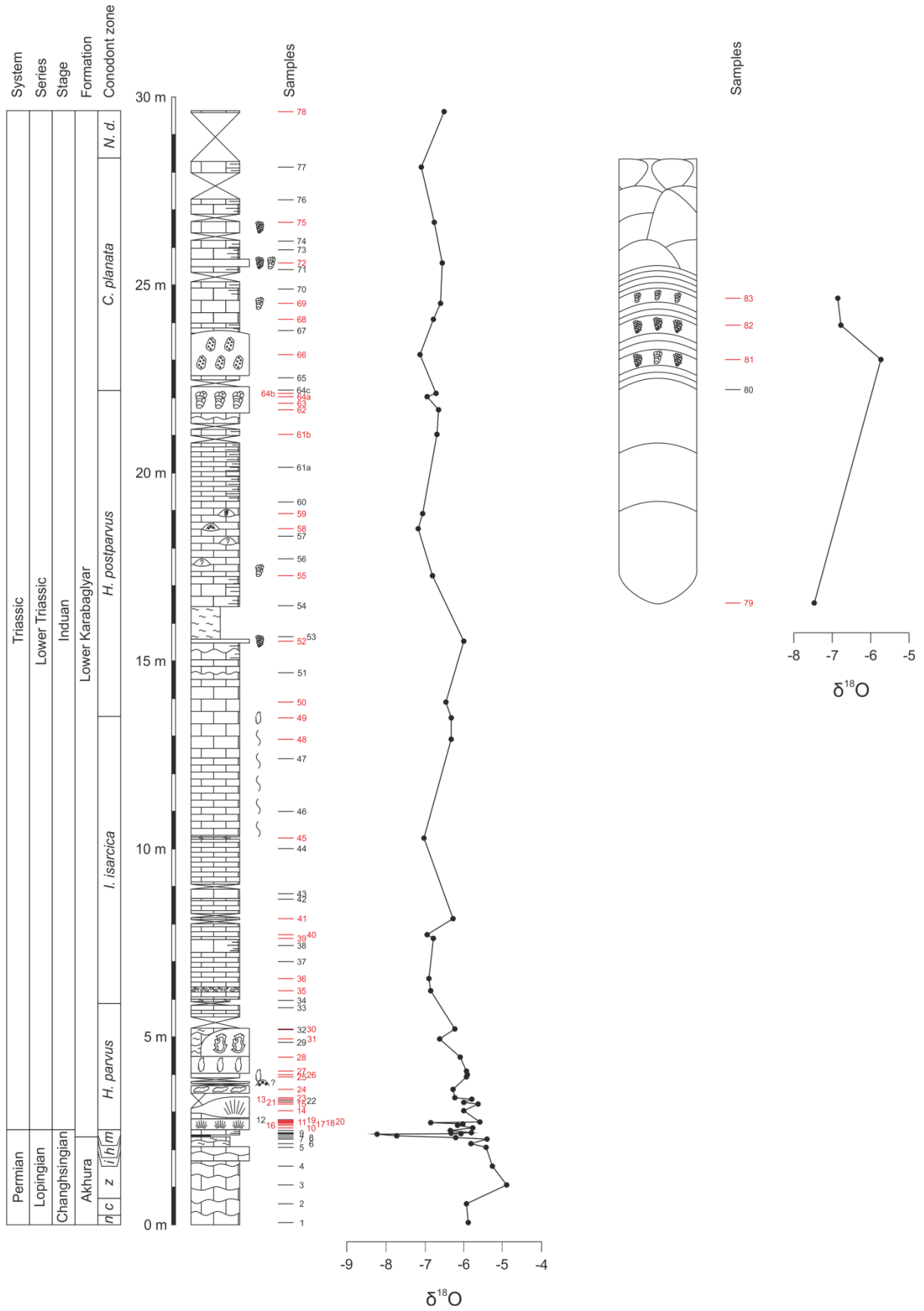
**Fig. 32:** The $\delta^{18}O_{sediment}$ curve from Zangakatun. The $\delta^{18}O_{sediment}$ values were measured on the bioclastic wackestone that surrounds the crystals. For the legend see Fig. 9. For explanation see text.
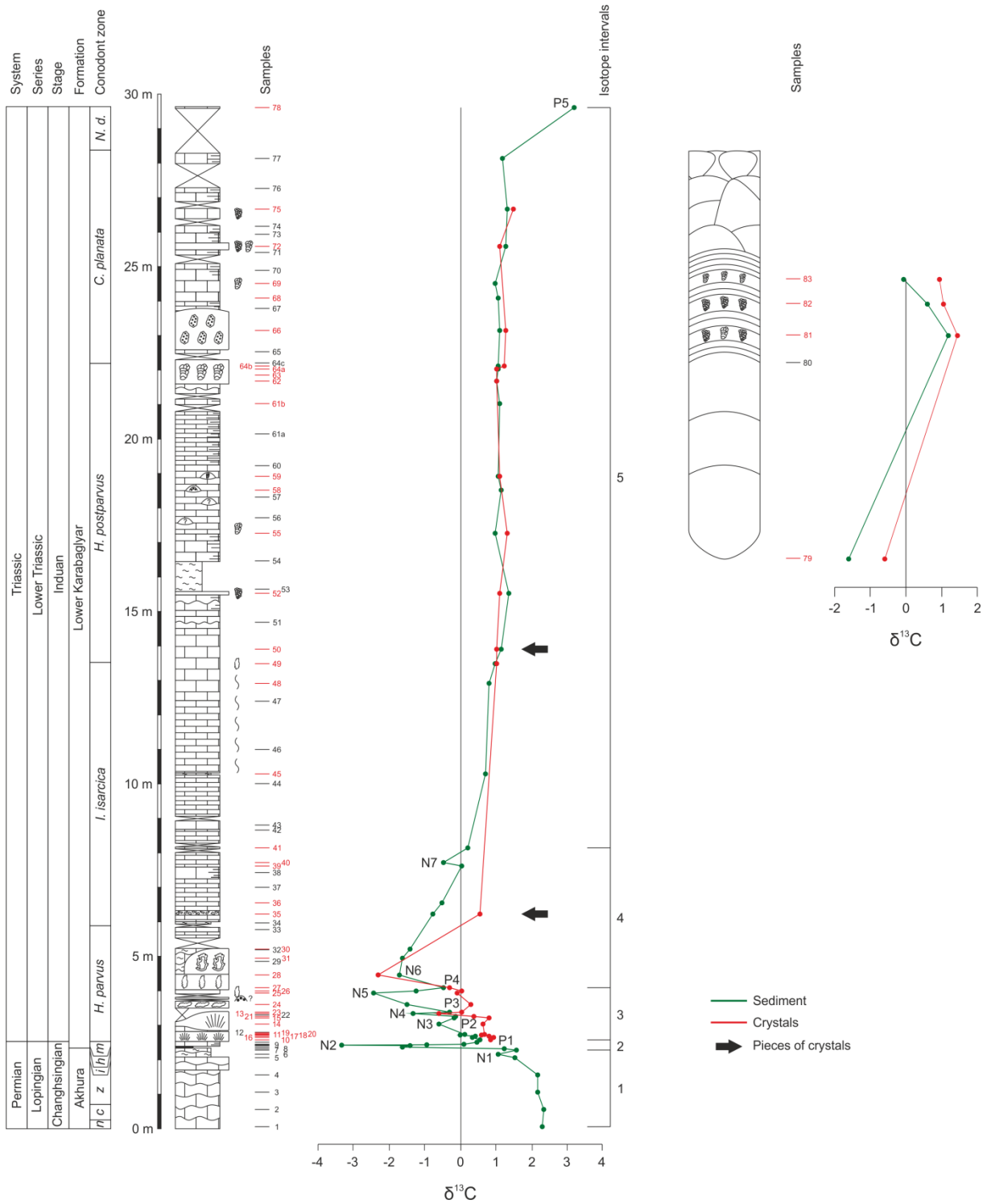
**Fig. 33:** The $\delta^{13}C_{sediment}$ (green) and $\delta^{13}C_{crystal}$ (red) values from Zangakatun. The difference between these values in the lower microbialites is well visible. The arrows mark samples in which no in situ crystals but pieces of crystals were measured. For the legend see Fig. 9. For explanation see text.

crystals do not always show the same trend e.g. sample 24, where the $\delta^{13}C_{sediment}$ value is 1.2‰ more negative than the previous $\delta^{13}C_{sediment}$ value but the $\delta^{13}C_{crystal}$ value is 0.3‰ more positive than the previous one. Sample 27 shows the opposite. The $\delta^{13}C_{sediment}$ value is 0.8‰ more positive than the previous one but the $\delta^{13}C_{crystal}$ value is 0.3‰ more negative. On top of this interval the $\delta^{13}C_{sediment}$ and

$\delta^{13}C_{crystal}$ values are almost the same. The differences between $\delta^{13}C_{sediment}$ and $\delta^{13}C_{crystal}$ vary between only 0.2‰ in sample 27 and 2.3‰ in sample 25.

In interval 4 only two crystals from the diffused shaped crystals and one piece of a crystal from the breccia were measured. The $\delta^{13}C_{crystals}$ value from the bedded part below the thrombolitic hill decreases more than the corresponding $\delta^{13}C_{sediment}$ value does and reaches -2.1‰. The measured piece of a crystal from sample 35 has a $\delta^{13}C$ value from 0.5‰ and is 1.3‰ more positive than the corresponding sediment (-0.8‰).

The $\delta^{13}C_{crystal}$ record measured in interval 5 also reaches a plateau just like the $\delta^{13}C_{sediment}$ record but because of missing samples between sample 35 and sample 49 it cannot be said for sure that this plateau already starts in the middle of interval 4 or at the beginning of interval 5. The $\delta^{13}C_{crystal}$ values are very similar to the corresponding $\delta^{13}C_{sediment}$ values and are both more positive as well as more negative than the sediment. The maximum differences between $\delta^{13}C_{crystal}$ and $\delta^{13}C_{sediment}$ amount to 0.4‰ and in sample 63 they are the same.

The $\delta^{13}C_{crystal}$ values from the huge microbialite are all more positive than the corresponding sediment and show the same trend as the $\delta^{13}C_{sediment}$ values do. The differences between them vary between 0.2‰ and 1‰.


## *Comparison between the $\delta^{18}O_{sediment}$ and $\delta^{18}O_{crystal}$ values*

A comparison between the $\delta^{18}O$ values of the crystals and the surrounding bioclastic wackestone shows that the $\delta^{18}O_{crystal}$ values are more negative than the corresponding $\delta^{18}O_{sediment}$ values. The $\delta^{18}O_{crystal}$ values are up to 1.7‰ more negative. The only exceptions are sample 55 and 59 where the $\delta^{18}O_{crystal}$ values are 0.1‰ more positive than the corresponding $\delta^{18}O_{sediment}$ values. As the $\delta^{18}O_{sediment}$ values the $\delta^{18}O_{crystal}$ values show fluctuations in the lower half of the *H. parvus* zone and vary between -7.6‰ and -6.1‰. After these fluctuations the $\delta^{18}O_{crystal}$ values become more or less stable and vary between -7.9‰ and -6.6‰ (Fig. 34).

A cross-plot between $\delta^{13}C$ values and $\delta^{18}O$ values from the bioclastic wackestone as well as from the crystals does not show any covariance (Fig. 35).


### 5.5.3. $\delta^{13}C$ values from the laminated Crystals from Type 1

To ascertain whether the $\delta^{13}C$ values vary within the laminated crystals from type 1, such crystals from samples 15 and 17 were analysed. The samples were drilled at a distance of 0.5 mm. Also crystals from type 2 and the surrounding bioclastic wackestone were analysed (Fig. 36). Furthermore, mottled and laminated parts from ten crystals from type 1 were measured (Fig. 37).

In sample 15 two neighbouring crystals were drilled. The $\delta^{13}C$ values from the left crystal vary between 0.6‰ and 0.9‰ with an average of 0.7‰. The right crystal has an average $\delta^{13}C$ value of 0.6‰ with values varying between 0.4‰ and 0.8‰. The maximum difference between the highest and the lowest $\delta^{13}C$ value is 0.3‰ for the left and 0.2‰ for the right crystal. The $\delta^{13}C$ values are thus not varying much, just above the measurement uncertainties, and are more or less constant. Both crystals plot on average by 0.6‰ and show the same trend in the middle part.

In sample 17 only one crystal was drilled. The $\delta^{13}C$ values vary between 0.7‰ and 0.9‰. The maximum difference between the $\delta^{13}C$ values is 0.2‰, which means that these values, as well as the ones from sample 15, are more or less constant.
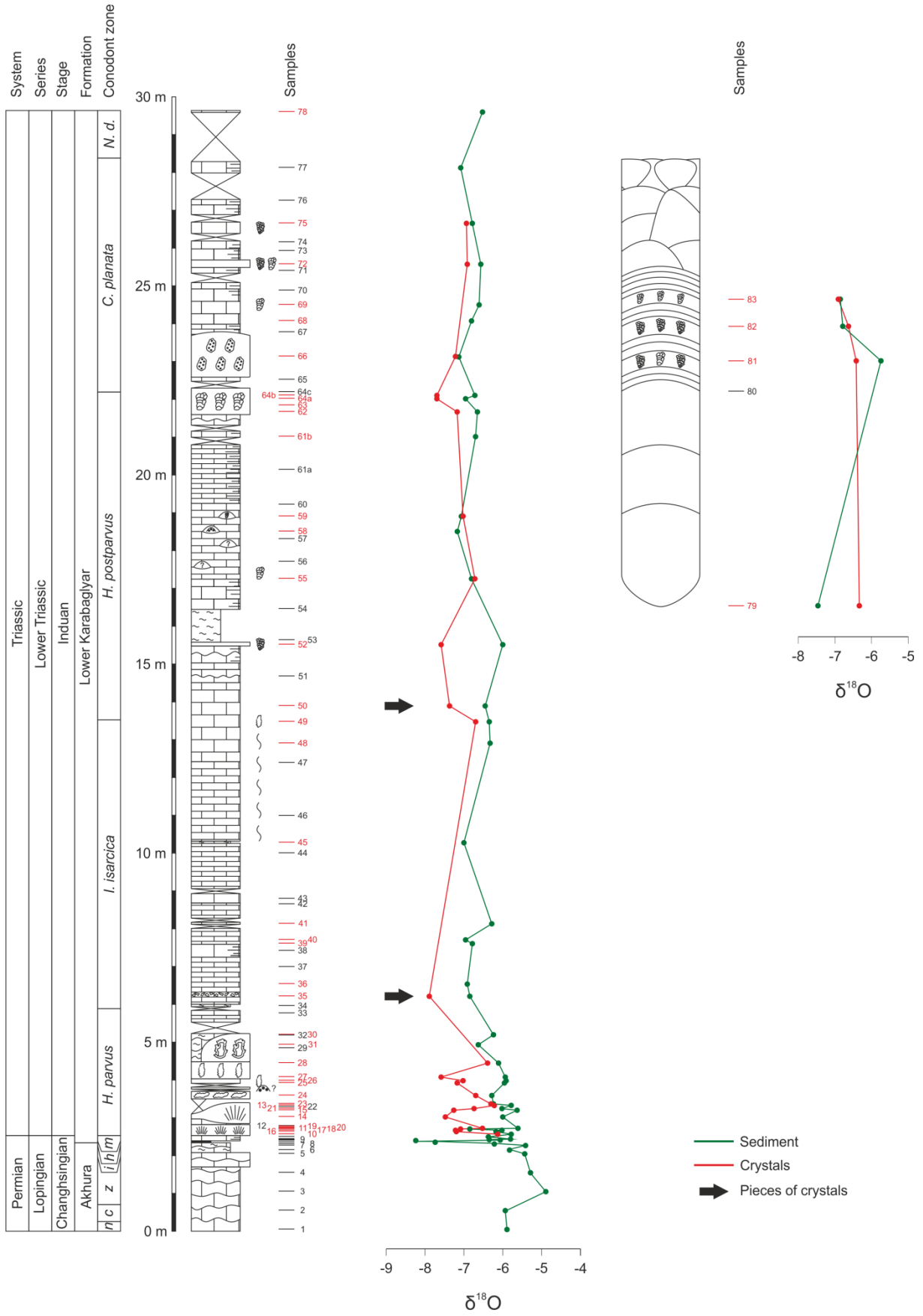
**Fig. 34:** The $\delta^{18}O_{sediment}$ (green) and $\delta^{18}O_{crystal}$ (red) values. The $\delta^{18}O_{crystal}$ values are up to 1.7‰ more negative. For legend see Fig. 9. For explanation see text.
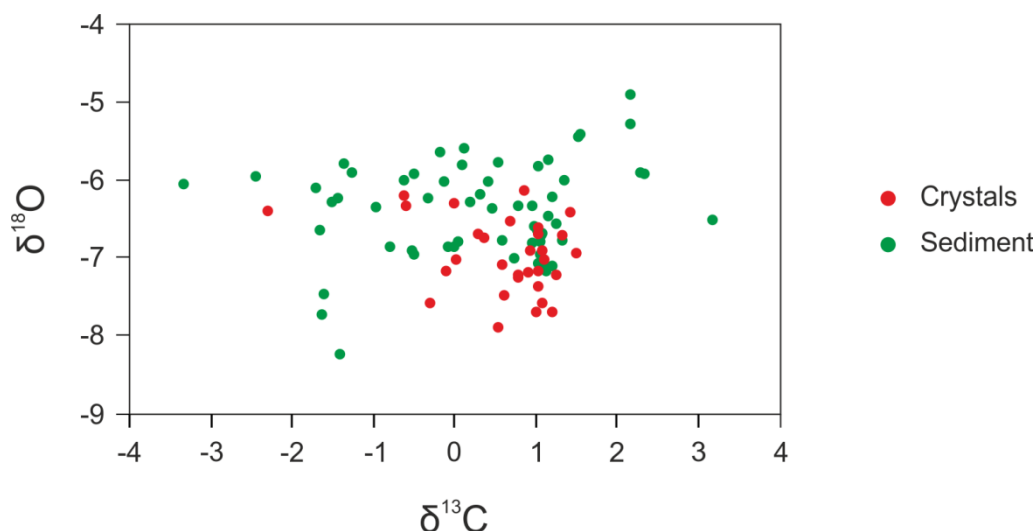
**Fig. 35:** A cross-plot between the $\delta^{13}C$ values and the $\delta^{18}O$ values. It does not show any covariance between the two variables. The green data points are from the $\delta^{13}C_{sediment}$ and $\delta^{18}O_{sediment}$ values and the red ones are from the $\delta^{13}C_{crystal}$ and $\delta^{13}O_{crystal}$ values.

From both samples also the $\delta^{13}C_{crystal}$ values from crystal type 2 were analysed and interestingly both of them are exactly the same, namely 0.8‰. That means that these crystals from type 2 are slightly more positive as well as more negative than the corresponding laminated crystal(s). In both samples the sediment is more negative than the crystals and plots at -0.2‰ for sample 15 and at -0.4‰ for sample 17.

Something similar applies for the $\delta^{18}O$ values. In sample 15 the $\delta^{18}O$ values vary between -6.4‰ and -7.1‰ in the left and between -6.6‰ and -6.8‰ in the right crystal. The average values are -6.8‰ for the left and -6.8‰ for the right crystal. In the crystal from sample 17 the $\delta^{18}O$ values vary between -7.2‰ and -6.6‰ with an average value of -6.8‰. Variation is minimal and almost absent. The $\delta^{18}O$ values from the crystals of crystal type 2 are -7.3‰ for sample 15 and -7.2‰ for sample 17, meaning that both are more negative than the laminated crystals, respectively. The $\delta^{18}O_{sediment}$ values are more positive than all $\delta^{18}O_{crystal}$ values and plot at -5.6‰ (sample 15) and -6‰ (sample 17).

Measurements from the mottled and the laminated parts of the crystals revealed that the $\delta^{13}C_{mottled}$ values from crystals with a higher relative outcrop position are more positive than the $\delta^{13}C_{laminated}$ values (Fig. 37). The differences between $\delta^{13}C_{mottled}$ and $\delta^{13}C_{laminated}$ in these upper crystals vary between 0‰ and 0.4‰. In the lower crystals the $\delta^{13}C_{mottled}$ values are more negative than the $\delta^{13}C_{laminated}$ values or equal. In both crystals the difference between $\delta^{13}C_{mottled}$ and $\delta^{13}C_{laminated}$ is 0.1‰. The $\delta^{18}O$ values show another trend. In only one sample the $\delta^{18}O_{mottled}$ value is more positive than the corresponding $\delta^{18}O_{laminated}$ value. The difference accounts for 0.1‰. In one sample the $\delta^{18}O$ values are equal and in the remaining samples $\delta^{18}O_{mottled}$ is more negative than $\delta^{18}O_{laminated}$. The difference varies between 0.1‰ and 0.9‰.

### 5.5.4. Further Results

The crystals from sample 30 belong to crystal type 5 and their central parts and their envelopes do not only show conspicuous differences in their visual appearance but also in their $\delta^{13}C$ values. The
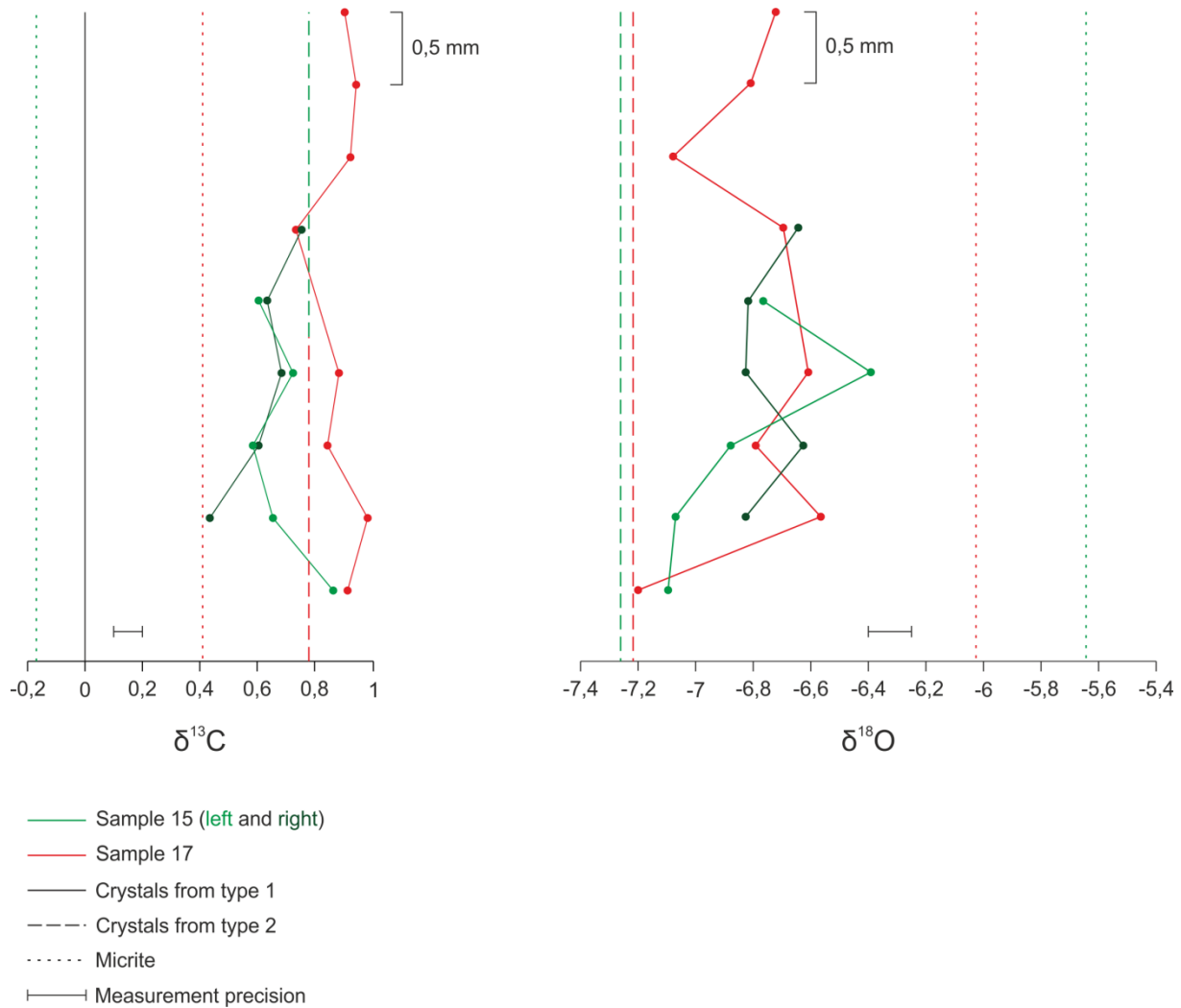
**Fig. 36:** $\delta^{13}$C values (left) and $\delta^{13}$O values (right) from laminated crystals of type 1. Samples from the laminated crystals were taken at a distance of 0.5 mm. For description see text.

$\delta^{13}$C value from the central part accounts to -3.1‰ but the one from the envelope has only -1.6‰, which makes a difference from 1.5‰.

In sample 16a the crystals of type 1 and 2 have $\delta^{13}$C values of 0.9‰ and 1‰ but the type 2 crystals from sample 16b have a $\delta^{13}$C value of -0.9‰, which makes a difference of almost 2‰. There is also a noticable difference at the $\delta^{13}$C$_{sediment}$ values. The bioclastic wackestone from sample 16a has a $\delta^{13}$C value of 0.3‰ but the one from sample 16b has a $\delta^{13}$C$_{sediment}$ value of -1.1‰. That makes a difference of 1.4‰. A more precise observation of the thin section from sample 16b reveals that in the measured part small cracks occur.

Additional to the crystals from type 2 and the bioclastic wackestone also a sponge from sponge type 1 was analysed from sample 16b. The bioclastic wackestone as well as the sponge (sponge type 1) have the same $\delta^{13}$C value of -1.1‰. In sample 49 the $\delta^{13}$C$_{sediment}$ account for 1‰ and $\delta^{13}$C$_{sponge}$ (sponge type 3) for 1.2‰, which makes a difference of only 0.2‰. As the sediment the crystal from this sample plots at 1.‰.
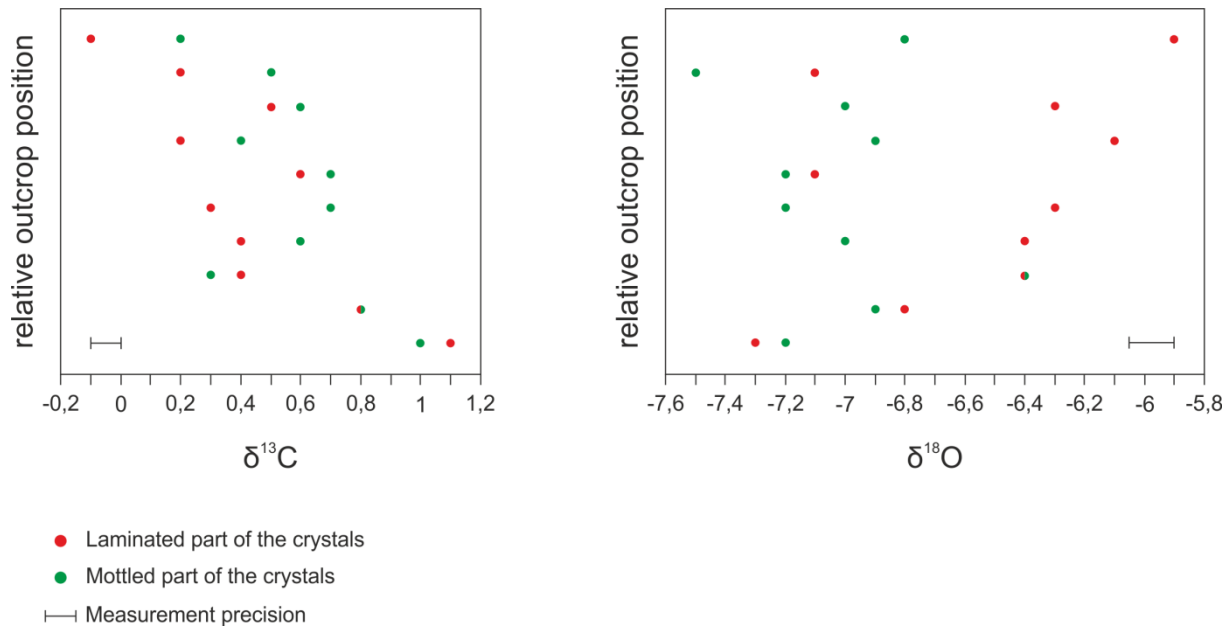
**Fig. 37:** $\delta^{13}$C values (left) and $\delta^{13}$O values (right) from the laminated part of the crystals from type 1 (red) and their mottled base (green). For explanation see text.

## 6. Interpretation and Discussion

In all three investigated sections in Armenia two phases of microbial growth occurred during the Griesbachian. The first phase led to the formation of diffused shaped crystals and CCFs. The CCFs predominantly but not-exclusively consist of the laminated crystal of type 1 and crystals of type 2. The second phase is characterized by the occurrence of diffused shaped crystals. Microstructures that resemble the ones from thrombolites and stromatolites were also formed during the second microbial growth phase but in none of the investigated thin sections a typically microbialitic microstructure was observed. Therefore the question comes in mind whether the diffused shaped crystals are real microbialites. Although the microstructure is not typically microbialitic the meso-, macro- and megastructures (scales defined by Shapiro 2000, see also chapter 4) are and therefore I interpret them as microbialites.

As already mentioned the CCFs do not only consist of crystals from type 1 and 2. They also consist of crystals that have the same shape as the ones from type 1 and 2 but their internal structure is different and resembles the crystals from type 4 and 6. One possible explanation for the different internal structure but the same shape could be differences in the microbial community. Fenton and Fenton (1937) already assumed that stromatolite morphotypes reflect particular microbial communities and Semikhatov et al. (1979) suggested that Proterozoic stromatolite fabrics, and possibly morphotypes too, reflect the microbial evolution (Riding 2000). Also Riding (1994) assumed that the Early Paleozoic development of dendrolites and thrombolites partly represent cyanobacterial evolution. Studies from Logan (1974) and Logan et al. (1974) have shown that scalloped lamination can be produced by the reticulate mat forming cyanobacteria *Lyngbya* whereas Logan et al. (1974) and Monty (1976) showed that mats dominated by coccoid microbes, e.g. the cyanobacteria *Entophysalis*, commonly produce clotted fabrics (Browne et al. 2000). Because investigations on biomarkers failed I cannot say whether the microbial community really changed or not but differences in the internal structure of the microbialites, also in neighbouring ones, could be the result of differences in the microbial community and heterogeneities within microbial mats. Nevertheless, the internal structure and morphology of microbialites does not only reflect the microbial community composition but also the physical and geochemical conditions inherent to their environment (Grotzinger and Knoll 1999, Planavsky and Grey 2008, Power et al. 2011), therefore a possible influence of environmental factors should not be excluded.

The bushy crystals of type 7, which occur in samples with a mainly dendrolitic structure, are more similar to botryoidal crystals that grew on each other rather than to microbial microstructures. Nevertheless, these botryoidal crystals also occur together with the cloudy crystals of type 6, which more often show a thrombolitic mesostructure than a dendrolitic one. The botryoidal crystals from type 7 possibly used the microbialites as nucleation sites. After the cessation of crystal growth microbes started to settle down on the crystals and the next crystal generation used these microbes as a nucleation site again. Such a case is reported from an open pit pond by Power et al. (2011). They investigated columnar microbialites with an internal spherulitic fabric. The spherulites consist of acicular aragonite crystals. The centers include microbial remnants as well as detrital particles. A difference between these spherulites and the crystals of type 7 is that the crystals of type 7 do not contain any detrital particles. The substantial growth of individual spherulites occurred abiotically and pauses in spherulite growth allowed the microbes to colonize the spherulites again. Such a scenario could also have happened in Armenia during the Early Triassic. Power et al. (2011) assume that a combination of a low sedimentation rate, high calcification rate and low microbial growth rate is the reason for the formation of such columnar microbialites.

63

## 6.1. Did the Calcium Carbonate Crystal Fans and Microbialites grow in or on the Sediment?

First hints whether the CCFs and microbialites grew in or on the sediment are given by the asymmetrical growth of the giant microbialites in Zangakatun and Vedi (Fig. 10e and Fig. 14). This asymmetrical growth indicates the influence of a steady bottom current condition (Fig. 38a (right)). A bottom current cannot influence the growth of microbialites when they are within the sediment, therefore the microbialites must have grown on the sediment surface.

Thin section observations give further indications that the microbialites and CCFs grew on the sediment. Heindel et al. (2013) reported calyx-shaped crystal fans of Late Dienerian to Early Smithian (Early Triassic) age that show a displacive growth in soft sediment during early diagenesis. This displacive growth is evident from downward-facing crystal fans that deformed the lamination of the background sediment as a consequence of crystal growth. In none of the investigated thin sections from Armenia any structures were found which would indicate that the crystals pushed the sediment away.

The organisms between the crystals of the CCFs were probably accumulated during storm events. An accumulation of these organisms was only possible when the crystals protruded from the sediment. How far the microbialites protruded the sediment is not clear.

Another evidence that the growth of both microbialites and CCFs happened on the sediment surface are the sponge spicules that fit perfectly to the crystal margins. These spicules indicate that the CCFs and microbialites must have grown before the sponges occurred. After the crystal's growth the sponges started to settle down between the crystals and adjusted their shape as well as the form of their spicules to the available space between the crystals and to the crystal's morphology. It is well known that sponges cannot live inside the sediment, therefore the microbialites and the CCFs must have grown on the sediment too.

## 6.2. Is there a Connection between the Sponges and the Microbialites and Calcium Carbonate Crystal Fans?

Sponges in association with microbialites were already reported from PTB sections in Iran (Horacek et al. 2007b, Richoz et al. 2010, Leda et al. 2014), Lower and Middle Triassic carbonate successions of the Western Tethys domain meaning the Alps, Carpathians and the Germanic Basin (Szulc 2007) and late Early Triassic microbialites from Western USA (Brayard et al. 2011, Marenco et al. 2012, Olivieri et al. 2014, Luo et al. 2014, Vennin et al. 2015). The Upper Permian sponges in Iran were interpreted in different ways, namely as filaments of probably fungal origin (Horacek et al. 2007b), a mesh of algal filaments (Richoz et al. 2010) and as remains of calcified sponge spicules with predominant triaxon-like morphologies probably belonging to the genus Lithistida (Leda et al. 2014). Ezaki et al. (2008) reported from sponge-like textures in Earliest Triassic thrombolites from the Yangtze Platform (China). Hypercalcified sponges, sphinctozoan demosponges and hexactinellids were reported from Smithian and Spathian (Olenekian, Lower Triassic) microbialites from Western USA (Brayard et al. 2011, Vennin et al. 2015). According to Szulc (2007) the main sponge components of Middle Triassic stromatolites seem to be dictyid Hexactinellidea. Luo and Reitner (2014) suggest that sponges associated with Anisian microbialites from Poland represent keratose demosponges. The Griesbachian sponges from Armenia could also be keratose demosponges (Reitner J., personal communication).
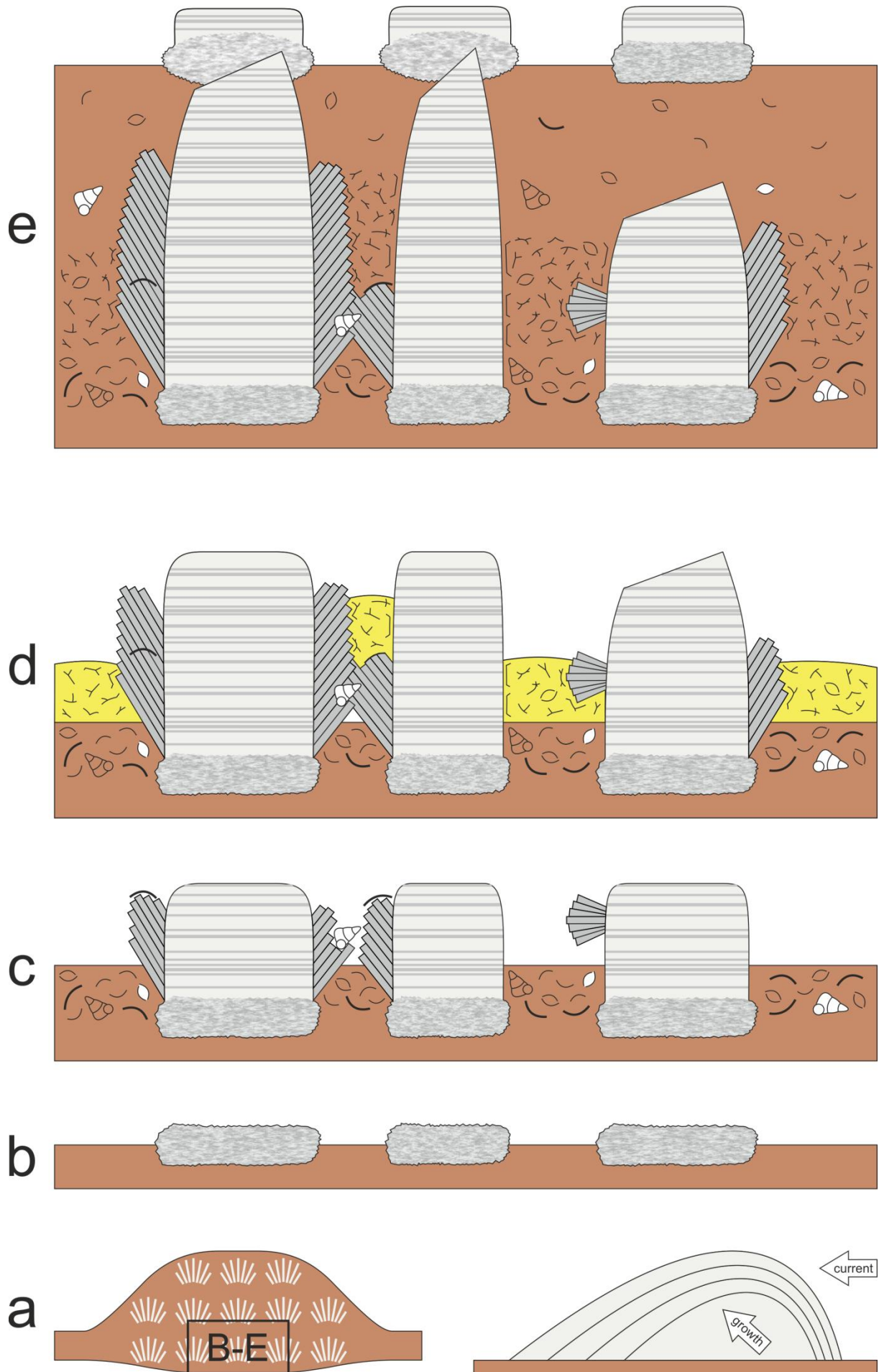
**← Fig. 38:** A model explaining the formation of the CCFs and microbialites. **(a)** The growth forms of the microbialites. The right picture shows the asymmetrical growth of the giant microbialites that was caused by a bottom current. The left picture shows a mound from the CCFs. The cycle of crystal growth is indicated. **(b) – (e)** Stage 1 to 4 of crystal growth. For explanation see text.

As already mentioned before, the sponge spicules that fit perfectly to the crystal margins indicate that the laminated crystals and microbialites must have grown before the sponges settled down. Furthermore, it seems that the occurrence of sponges within the microbialites and CCFs is irregular. On the one hand the crystals can be completely surrounded by sponges. On the other hand sponges surrounding the crystals of the very same microbialite or CCF can be less abundant or even completely absent. For all this reasons it can be concluded that the sponges were not necessary for the appearance, the formation and the growth of both the microbialites and the CCFs.

At a PTB section in the Julfa region (northwest Iran) sponges resembling the ones from type 1 already occur in the latest Permian *Paratirolites* Limestone as well as in the Boundary Shale without any microbialites (Leda et al. 2014). Therefore it can be concluded that the sponges and the microbialites were independent from each other. Leda et al. (2014) say that the irregularly distributed spicules must have been reworked prior to final deposition. They also present a picture from the topmost *Paratirolites* Limestone showing micrite pebbles of the micrite-clast wackestone underlying the sponge packstone horizon (Fig. 9c from Leda et al. 2014). They interpret the clasts to have been reworked and transported to the sponge packstone horizon but in my opinion the sponge spicules seem to enclose the micrite pebbles and fit perfectly to their margins and it seems that the sponges adjusted their shape to the micrite pebbles containing substrate. This confirms my assumption that the sponges adjusted their shape to the available space between the microbialites and that the irregularly distributed spicules were originally arranged in this way.

Some sponge spicules were pierced by crystals of type 2 indicating that the sponges must have grown before these crystals (Fig.39). On the other hand some sponge spicules also fit perfectly to these crystal's margins. For this reason it cannot be said for sure whether the crystals of type 2 developed before the sponge's appearance or afterwards. It is also possible that the growth of both the crystals of type 2 and the sponges happened simultaneously.

It is conspicuous that the sponges are restricted to the CCFs and microbialites (Fig. 17). The only exception could be sample 50 from Zangakatun. This suggests that the sponges should have benefited from the presence of the CCFs and microbialites but it is not clear in which way. It is possible that the microbialites provided food or nutrients for the sponges.
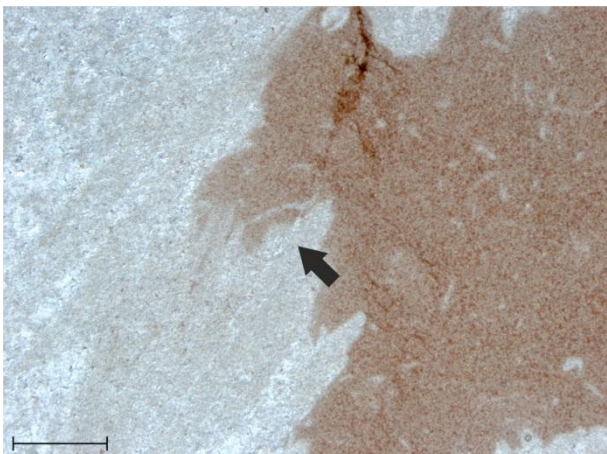


**Fig. 39:** Sponge spicule that was pierced by a crystal of type 2 (black arrow). Sample 17. Scale bar = 1 mm.

Since the CCFs are for the most part preserved in their upward position I believe that the sponges were important to give these elongated crystals stability and prevented them to immediately fall over during storm events. Nevertheless, some storms were strong enough to overturn the CCFs together with the surrounding sponges. Furthermore, broken pieces of crystals were found in a breccia.

## 6.3. Comparison of the $\delta^{13}C_{sediment}$ Curve with others

C isotope studies in Vedi and Zangakatun have already been published by Baud et al. (1989) and Zakharov et al. (2005). Although my $\delta^{13}C$ curve has a higher resolution, all curves show the same trend. However, the $\delta^{13}C$ values of this study are more negative. The positive peak P5 is not recorded in Baud et al. (1989) and Zakharov et al. (2005).

Richoz et al. (2010) performed a high-resolution C isotope study on different sections in Iran and Oman. They were able to discriminate nine successive isotopic events (IE 0-8) which can be correlated with some of the isotopic excursions in Zangakatun although the conodont zones do not always correlate well. Richoz et al. (2010) separated the negative excursions in four distinct parts:

1) A first drop in the Late Wuchiapingian (IE 0). This drop is not seen in the $\delta^{13}C$ curve of this study because it starts higher up in the section but it can be seen in the studies from Baud et al. (1989) and Zakharov et al. (2005).

2) A second decrease (IE 1-2) starts at the base of the Changhsingian *Dzhulfites* ammonoid beds and continues gradually until the extinction event. No important second order variations have been detected. IE 1 starts in the lower *Dzhulfites* beds with a gentle slope until the *Paratirolites* beds and then becomes more rapid until the top of the *C. iranica* zone. This regular decrease reaches a first minimum (IE 2) at the top of the *C. jolfensis* zone. This zone corresponds to the lithological boundary as well as to the event boundary and is the same as the *C. hauschkei* zone in Zangakatun. Richoz et al. (2010) term the decrease between IE 1 and IE 2 pre-extinction event decrease.

In Zangakatun the $\delta^{13}C$ values start to decrease until N1, which lies within the *C. iranica* zone but in the same zone the $\delta^{13}C$ values start to rise again. N2, in contrast to IE 2, does not lie in the *C. hauschkei* (=*C. jolfensis*) zone but in the overlaying *C. meishanensis – H. praeparvus* zone and is also overlaying the Boundary Shale and therefore the mass extinction event. It cannot be excluded that the extremely negative $\delta^{13}C$ value of N2 is of diagenetic origin. The negative excursion between N1 and N2 lies within the *C. hauschkei* zone and could correspond to IE 2.

3) Stationary to slightly increasing values for the first part of the *C. meishanensis – H. praeparvus* zone (IE 2 to IE 3). IE 3 is a slight increase or a plateau of the $\delta^{13}C$ values. Its maximum increase lies within the *C. meishanensis – H. praeparvus* zone.

After N2 the $\delta^{13}C$ values in Zangakatun increase in the *C. meishanensis – H. praeparvus* zone but the most positive peak (P1) lies at the base of the overlaying *H. parvus* zone.

4) A post-extinction event decrease (IE 3 to IE 7) that shows several second-order variations. It starts at the top of the *C. meishanensis – H. praeparvus* zone and reaches its minimum in the *I. isarcica* zone. After the IE 3 maximum follows a decrease. The minimum of this drop (IE 4) lies within the lower part of the *H. parvus* zone and could correspond to N3, which follows the positive excursion P1 and also lies within the *H. parvus* zone. IE 5 and IE 6 are two small positive peaks following IE 4, whereas the minimum reached after IE 6 is always lower than the one from IE 4. IE 5 could be represented in Zangakatun by the positive peaks P2 and P3. P4 probably corresponds to IE 6

because the following peak N6 is more negative than N3. IE 7 is the minimum of the negative C isotope excursion. It corresponds to the lower part of the *I. isarcica* zone and is not seen in Zangakatun.

IE 8 is a positive excursion that starts within the *I. isarcica* zone and can be correlated with the plateau reached in Zangakatun's isotope interval 5.

The first CCFs in Iran reported by Richoz et al. (2010) occur after the positive excursion IE 3. Because the first appearance of the Armenian CCFs happened simultaneously with P1, which happened before IE 3, the Armenian CCFs appeared before the ones in Iran.

## 6.4. The Difference between the $\delta^{13}C_{sediment}$ and $\delta^{13}C_{crystal}$ Values in the lower Microbialites

Present-day and fossil stromatolites commonly display the isotopic signatures of both the surrounding sediment as well as the primary microbial biomass (Schidlowski 2000). A small isotopic difference between the microbialites and the surrounding matrix C isotope signatures means that the microbialites grew in isotopic equilibrium with the surrounding seawater. This is true for the upper thrombolites and dendrolites that formed during the second microbial growth phase in which the maximum difference between $\delta^{13}C_{sediment}$ and $\delta^{13}C_{crystal}$ is only 0.4‰. However, the laminated crystals and the other microbialites that formed during the first microbial growth phase show a difference between the $\delta^{13}C_{sediment}$ and $\delta^{13}C_{crystal}$ values of up to 2.3‰. C isotope studies on PTBMs in China showed little differences (<0.5%) between the $\delta^{13}C$ values of microbialite branches and adjacent micritic sediment (Mu et al. 2009, Kershaw et al. 2012, Collin et al. 2014). Isotope studies from Neoproterozoic CCFs from Brazil showed no significant differences between $\delta^{13}C_{crystal}$ and $\delta^{13}C_{matrix}$ (Vieira et al. 2015) and also Paleoproterozoic CCFs from Canada and middle Ediacaran CCFs from the USA show little isotopic difference between the crystals and the surrounding matrix (Bergmann et al. 2013). A comparison of stromatolitic micrite and cements of Proterozoic age (about 900 Ma) from Mauritania also revealed that no biologically-related $^{13}C$ fractionation occurred (Fairchild et al. 1990). So, what is the reason for the isotopic fractionation in the lower microbialites?

One possibility is that diagenetic processes led to a fractionation and caused the differences between $\delta^{13}C_{sediment}$ and $\delta^{13}C_{crystal}$. According to Chilingar et al. (1967) changes in isotopes are commonly assumed with pseudomorphosis, recrystallization and possible grain growth. The thin section analyses showed that pseudomorphosis and recrystallization undoubtably took place. Other evidences for diagenesis are the formation of stylolites and dolomitization. In fact, dolomitization is very small and the dolomite crystals found in the sediment could also be allochthonous. The results from the cathodoluminescence show zoned sub-crystals within the laminated crystals of the CCFs with up to four zones meaning four phases of recrystallization. The sub-crystals of the upper microbialites do not show so many zones, meaning less phases of recrystallization. Even if more phases of recrystallization led to a stronger fractionation on the $\delta^{13}C_{crystal}$ values of the lower microbialites it is unlikely that only recrystallization would cause such a big difference between the $\delta^{13}C_{sediment}$ and $\delta^{13}C_{crystal}$ values. Apart from this, the cross-plot from the $\delta^{13}C$ and $\delta^{18}O$ values does not show any diagenetic overprint. Therefore, diagenesis probably did not cause the difference between $\delta^{13}C_{sediment}$ and $\delta^{13}C_{crystal}$.

It is conspicuous that the difference between $\delta^{13}C_{sediment}$ and $\delta^{13}C_{crystal}$ occurs in the microbialites, which are mostly surrounded by sponges of type 1 and 2. It is possible that the microbialites did grow in isotopic equilibrium with the ambient seawater and the sponges caused a fractionation. This

would mean that the $\delta^{13}C$ values from the microbialites represent the $\delta^{13}C$ values of the seawater and the $\delta^{13}C$ signal of the sediment is actually an altered $\delta^{13}C$ sponge signal. However, isotope analyses on sediment containing sponge spicules as well as sediment without sponge spicules revealed that the differences between these two $\delta^{13}C$ values are 0‰ and 0.2‰. Furthermore, the upper microbialites that are surrounded by sponges do not show such big differences between $\delta^{13}C_{sediment}$ and $\delta^{13}C_{crystal}$ values. Moreover, several C and O isotope studies on modern sclerosponges from Jamaica (Druffel and Benavides 1986), chaetetid sponges (Reitner and Gautret 1996), demosponges from the Caribbean and Coral Sea (Böhm et al. 1996) and Caribbean coralline sponges (Böhm et al. 2000) showed that all these sponges grew in isotopic equilibrium with the ambient seawater. Isotopic equilibrium in the skeletons of most coralline sponges was also shown by several authors (Druffel and Benavides 1986, Reitner 1992, Joachimski et al. 1995, Wörheide 1998). Also fossil demosponges and coralline sponges show no significant fractionations, although there are exceptions in some calcareous sponges (Calcinea; Reitner J., personal communication, 11. 01. 2016). For all these reasons it is not likely that the sponges from type 1 and 2 are the reason for the difference between $\delta^{13}C_{sediment}$ and $\delta^{13}C_{crystal}$ values. That means that the $\delta^{13}C_{sediment}$ values represent the $\delta^{13}C$ signals from the surrounding seawater and that the fractionation of the $\delta^{13}C_{crystal}$ values must have another reason.

Abiotic as well as biotic processes that lead to the precipitation of carbonate influence their C and O isotopic composition (Léveillé et al. 2007, Brady et al. 2010, Power et al. 2011). The phototrophic community of microbial mats typically consists of cyanobacteria, whereas the heterotrophic community includes anaerobes, such as sulfate-reducing bacteria (SRB) and methanogenic bacteria (Visscher et al. 1991, Pierson et al. 1992, Bauld et al. 1992, Des Marais 1995, Stal 2000, Visscher et al. 2000, Buckley et al. 2008, Dupraz et al. 2009). Both autotrophic and heterotrophic metabolisms can influence the concentration and isotopic composition of the dissolved inorganic carbon (DIC; Merz 1992, Andres et al. 2006, Breitbart et al. 2009, Brady et al. 2010). Carbonates that precipitate from this DIC record the DIC's $\delta^{13}C$ values, including any microbial effects on the DIC's isotopic composition. Heterotrophic activity during the degradation of organic matter leads to a depletion of $^{13}C$ in the residual DIC (Burne and Moore 1987, Guo et al. 1996, Thompson et al. 1997, Sumner 2001, Brady et al. 2010). Breitbart et al. (2009) report from modern freshwater microbialites in Cuatro Ciénegas (Mexico) in which the DIC is depleted in $^{13}C$ due to heterotrophic respiration of photoautotrophic biomass. Because of the abundance of sulfate and the genomic and isotopic evidence for sulfate reduction they concluded that sulfate reduction was the dominant heterotrophic process influencing microbialite precipitation. During photosynthesis $^{12}C$ is preferentially incorporated into the cell biomass resulting in a $^{13}C$-enrichment of the residual DIC (O'Leary 1988, Brady et al. 2010). This means that photosynthetic activity can result in carbonates that are enriched in $\delta^{13}C$. Such carbonates are not only reported from freshwater lakes with high levels of photosynthetic activity (Hollander and McKenzie 1991, Thompson et al. 1997, Brady et al. 2010) but also from saline ponds, shallow lakes with high methane production and hot spring travertines (Guo et al. 1996, Valero-Garcés et al. 1999, Gu et al. 2004, Brady et al. 2010). Guo et al. (1996) investigated modern and early Holocene to Pleistocene hot-spring travertine carbonates from central Italy that among others consist of crystalline shrubs. These crystalline shrubs have $\delta^{13}C$ values that are 0.5-6‰ higher than values from associated abiotic precipitates. They assume that this difference is probably due to microbial activity. Thompson et al. (1997) reported from annual whiting events in Fayetteville Green Lake (New York). The $\delta^{13}C$ values of DIC show a seasonal variability and vary between -9.5‰ in winter and -6.2‰ in summer. The enrichment of 2.3‰ during summertime is caused by the photosynthetic activity of cyanobacterial picoplankton. Brady et al. (2010) showed that carbonate

$\delta^{13}$C values from micro-stromatolitic nodules, in association with freshwater microbialites, from Pavilion Lake (British Columbia) are enriched by up to 3.6‰ (1-2‰ on average) compared to predicted abiotic carbonate $\delta^{13}$C values from measured DIC. $\delta^{13}$C values of microbial photosynthetically influenced precipitations within the nodule's microenvironment were consistent with the enriched $\delta^{13}$C values. According to their opinion the enriched $\delta^{13}$C values represent biosignatures that formed through a predominance of photosynthetic influences over heterotrophic influences and are caused by microbial activity rather than physical processes. The already mentioned columnar microbialites with an internal spherulitic fabric investigated by Power et al. (2011) show isotopic differences between aragonite associated with biomass and aragonite without biomass. The $\delta^{13}$C values of aragonite associated with biomass are enriched by 0.8‰ compared to $\delta^{13}$C values of aragonite without biomass. They suggest that this difference is caused by the modest removal of isotopically light DIC by phototrophs. They further assume that photosynthesis is a key process in initiating aragonite precipitation.

The activity of phototrophs seems to be the most plausible explanation for the difference between $\delta^{13}$C$_{sediment}$ and $\delta^{13}$C$_{crystal}$ in the microbialites and CCFs that formed during the first microbial growth phase. But that does not automatically mean that there was no photosynthesis in the upper microbialites. A study from Andres et al. (2006) on modern Bahamian stromatolites shows spatial associations from Cyanobacteria with aragonite containing heterotrophic isotope signatures. They suggested that more aragonite precipitated when and where respiration influenced local DIC and not during peak photosynthesis, whereas respiration is consistent with sulfate reduction and EPS (extracellular polymeric substance) release of Ca$^{2+}$ during decay. Andres et al. (2006) further suggest that the absence of an autotrophic isotope signature in the rock does not imply the absence of photosynthetic organisms. Therefore, it is probable that the upper microbialites, in contrast to the microbialites and CCFs from the first microbial growth phase, precipitated during phases when photosynthesis had less influence than heterotrophic processes, such as sulfate reduction.

## 6.5. The Formation of the laminated Crystals from the Calcium Carbonate Crystal Fans

CCFs are already known from other PTB sections around the world (Leda et al. 2014) such as North America (Woods et al. 1999, Pruss et al. 2005, Woods and Bottjer 2000, Woods 2005), China (Kershaw et al. 1999), Iran (Heydari et al. 2000, Richoz et al. 2010) and Oman (Baud et al. 2007). According to Leda et al. (2014) they have already been interpreted as thrombolites (Taraz et al. 1981, Heydari et al. 2000, 2001), digitate or branching laminated stromatolites (Baud et al. 2005a, 2005b, 2007), microbialites (Fang 2005), dendrolites (Richoz 2006), synsedimentary seafloor carbonate cements (Heydari et al. 2003, 2008) or carbonate seafloor-precipitated fans (Richoz et al. 2010). It is still debated whether CCFs are of biotic or abiotic origin and whether their formation conditions were oxic or anoxic (e.g., Woods et al. 1999, 2007, Wignall and Twitchett 2002, Heydari et al. 2000, 2001, 2003, 2008, Wignall et al. 2005, Leda et al. 2014). Several authors (Knoll et al. 1996, Kershaw et al. 1999, Woods et al. 1999, 2007, Heydari et al. 2003, Pruss and Bottjer 2004, Leda et al. 2014) suggested that CO$_2$ degassing from the upwelling of CaCO$_3$ supersaturated anoxic waters caused by bacterial sulphate reduction resulted in the formation of CCFs. Woods et al. (1999) interpreted the CCFs as inorganic and synsedimentary cements whose precipitation took place at the interface between anoxic and oxygenated water masses (Leda et al. 2014). Precipitation and preservation of carbonates can also be promoted by increased chemical weathering processes on land, which lead to

an enhanced $Ca^{2+}$ and $HCO_3^-$ input into the oceans (Leda et al. 2014). Because no obvious anoxia has been recorded in the PTB sections in Iran (Heydari et al. 2003, Kozur 2005, 2007, Richoz 2006) Leda et al. (2014) assumed that enhanced silicate weathering resulting in an increased total alkalinity is the reason for the formation of the CCFs. They further suggest that pulses of $CaCO_3$ oversaturation explain the synsedimentary formation of the CCFs and that $CaCO_3$ supersaturated water also promoted the recrystallization of the matrix and/or precipitation of the crystals. According to Clarkson et al. (2015) not only silicate weathering but also increased pyrite deposition, increased carbonate weathering and a decrease in shallow marine carbonate depositional area could have caused an increase in alkalinity.

Exclusively based on mineralogical and textural data it is not possible to distinguish whether carbonate precipitation was induced by abiotic processes (e.g. $CO_2$ degassing, evaporation, changes in temperature, dissolution, re-precipitation) or biotic processes (e.g. photosynthesis, methanogenesis, sulfate reduction; Léveillé et al. 2007, Power et al. 2011). Because of the fine laminated texture of CCF crystals that bind micrite and micropeloids Baud et al. (2007) interpreted the CCFs to be biotic and microbial in origin. Because of the bound micrite and micropeloids as well as the wavy lamination the CCFs could be stromatolites but the shape of these crystals is not typical for stromatolites. Their shape would better fit to the idea that these crystals formed synsedimentary on the seafloor due to $CaCO_3$ supersaturation. But as Leda et al. (2014) already mentioned, the lamination of the crystals cannot be explained easily by inorganic, spontaneous calcite crystal growth because in this case the lamination would not be wavy but straight. In my opinion the laminated crystals are synsedimentary calcium carbonate crystals that were influenced by phototrophic microorganisms. The presence of phototrophic microbes led to the wavy lamination as well as to the C isotope signatures of these crystals. Apart from that, photosynthesis under supersaturation could be a key factor in the initiation of the formation of the CCFs, but the exact reason for the required $CaCO_3$ oversaturation of the ambient seawater to form these crystals is still uncertain.

The mottled base of the crystals could be microbialites that acted as nucleation sites for the laminated crystals. The idea is that the change from the mottled structure at the base to the laminated one could represent a change in the microbial community, meaning that at the beginning the microbialites were dominated by heterotrophs and later by phototrophs (Peckmann J. and Richoz S., personal communication). In this case the $\delta^{13}C_{laminated}$ values should be more positive than the $\delta^{13}C_{mottled}$ values. In fact the $\delta^{13}C_{laminated}$ values are mostly more negative than the $\delta^{13}C_{mottled}$ values, therefore the $\delta^{13}C$ values do not show such a change in the microbial community. Another possibility is that the microbial community that formed the mottled part of the crystals as well as the microbial community that formed the laminated part were both dominated by phototrophs but the rest of the microbial community changed, which resulted in the change from the mottled to the laminated microstructure. It is also possible that not the microbial community but the environmental conditions changed and caused the change of the microstructure. Nevertheless, it is not clear why only the crystals of type 1 show a lamination and not the co-occurring other crystal types.

When the laminated crystals of type 1 really represent some kind of stromatolites the darker laminae could contain some organic matter. In this case the darker laminae must have been brighter under the fluorescence microscope but in fact they were not. This would indicate that there is no organic matter in the darker layers of the laminated crystals. It should be pointed out that the results from the fluorescence microscopy are not completely trustworthy because the magnification was probably not high enough. This means that not the real signal from the sample but extraneous fluorescence or internal reflections or refractions of the fluorescent light was seen under the microscope.

Unfortunately it was not possible to compare $\delta^{13}C$ values from the darker and brighter laminae because it was not possible to distinguish them in the hand specimen. Instead laminated crystals from two samples were analysed to see whether heterogeneities within the crystals exist. The $\delta^{13}C$ values indeed vary within the crystals but these variations are small (maximal 0.3‰). Isotopic heterogeneity was also reported from the Late Dienerian to Early Smithian calyx-shaped CCFs (Heindel et al. 2013) and within crusts from modern Bahamian stromatolites (Anders et al. 2006).

## 6.6.   Palaeoenvironmental Conditions

The micritic matrix is an indication to low wave energies but in contrast to that the accumulations of organisms as well as brecciated crystals indicate high-energy conditions and are probably the results of storm events. That means that the microbialites were formed below the fair-weather wave base and above the storm wave base. Because the outcrop in Vedi contains more shale layers the microbialites in Vedi were probably formed in deeper water depths than the ones from Zangakatun and Ogbin. Furthermore, the missing accumulations of organisms in Vedi possibly indicate that these carbonates were already deposited below the storm wave base. According to Kershaw et al. (2012) the maximum depth of PTBMs seems to be deeper than the pre-extinction Permian reefs but an exact determination of the depth is not possible.

There are strong indications of low-oxygen processes across the PTB extinction event (Kershaw et al. 2012) and at the main locations of PTBMs, namely the Palaeotethys (Kershaw et al. 2007) and the Neotethys (Baud et al. 2005a, 2007), evidences for low-oxygen conditions exist (Bond and Wignall 2010, Chen et al. 2011, Liao et al. 2010, Forel 2013). Such evidences are pyrite framboids (Bond and Wignall 2010) that are described in many low-oxygen areas around the world (Kershaw et al. 2012). Liao et al. (2010) gave the first evidence of pyrite framboids within PTBMs. They found these pyrite framboids in both the microbial branches as well as in the surrounding micrite. However, microbialites are often associated with organisms like ostracods (e.g. Crasquin-Soleau et al. 2004a, 2004b, 2006, Crasquin-Soleau and Kershaw 2005, Forel et al. 2009, 2013a, 2013b, Forel 2012, 2013), micro-gastropods and micro-brachiopods, foraminifers, bivalves, ammonoids and conodonts (e.g. Baud et al. 1997, Groves et al. 2005, Richoz 2006, Brühwiler et al. 2008, Ezaki et al. 2008, Kaim et al. 2010, Hautmann et al. 2011, Frisk et al. 2012, Forel 2013). Some of these shelly fossils are encased within PTBMs (Yang et al. 2011, Kershaw et al. 2012), which is also the case in the Armenian microbialites. All these organisms needed oxygen to survive and therefore contradict the idea of total anoxia (Kershaw et al. 2012, Forel 2013). One possible solution for this contradiction is that the shallow-marine environment in which the PTBMs formed was oxygenated but experienced episodic upwelling of low-oxygenated water or rises in the chemocline causing anoxic conditions in which the pyrite framboids were formed (Kershaw et al. 2012). Another explanation could be that rapid changes in oxygenation, which allowed shelly faunas to develop when oxygen levels were generally higher, whereas microbialite's calcium carbonate formed during periods of low oxygen levels (Kershaw et al. 2012). A third explanation for the co-occurrence of pyrite framboids and shelly fossils could be that pyrite framboids formed in anoxic deep water and then were upwelled. If the upwelled water carried suspended pyrite framboids up into the mixed layer advective currents could have drawn them to the shelf areas where they have been deposited in aerated sediments. When the pyrite framboids were buried quickly by active sedimentation on the shelf, e.g. from sediment precipitation, the preservation of these framboids is likely (Kershaw 2015). Lethiers and Whatley (1994) used ostracod faunas to estimate the levels of oxygenation. They concluded that the ostracod

faunas associated with PTBMs reflect dysoxia but the ostracod faunas that lived after the formation of PTBMs indicate oxic conditions (Forel 2013). However, the PTBMs may have grown in dysoxic water but the photosynthetic activity of the microbial community possibly created an oxygenated micro-environment in which the benthic organisms where able to survive (Kershaw et al. 2012, Forel 2013). Such a case is reported from Gingras et al. (2011) from microbial mats in a hypersaline lagoon in Venezuela. There are raised oxygen levels in association with the microbial mats but the overlying water as well as the underlying sediment are both poorly oxygenated. The fossil distributions, especially the ones from Zangakatun and Ogbin, show that the fauna associated with microbialites and CCFs is more diverse and also comprises a higher number of organisms. This matches the theory that the microbialites growing in dysoxic water created a micro-environment with better conditions for the associated organisms. Nevertheless, organisms also occur in sediments without microbial carbonates, therefore oxic conditions must have been present. Bioturbation, not only visible in the field but also in some thin sections, indicate that the sediment must have been, maybe not always but at least episodically, well oxygenated.

Ocean acidification was proposed as one mechanism that led to the end-Permian mass extinction (EPE; Payne et al. 2010). However, studies on B isotopes from Clarkson et al. (2015) from two locations in the United Arab Emirates revealed that pH increased in the Upper Permian and then remained relatively stable into the early Griesbachian, meaning that pH was relatively stable during the first extinction pulse in the Upper Permian as well as during the period of C cycle perturbations. They further recorded a rapid decrease of $\delta^{11}B$ after the $\delta^{13}C$ increase that coincides with the second extinction pulse, which in turn coincides with the temporary loss of abiotic and microbial carbonates throughout the Tethys (Baud et al. 2007, Richoz et al. 2010, Clarkson et al. 2015). The sharp drop of pH of around 0.6-0.7 is recorded at the base of the *I. isarcica* conodont zone. After this rapid decrease in pH the $\delta^{11}B$ values quickly reached values nearly as high as before the decrease (Clarkson et al. 2015). For Armenia this means that the pH stayed stable during the Permian-Triassic transition and during the first microbial growth phase. The *I. isarcica* zone comprises most of the interval between both microbial growth phases, therefore a decreased pH could be a reason for the absence of microbialites. A somewhat lower pH during the second microbial growth phase than during the first one could be a possibly explanation for the fact that during the second microbial growth phase no CCFs were formed. When pH was already higher during the Upper Permian, what is the reason why the CCFs only grew in the Lower Triassic and not in the Upper Permian? Baud et al. (2007) proposed that the extinction of skeletal metazoans was enough to promote the formations of PTBMs and $CaCO_3$ supersaturation was not necessarily needed (Kershaw et al. 2012). In this case a further small increase in pH could have led to the formation of the CCFs. This would explain why CCFs did not already form in the Upper Permian before the EPE. The fact that CCFs do not occur in all PTB sections could further imply that a global supersaturation was necessary but not sufficient to produce the CCFs and that other factors have to be deciphered. This is confirmed by the study from Clarkson et al. (2015) since there are no CCFs in the United Arab Emirates although pH values were elevated.

## 6.7. A Model explaining the Formation of the Calcium Carbonate Crystal Fans and the Microbialites

With all these information I tried to reconstruct the formation of the CCFs and the microbialites. The four stages of the model are illustrated in Fig. 38b-e.

Stage 1: Microbialites started to grow on the sediment surface and produced a mottled internal fabric.

Stage 2: $CaCO_3$ supersaturation caused the formation of synsedimentary crystals of type 1 that used the microbialites as nucleation sites. The exact reason for this $CaCO_3$ supersaturation is not clear. The activity of photoautotroph microorganisms caused both the lamination of the crystals and the fractionation of the C isotopes. Crystals of type 2 started to grow soon after the laminated crystals of type 1. This is supported by the $\delta^{13}C$ values of the crystals from type 2 that are more similar to the $\delta^{13}C$ values from the laminated crystals of type 1 than the surrounding sediment. The crystals of type 2 sometimes coalesced, which caused the wall-like arrangement of the crystals seen in thin sections cut perpendicular to the crystals growth direction. Some organisms, mainly ostracods, foraminifers and gastropods lived in the space between the crystals. During a storm event organisms were accumulated between the crystals. Some of these organisms lay down on the crystals.

Stage 3: Both the crystals from type 1 and 2 continued to grow and sometimes enclosed organisms. Some organisms were not enclosed but stopped the crystal's growth. The sponges settled down on the accumulations of organisms and started to fill the spaces between the crystals. While doing this they adjusted their shape to the available space and their spicules to the crystal margins.

Stage 4: The crystals from type 1 and 2 continued to grow and partly enclosed the sponge spicules. This could have happened while the sponges were still alive. Nevertheless, after their death the sponges were covered by sediment fast enough to preserve the original position of their spicules. After some time of sedimentation the microbialites settled down on the sediment as well as on the crystals and the whole cycle started again.

Even if this model shows only the formations of the crystals from the CCFs it is also valid for the co-occuring microbialites as well as for the microbialites that formed during the second microbial growth phase. It should be pointed out that the accumulations of organisms do not occur between all crystals of type 1 and 2 and microbialites. In fact they are very rare. In this case the sponges did not settle down on these accumulations but only on the sediment and possibly also on the microbialites. In other samples the laminated crystals and microbialites are completely surrounded by sponges and the overlaying sediment layer is missing, meaning that the sponges were not covered by sediment. There are also samples in which the sponges are missing and the laminated crystals and microbialites are completely surrounded by sediment. Furthermore, the cyclicity of the events described above, which is also indicated in Fig. 38a (left), was only observed in a few samples.

# 7. Conclusion

The PTBMs and CCFs from the three investigated outcrops in Armenia formed during two microbial growth phases in the Griesbachian. The thrombolites, dendrolites and CCFs formed banks as well as mound with variable internal structures. The microbialites that flourished during the first microbial growth phase co-occur with CCFs. The laminated crystals of the CCFs are possibly synsedimentary calcium carbonate crystals that were influenced by photoautotroph microorganisms. The laminated crystals formed due to a $CaCO_3$ supersaturation of the ambient seawater and used microbialites as nucleation sites. The activity of photoautotrophs did not only cause the wavy lamination of the crystals but also their enrichment in the heavier $^{13}C$. The exact reason for the $CaCO_3$ supersaturation is still uncertain.

Thin section analyses revealed that the CCFs and microbialites formed on the sediment surface between the fair-weather wave base and the storm wave base. During their formation anoxic conditions were not reached but periodical dysoxia cannot be excluded. The micritic matrix contains sponges, ostracods, foraminifers of the genus *Earlandia* and *Rectocornuspira*, gastropods, bivalves and ammonoids.

It seems that the sponges were not necessary for the initiation and formation of the microbialites. Sponge spicules that fit perfectly to the crystal margins indicate that the sponges settled down after the growth of microbialites and CCFs. They had to adjust their shape to the available space between the microbialites and CCFs as well as their spicule morphologies to the crystal margins. Because sponges are almost restricted to CCFs and microbialites it can be concluded that the microbialites provided some advantages to the sponges, which still have to be understood in detail. Furthermore, sponges were important for the stability of the CCFs.

C isotope studies showed that the $\delta^{13}C_{sediment}$ curve from Zangakatun is comparable with previous C isotope studies of this outcrop. Furthermore, the $\delta^{13}C_{sediment}$ curve can be well correlated with C isotope curves from Iran and Oman. A comparison between the $\delta^{13}C_{sediment}$ and the $\delta^{13}C_{crystal}$ values showed that the microbialites that formed during the second microbial growth phase grew in isotopic equilibrium with the ambient seawater, whereas the CCFs and the microbialites that formed during the first microbial growth phase show more positive $\delta^{13}C$ values than the corresponding micrite. This difference between the $\delta^{13}C_{sediment}$ and $\delta^{13}C_{crystal}$ values is probably due to the activity of photoautotrophs. The second phase of microbialites possibly shows a higher proportion of heterotroph organisms in the microbial community or a smaller supersaturation of the ambient seawater.

# 8. References

**Aguliar M.I., Osendi M.L. (1982):** *Fluorescence of Mn$^{2+}$ in CaCO$_3$.* Journal of Luminescence 27, 365-375

**Algeo T.J., Chen Z.Q., Fraiser M.L., Twitchett R.J. (2011):** *Terrestrial-marine teleconnections in the collapse and rebuilding of Early Triassic marine ecosystems.* Palaeogeography, Palaeoclimatology, Palaeoecology 308, 1-11

**Algeo T.J., Twitchett R.J. (2010):** *Anomalous Early Triassic sediment fluxes due to elevated weathering rates and their biological consequences.* Geology 38, 1023-1026

**Andres M.S., Sumner D.Y., Reid R.P., Swart P.K. (2006):** *Isotopic fingerprints of microbial respiration in aragonite from Bahamian stromatolites.* Geology 34, 973-976

**Atudorei N.-V. (1999):** *Constraints on the Upper Permian to Upper Triassic marine carbon isotope curve: case studies from the Tethys.* PhD Thesis, Lausanne University, p. 155

**Barrier E., Vrielynck B. (2008***): Palaeotectonic map of the Middle East, Atlas of 14 maps, Tectonosedimentary-Palinspastic maps from Late Norian to Pliocene.* Commission for the Geologic Map of the World (CCMW, CCGM), Paris, France

**Basu A.R., Petaev M.I., Poreda R.J., Jacobsen S.B., Becker L. (2003):** *Chondritic meteorite fragments associated with the Permian-Triassic boundary in Antarctica.* Science 302, 1388-1392

**Baud A. (1998):** *Marine carbonate and siliceous factories: global Change after the end of Permian Mass Extinction.* 15th International Sedimentological Congress Alicante (Spain), Abstract book, p. 180

**Baud A., Atudorei V., Richoz S. (2005a):** *Sea-floor carbonate fans and calcimicrobial mounds in the lower Triassic red limestone of the Alwa formation, baid Exotic, Eastern Oman Mountains.* In: IAS (ed.): 24$^{th}$ IAS meeting of sedimentology, Muscat, Oman, p. 31

**Baud A., Atudorei V., Sharp Z. (1996):** *Late Permian and Early Triassic evolution of the Northern Indian margin: carbon isotope and sequence stratigraphy.* Geodinamica Acta 9, 57-77

**Baud A., Cirilli S., Marcoux J. (1997):** *Biotic response to mass extinction: the lowermost Triassic microbialites.* Facies 36, 238-242

**Baud A., Magaritz M., Holser W.T. (1989):** *Permian-Triassic of the Tethys: Carbon isotope studies.* Geologische Rundschau 78 (2), 649-677

**Baud A., Richoz S. (2004):** *The Lower Triassic microbialites and precipitates: environmental control, distribution in space and time.* In: Camoin G., Gautret P. (eds.): Microbialites and microbial communities in sedimentary systems, Publications AST, Paris, 15-17

**Baud A., Richoz S., Marcoux J. (2005b):** *Calcimicrobial cap rocks from the basal Triassic units: western Taurus occurrences (SW Turkey).* Comptes Rendus Palevol 4, 569-582

**Baud A., Richoz S., Pruss S. (2007):** *The lower Triassic anachronistic carbonate facies in space and time.* Global and Planetary Change 55, 81-89

**Bauld J., D'Amelio E., Farmer J.D., (1992):** *Modern microbial mats.* In: Schopf J.W., Klein C. (eds.): The Proterozoic Biosphere. Cambridge University Press, NewYork, 261-270

**Bazhenov M., Burtman V. S., Levashova N. (1996):** *Lower and Middle Jurassic paleomagnetic results from the south Lesser Caucasus and the evolution of the Mesozoic Tethys Ocean.* Earth and Planetary Science Letters 141, 79-89

**Becker L., Poreda R.J., Basu A.R., Pope K.O., Harrison T.M., Nicholson C., Iasky R. (2004):** *Bedout: a possible end-Permian impact crater offshore of northwestern Australia.* Science 304, 1469-1476

**Becker L., Poreda R.J., Hunt A.G., Bunch T.E., Rampino M. (2001):** *Impact event at the Permian-Triassic boundary: Evidence from extraterrestrial noble gases in fullerenes.* Science 291, 1530-1533

References

**Belov A.A., Bragin N.Y., Vishnevskaya V. S. Satian M. A., Sokolov S. D. (1991):** *New data about the age of the ophiolites of Vedi (Armenia).* Reports of the USSR Academy of Science 321, 784-787 (in Russian)

**Bergmann K.D., Grotzinger J.P., Fischer W.W. (2013):** *Biological influences on seafloor carbonate precipitation.* Palaios 28, 99-115

**Berner R.A. (2002):** *Examination of hypotheses for the Permo–Triassic boundary extinction by carbon cycle modeling.* Proceedings of the National Academy of Sciences 99, 4172-4177

**Birgel D., Elvert M., Han X., Peckmann J. (2008):** *$^{13}$C-depleted biphytanic diacids as tracers of past anaerobic oxidation of methane.* Organic Geochemistry 39, 152-156

**Birgel D., Thiel V., Hinrichs K.U., Elvert M., Campbell K.A., Reitner J., Farmer J.D., Peckmann J. (2006):** *Lipid biomarker patterns of methane-seep microbialites from the Mesozoic convergent margin of California.* Organic Geochemistry 37, 1289-1302

**Boggs S., Krinsley D. (2006):** *Application of cathodoluminescence imaging to the study of sedimentary rocks.* Cambridge University Press, New York

**Böhm F., Joachimsk, M.M., Lehnert H., Morgenroth G., Kretschmer W., Vacelet J., Dullo W.C. (1996):** *Carbon isotope records from extant Caribbean and South Pacific sponges: Evolution of $\delta^{13}$C in surface water DIC.* Earth and Planetary Science Letters 139, 291-303

**Böhm F., Joachimski M.M., Dullo W.C., Eisenhauer A., Lehnert H., Reitner J., Wörheide G. (2000):** *Oxygen isotope fractionation in marine aragonite of coralline sponges.* Geochimica et Cosmochimica Acta 64 (10), 1695-1703

**Bond D.P., Wignall P.B. (2010):** *Pyrite framboid study of marine Permian–Triassic boundary sections: a complex anoxic event and its relationship to contemporaneous mass extinction.* Geological Society of America Bulletin 122, 1265-1279

**Brady A.L., Slater G.F., Omelon C.R., Southam G., Druschel G., Andersen D.T., Hawes I., Laval B., Lim D.S.S. (2010):** *Photosynthetic isotope biosignatures in laminated micro-stromatolitic and non-laminated nodules associated with modern, freshwater microbialites in Pavilion Lake, BC.* Chemical Geology 274, 56-67

**Brayard A., Vennin E., Olivier N., Bylund K.G., Jenks J., Stephen D.A., Bucher H., Hofmann R., Goudemand N., Escargual G. (2011):** *Transient metazoan reefs in the aftermath of the end-Permian mass extinction.* Nature Geoscience 4, 693-697

**Breitbart M., Hoare A., Nitti A., Siefert J., Haynes M., Dinsdale E., Edwards R., Souza V., Rohwer F., Hollander D. (2009):** *Metagenomic and stable isotopic analyses of modern freshwater microbialites in Cuatro Ciénegas, Mexico.* Environmental Microbiology 11, 16-34

**Browne K.M., Golubic S., Seong-Joo L. (2000):** *Shallow Marine Microbial Carbonate Deposits.* In: Riding R.E., Awramik S.M. (eds): Microbial sediments. Springer Berlin Heidelberg, 223-249

**Brühwiler T., Brayard A., Bucher H., Guodun K. (2008):** *Griesbachian and Dienerian (Early Triassic) ammonoid faunas from northwestern Guangxi and southern Guizhou (south China).* Palaeontology 51, 1151-1180

**Buckley D.H., Baumgartner L.K., Visscher P.T. (2008):** *Vertical distribution of methane metabolism in microbial mats of the Great Sippewissett Salt Marsh.* Environmental microbiology 10, 967-977

**Burgess S.D., Bowring S., Shen S.Z. (2014):** *High-precision timeline for Earth's most severe extinction.* Proceedings of the National Academy of Sciences 111, 3316-3321

**Burne R.V., Moore L.S. (1987):** *Microbialites: organosedimentary deposits of benthic microbial communities.* Palaios 2, 241-254

# References

**Campbell I.H., Hill R.I., Williams I.S., Czamanske G.K., Kunikov V.E., Stepanov V. (1992):** *Synchronism of the Siberian Traps and the Permian-Triassic boundary.* In: 29th International Geological Congress, Resumes, Kyoto, p. 65

**Cercone K.R., Pedone V.A. (1987):** *Fluorescence (Photoluminescence) of carbonate rocks: Instrumental and analytical sources of observational error.* Journal of Sedimentary Petrology 57, 780-782

**Chen L., Wang Y., Xie S., Kershaw S., Dong M., Yang H., Liu H., Algeo, T.J. (2011):** *Molecular records of microbialites following the end-Permian mass extinction in Chongyang, Hubei Province, South China.* Palaeogeography, Palaeoclimatology, Palaeoecology 308, 151-159

**Chen Z.Q., Benton M.J. (2012):** *The timing and pattern of biotic recovery following the end-Permian mass extinction.* Nature Geoscience 5, 375-383

**Chen Z.Q., Tong J., Liao Z.T., Chen J. (2010):** *Structural changes of marine communities over the Permian-Triassic transition: ecologically assessing the end-Permian mass extinction and its aftermath.* Global and Planetary Change 73, 123-140

**Chilingar G.V., Bissell H.J., Wolf K.H. (1967):** *Diagenesis of carbonate rocks.* Developments in sedimentology 8, 179-322

**Clarkson M.O., Kasemann S.A., Wood R.A., Lenton T.M., Daines S.J., Richoz S., Ohnemueller F., Meixner A. Poulton S.W., Tipper E.T. (2015).** *Ocean acidification and the Permo-Triassic mass extinction.* Science 348, 229-232

**Clarkson M.O., Richoz S., Wood R.A., Maurer F., Krystyn L., McGurty D.J., Astratti D. (2013).** *A new high-resolution $\delta^{13}C$ record for the Early Triassic: insights from the Arabian Platform.* Gondwana Research 24, 233-242

**Clough J.G., Goldhammer R.K. (2000):** *Evolution of the Neoproterozoic Katakturuk dolomite ramp complex, northeastern Brooks Range, Alaska.* In: Grotzinger J.P., James N.P. (eds.): Carbonate Sedimentation and Diagenesis in the Evolving Precambrian World. Society for Sedimentary Geology (SEPM) Special Publication 67, 209–241

**Collin P.Y., Kershaw S., Tribovillard N., Forel M.B., Crasquin S. (2014):** *Geochemistry of post-extinction microbialites as a powerful tool to assess the oxygenation of shallow marine water in the immediate aftermath of the end-Permian mass extinction.* International Journal of Earth Sciences 104, 1025-1037

**Crasquin-Soleau S., Galfetti T., Bucher H., Brayard A. (2006):** *Palaeoecological changes after the end-Permian mass extinction: Early Triassic ostracods from northwestern Guanxi Province, South China.* Rivista Italiana di Paleontologia e Stratigrafia 112, 55-75

**Crasquin-Soleau S., Kershaw S. (2005):** *Ostracod fauna from the Permian-Triassic boundary interval of South China (Huaying Mountains, eastern Sichuan Province): palaeoenvironmental significance.* Palaeogeography, Palaeoclimatology, Palaeoecology 217, 131-141

**Crasquin-Soleau S., Marcoux J., Angiolini L., Nicora A. (2004a):** *Palaeocopida (Ostracoda) across the Permian-Triassic events: new data from southwestern Taurus (Turkey).* Journal of Micropalaeontology 23, 67-76

**Crasquin-Soleau S., Marcoux J., Angiolini L., Richoz S., Nicora A., Baud A., Bertho Y. (2004b):** *A new ostracode fauna from the Permian-Triassic boundary in Turkey (Taurus, Antalya Nappes).* Micropaleontology 50, 281-295

**Danelian T., Asatryan G., Sahakyan L., Galoyan G.H., Sosson M., Avagyan A. (2010):** *New and revised Radiolarian biochronology for the sedimentary cover of ophiolites in the Lesser Caucasus (Armenia).* In: Sosson M., Kaymakci N., Stephenson R.A., Bergerat F., Starostenko V. (eds.):

Sedimentary Basin Tectonics from the Black Sea and Caucasus to the Arabian Platform. Geological Society, London, Special Publications 340, 383-391

**Danelian T., Asatryan G., Sosson M., Person A., Sahakyan L., Galoyan G. (2008):** *Discovery of two distinct Middle Jurassic Radiolarian assemblages in the sedimentary cover of the Vedi ophiolite (Lesser Caucasus, Armenia).* Comptes Rendus Palevol 7, 324-334

**de Wit M.J., Ghosh J.G., de Villiers S., Rakotosolofo N., Alexander J., Tripathi A., Looy C. (2002):** *Multiple Organic Carbon Isotope Reversals across the Permo-Triassic Boundary of Terrestrial Gondwana Sequences: Clues to Extinction Patterns and Delayed Ecosystem Recovery.* The Journal of Geology 110, 227-240

**Dellenbach J. (1964):** Contribution á l'étude géologique de la région située à l'est de Teheran (Iran). PhD Thesis, Université de Strasbourg, 1-117

**Des Marais D.J. (1995):** *The biogeochemistry of hypersaline microbial mats.* In: Jones J.G. (ed): Advances in microbial ecology, Springer US, 251-274

**Dravis J.J., Yurewicz D.A. (1985):** *Enhanced Carbonate Petrography using Fluorescence Microscopy.* Journal of Sedimentary Petrology 55, 795-804

**Druffel E.R., Benavides L.M. (1986):** *Input of excess $CO_2$ to the surface ocean based on $^{13}C/^{12}C$ ratios in a banded Jamaican sclerosponge.* Nature 321, 58-61

**Dunham R.J. (1962):** *Classification of carbonate rocks according to depositional texture.* In: Ham W.E. (ed.): Classification of carbonate rocks. A symposium. American Association of Petroleum Geologist Memoir 1, 108-171

**Dupraz C., Reid R.P., Braissant O., Decho A.W., Norman R.S., Visscher P.T. (2009):** *Processes of carbonate precipitation in modern microbial mats.* Earth-Science Reviews 96, 141-162

**Eghoyan V.L. (1955):** *The Upper-Cretaceous Deposits of the South-Western Part of Armenian SSR.* Academia of Sciences of the Armenian SSR, Yerevan (in Russian)

**Embry A.F., Klovan J.E. (1971):** *A late Devonian reef tract on northeastern Banks Island, NWT.* Bulletin of Canadian Petroleum Geology 19, 730-781

**Erwin D.H. (1993):** *The Great Paleozoic Crisis: life and death in the Permian. The Perspectives in Paleobiology and Earth History.* Columbia University Press, New York, 327

**Erwin D.H., Bowring S.A., Jin Y.-G. (2002):** *End-Permian mass-extinctions: a review.* In: Koeberl C., MacLeod K.G. (eds.): Catastrophic Events and Mass Extinctions: Impacts and Beyond. Geological Society of America Special Paper 356, 353–383

**Ezaki Y., Liu J., Nagano T., Adachi N. (2008):** *Geobiological aspects of the earliest Triassic microbialites along the southern periphery of the tropical Yangtze Platform: initiation and cessation of a microbial regime.* Palaios 23, 356-369

**Fairchild I.J., Marshall J.D., Bertrand-Sarfati J. (1990):** *Stratigraphic shifts in carbon isotopes from Proterozoic stromatolitic carbonates (Mauritania): Influences of primary mineralogy and diagenesis.* American Journal of Science 290, 46-79

**Fang Z.J. (2005):** *Comments on Heydari E., Hassanzadeh J., Wade W.J., Ghazi A.M. (2003): Permian-Triassic boundary interval in the Abadeh section of Iran with implications for mass extinctions: part 1 – Sedimentology.* Palaeogeography, Palaeoclimatology, Palaeoecology 217, 311-313

**Fenton F.G., Fenton M.A. (1937):** *Belt series of the north: stratigraphy, sedimentation, paleontology.* Geological Society of America Bulletin 48, 1873-1969

**Flügel E. (2002):** *Triassic reef patterns.* In: Kiessling W., Flügel E., Golonka J. (eds.): Phanerozoic Reef Patterns. SEPM (Society for Sedimentary Geology) Special Publication 72, 391-463

**Flügel E. (2010):** *Microfacies of carbonate rocks: Applications, Interpretation and Application.* Springer Berlin Heidelberg

**Font E., Nédélec A., Trindade R.I.F., Macouin M., Charrière A. (2006):** *Chemostratigraphy of the Neoproterozoic Mirassol d'Oeste cap dolostones (Mato Grosso, Brazil): an alternative model for Marinoan cap dolostone formation.* Earth and Planetary Science Letters 250, 89-103

**Forel M.B. (2012):** *Ostracods (Crustacea) associated with microbialites across the Permian-Triassic boundary in Dajiang (Guizhou Province, south China).* European Journal of Taxonomy 19, 1-34

**Forel M.B. (2013):** *The Permian-Triassic mass extinction: Ostracods (Crustacea) and microbialites.* Comptes Rendus Geoscience 345, 203-211

**Forel M.B., Crasquin S., Hips K., Kershaw S., Collin P.Y., Haas J. (2013a):** *Ostracods (Crustacea) from Permian-Triassic Boundary of Bálvány North section (Bükk Mountains, Hungary).* Acta Palaeontologica Polonica 58, 195-219

**Forel M.B., Crasquin S., Kershaw S., Collin P.Y. (2013b):** *In the aftermath of the end-Permian extinction: the microbialite refuge?* Terra Nova 25, 137-143

**Forel M.B., Crasquin S., Kershaw S., Feng Q.L., Collin P.Y. (2009):** *Ostracods (Crustacea) and water oxygenation in the earliest Triassic of South China: implications for oceanic events at the end-Permian mass extinction.* Australian Journal of Earth Sciences 56, 815-823

**Friesenbichler E., Baud A., Krystyn L., Sahakyan L., Richoz S. (2015):** *Giant microbial build-ups of earliest Triassic in Armenia.* Berichte des Instituts für Erdwissenschaften der Karl-Franzens-Universität Graz 21, p. 113

**Frisk Å.M., Bucher H., Hautmann M., Baud A., Brosse M., Guodon K. (2012):** *Unusually diverse mollusc assemblages from the early Triassic (Griesbachian) of South China.* GSA Annual Meeting, Charlotte, p. 166

**Galfetti T., Bucher H., Ovtcharova M., Schaltegger U., Brayard A., Brühwiler T., Goudemand N., Weissert H., Hochuli P.A., Cordey F., Guodun K. (2007):** *Timing of the Early Triassic carbon cycle perturbations inferred from new U-Pb ages and ammonoid biochronozones.* Earth and Planetary Science Letters 258, 593-604

**Gealey W.K. (1988):** *Plate tectonic evolution of the Mediterranean-Middle East region.* Tectonophysics 155, 285-306

**Gingras M., Hagadorn J.W., Seilacher A., Lalonde S.V., Pecoits E., Petrash D., Konhauser K.O. (2011):** *Possible evolution of mobile animals in association with microbial mats.* Nature Geoscience 4, 372-375

**Götze J. (2002):** *Kathodolumineszenz-Mikroskopie und -Spektroskopie in den Geo- und Materialwissenschaften.* Mitteilungen der Österreichischen Mineralogischen Gesellschaft 147, 27-40

**Götze J. (2012):** *Application of Cathodoluminescence Microscopy and Spectroscopy in Geosciences.* Microscopy and Microanalyses 18, 1270-1284

**Greene S.E., Bottjer D.J., Corsetti F.A., Berelson W.M., Zonneveld J.P. (2012):** *A subseafloor carbonate factory across the Triassic-Jurassic transition.* Geology 40, 1043-1046

**Grey K. (1989):** *Handbook for the study of stromatolites and associated structures.* In: Kennard J.M., Burne R.V. (eds.): Stromatolite Newsletter 14, 82-171

**Grice K., Cao C., Love G.D., Böttcher M.E., Twitchett R.J., Grosjean E., Summons R.E., Turgeon S.C., Dunning W., Jin Y. (2005):** *Photic zone euxinia during the Permian-Triassic superanoxic event.* Science 307, 706-709

**Grotzinger J.P., Knoll A.H. (1995):** *Anomalous carbonate precipitates: is the Precambrian the key to the Permian?* Palaios 10, 578-596

**Grotzinger J.P., Knoll A.H. (1999):** *Stromatolites in Precambrian carbonates: evolutionary mileposts or environmental dipsticks?* Annual Review of Earth and Planetary Sciences 27, 313–358

References

**Groves J.R., Altiner D., Rettori R. (2005):** *Extinction, survival, and recovery of lagenide foraminifers in the Permian-Triassic boundary interval, central Taurides, Turkey.* Journal of Paleontology 79, 1-38

**Gu B., Schelske C.L., Hodell D.A. (2004):** *Extreme $^{13}$C enrichments in a shallow hypereutrophic lake: Implications for carbon cycling.* Limnology and Oceanography 49, 1152-1159

**Guo L., Andrews J., Riding R., Dennis P., Dresser Q. (1996):** *Possible microbial effects on stable carbon isotopes in hot-spring travertines.* Journal of Sedimentary Research 66, 468-473

**Habermann D., Neuser R.D., Richter D.K. (2000):** *Quantitative high resolution analyses of $Mn^{2+}$ in sedimentary calcite.* In: Pagel M., Barbin V., Blanc P., Ohnenstetter (eds.): Cathodoluminescence in Geosciences. Springer Berlin Heidelberg, 331-358

**Habermann D., Neuser R.D., Richter D.R. (1996):** *REE-activated cathodoluminescence of calcite and dolomite: high-resolution spectrometric analysis of CL-emission (HRS-CL).* Sedimentary Geology 101, 1-7

**Hakobyan V.T. (1978):** *Biostratigraphy of the Upper Cretaceous Deposits of Armenia SSR.* Academia of Sciences of the Armenian SSR, Yerevan (in Russian)

**Hässig M., Rolland Y., Sahakyan L., Sosson M., Galoyan G., Avagyan A., Bosch D., Müller C. (2015):** *Multi-stage metamorphism in the South Armenian Block during the Late Jurassic to Early Cretaceous: Tectonics over south-dipping subduction of Northern branch of Neotethys.* Journal of Asian Sciences 102, 4-23

**Hautmann M., Bucher H., Brühwiler T., Goudemand N., Kaim A., Nützel A. (2011):** *An unusually diverse mollusc fauna from the earliest Triassic of South China and its implications for benthic recovery after the end-Permian biotic crisis.* Geobios 44, 71-85

**Hegenberger W. (1993):** *Stratigraphy and sedimentology of the late Precambrian Witvlei and Nama Groups east of Windhoek.* Geological Survey of Namibia Memoir 17, 82

**Heindel K., Richoz S., Birgel D., Brandner R., Klügel A., Krystyn L., Baud A., Horacek M., Mohtat T., Peckmann J. (2013):** *Biochemical formation of calyx-shaped carbonate crystal fans in the subsurface of the Early Triassic seafloor.* Gondwana Research 27, 840-861

**Heydari E., Arzani N., Hassanzadeh J. (2008):** *Mantle plume: the invisible serial killer – application to the Permian-Triassic boundary mass extinction.* Palaeogeography, Palaeoclimatology, Palaeoecology 264, 147-162

**Heydari E., Hassanzadeh J., Wade W.J. (2000):** *Geochemistry of central Tethyan Upper Permian and Lower Triassic strata, Abadeh region, Iran.* Sedimentary Geology 137, 85-99

**Heydari E., Hassanzadeh J., Wade W.J., Ghazi A.M. (2003):** *Permian-Triassic boundary interval in the Abadeh section of Iran with implications for mass extinction: part 1 – Sedimentology.* Palaeogeography, Palaeoclimatology, Palaeoecology 193, 405-423

**Heydari E., Wade W.J., Hassandzadeh J. (2001):** *Diagenetic origin of carbon and oxygen isotope composition of Permian-Triassic boundary strata.* Sedimentary Geology 143, 191-197

**Hips K., Haas J. (2006):** *Calcimicrobial stromatolites at the Permian-Triassic boundary in a western Tethyan section, Bükk Mountains, Hungary.* Sedimentary Geology 185, 239-253

**Hoffman P.F., Halverson G.P., Domack E.W., Husson J.M., Higgins J.A., Schrag D.P. (2007):** *Are basal Ediacaran (635 Ma) post-glacial "cap dolostones" diachronous?* Earth and Planetary Science Letters 258, 114-131

**Hoffman P.F., Schrag D.P. (2002):** *The snowball Earth hypothesis: testing the limits of global change.* Terra Nova 14, 129-155

**Hollander D.J., McKenzie J.A. (1991):** *$CO_2$ control on carbon-isotope fractionation during aqueous photosynthesis: A paleo-$pCO_2$ barometer.* Geology 19, 929-932

References

**Horacek M., Brandner R., Abart R. (2007a):** *Carbon isotope record of the P/T boundary and the Lower Triassic in the Southern Alps: evidence for rapid changes in storage of organic carbon.* Palaeogeography, Palaeoclimatology, Palaeoecology 252, 347-354

**Horacek M., Richoz S., Brandner R., Krystyn L., Spötl C. (2007b):** *Evidence for recurrent changes in Lower Triassic oceanic circulation of the Tethys: The δ¹³C record from marine sections in Iran.* Palaeogeography, Palaeoclimatology, Palaecology 252, 355-369

**Horacek M., Wang X., Grossman E.L., Richoz S., Cao Z. (2007c):** *The carbon-isotope curve from the Chaohu section, China: different trends at the Induan-Olenekian Boundary or diagenesis.* Albertiana 35, 41-45

**Irmis R.B., Whiteside J.H. (2011):** *Delayed recovery of non-marine tetrapods after the end-Permian mass extinction tracks global carbon cycle.* Proceedings of the Royal Society of London B, Biological Sciences 279, 1310-1318

**Isozaki Y. (1994):** *Superanoxia across the Permo-Triassic boundary: record in accreted deep-sea pelagic chert in Japan.* In: Embry A.F., Beauchamp B., Glass D.J. (eds.): Pangea. Global Environments and Resources. Canadian Society of Petroleum Geologists Memoir 17, 805-812

**Isozaki Y. (1997):** *Permo-Triassic boundary superanoxia and stratified superocean: records from lost deep sea.* Science 276, 235-238

**James N.P., Narbonne G.M., Kyser T.K. (2001):** *Late Neoproterozoic cap carbonates: Mackenzie Mountains, northwestern Canada: precipitation and global glacial meltdown.* Canadian Journal of Earth Sciences 38, 1229-1262

**Joachimski M.M., Böhm F., Lehnert H. (1995):** *Longterm Isotopic Trends from Caribbean Demosponges: Evidence for Isotopic Disequilibrium between Surface Waters and Atmosphere.* In: Lathuiliere B., Geister J. (eds.): Proceedings 2nd European Regional Meeting, International Society of Reef Studies, Publications du Service géologique du Luxembourg 29, 141-147

**Kaiho K., Kajiwara Y., Nakano T., Miura Y., Kawahata H., Tazaki K., Ueshima M., Chen Z.Q., Shi G.R. (2001):** *End-Permian catastrophe by a bolide impact: evidence of a gigantic release of sulfur from the mantle.* Geology 29, 815-818

**Kaim A., Nützel A., Bucher H., Brühwiler T., Goudemand N. (2010):** *Early Triassic (Late Griesbachian) gastropods from South China (Shanggan, Guangxi).* Swiss Journal of Geosciences 103, 121-128

**Kazmin V.G. (1991):** *Collision and rifting in the Tethys Ocean: geodynamic implication.* Tectonophysics 196, 371-384

**Kershaw S. (2015):** *Modern Black Sea oceanography applied to the end-Permian extinction event.* Journal of Palaeogeography 4(1), 52-62

**Kershaw S., Crasquin S., Collin P.Y., Li Y., Feng Q., Forel M.B. (2009):** *Microbialites as disaster forms in anachronistic facies following the end-Permian mass extinction: a discussion.* Australian Journal of Earth Sciences 56, 809-813

**Kershaw S., Crasquin S., Forel M.-B., Randon C., Collin P.Y., Kosun E., Richoz S., Baud A. (2011):** *Earliest Triassic microbialites in Çürük Dag, southern Turkey: composition, sequences and controls on formation.* Sedimentology 58, 739-755

**Kershaw S., Crasquin S., Li Y., Collin P.Y., Forel M.B., Mu X., Baud A., Wang Y., Xie S., Maurer F., Guo L. (2012):** *Microbialites and global environmental change across the Permian-Triassic boundary: a synthesis.* Geobiology 10, 25-47

**Kershaw S., Li Y., Crasquin-Soleau S., Feng Q., Mu X., Collin P.Y., Reynolds A., Guo L. (2007):** *Earliest Triassic microbialites in the South China block and other areas: controls on their growth and distribution.* Facies 53, 409-425

References

**Kershaw S., Zhang T., Lan G. (1999):** *A microbialites carbonate crust at the Permian-Triassic boundary in south China and its palaeoenvironmental significance.* Palaeogeography, Palaeoclimatology, Palaeoecology 146, 1-18

**Knipper A.L. (1975):** *The oceanic crust in the structures of the Alpine Folded Belt (South Europe, western part of Asia and Cuba).* Transactions 267, Moscow "Nauca" (in Russian)

**Knipper A.L., Khain E.V. (1980):** *Structural position of ophiolites of the Caucasus.* Ofioliti, Special Issue 2, 297-314

**Knoll A.H., Bambach R.K., Canfield D.E., Grotzinger J.P. (1996):** *Comparative Earth history and late Permian mass extinction.* Science 273, 452-457

**Kontoyannis C.G., Vagenas N.V. (2000):** *Calcium carbonate phase analysis using XRD and FT-Raman spectroscopy.* Analyst 125, 251-255

**Korte C., Kozur H.W. (2010):** *Carbon-isotope stratigraphy across the Permian–Triassic boundary: a review.* Journal of Asian Earth Sciences 39, 215-235

**Kozur H.W. (1998):** *Some aspects of the Permian–Triassic boundary (PTB) and of the possible causes for the biotic crisis around this boundary.* Palaeogeography, Palaeoclimatology, Palaeoecology 143, 227-272

**Kozur H.W. (2005):** *Pelagic uppermost Permian and the Permian-Triassic boundary conodonts of Iran. Part II: investigated sections and evaluation of the conodont faunas.* Hallesches Jahrbuch für Geowissenschaften Reihe B 19, 49-86

**Kozur H.W. (2007):** *Biostratigraphy and event stratigraphy in Iran around the Permian-Triassic Boundary (PTB): implications for the cause of the PTB biotic crisis.* Global and Planetary Change 55, 155-176

**Krull E.S., Lehrmann D.J., Druke D., Kessel B., Yu Y., Li R. (2004):** *Stable carbon isotope stratigraphy across the Permian-Triassic boundary in shallow marine carbonate platforms, Nanpanjiang Basin, south China.* Palaeogeography, Palaeoclimatology, Palaeoecology 204, 297-315

**Krull E.S., Retallack G.J. (2000):** *$\delta^{13}C$ depth profiles from paleosols across the Permian-Triassic boundary: Evidence for methane release.* Geological Society of America Bulletin 112, 1459-1472

**Krystyn L., Richoz S., Baud A., Twitchett R.J. (2003):** *A unique Permian-Triassic boundary section from the neotethyan Hawasina basin, Central Oman Mountains.* Palaeogeography, Palaeoclimatology, Palaeoecology 191, 329-344

**Leda L., Korn D., Ghaderi A., Hairapetian V., Struck U., Reimold W.U. (2014):** *Lithostratigraphy and carbonate microfacies across the Permian-Triassic boundary near Julfa (NW Iran) and in the Baghuk Mountains (Central Iran).* Facies 60, 295-325

**Lethiers F., Whatley R. (1994):** *The use of Ostracoda to reconstruct the oxygen levels of Late Palaeozoic oceans.* Marine Micropaleontology 24, 57-69

**Léveillé R.J., Longstaffe F.J., Fyfe W.S. (2007):** *An isotopic and geochemical study of carbonate-clay mineralization in basaltic caves: abiotic versus microbial processes.* Geobiology 5, 235-249

**Liao W., Wang Y., Kershaw S., Weng Z., Yang, H. (2010):** *Shallow-marine dysoxia across the Permian–Triassic boundary: evidence from pyrite framboids in the microbialite in South China.* Sedimentary Geology 232, 77-83

**Logan B.W. (1974):** *Inventory of diagenesis in Holocene-Recent carbonate sediments, Shark Bay, Western Australia.* American Association of Petroleum Geologists Memoir 22, 195-249

**Logan B.W., Hoffman P., Gebelein C.D. (1974):** *Algal mats, cryptalgal fabrics, and structures, Hamelin Pool, Western Australia.* American Association of Petroleum Geologists Memoir 22, 140-194

References

**Long D.A. (1977):** *Raman spectroscopy.* In: Staveley L.A.K. (ed.): The characterization of chemical purity organic compounds, Elsevier, 149-163

**Luo C., Reitner J. (2014):** *First report of fossil "keratose" demosponges in Phanerozoic carbonates: preservation and 3-D reconstruction.* Naturwissenschaften 101, 467-477

**Luo M., Zhong-Qjang C., Zhao L., Kershaw S., Huang J., Wu L., Yang H., Fang Y., Huang Y., Zhang Q., Hu S., Zhou C., Wen W., Jia Z. (2014):** *Early Middle Triassic stromatolites from the Luoping area, Yunnan Province, Southwest China: Geological features and environmental implications.* Palaeogeography, Palaeoclimotology, Palaeoecology 412, 124-140

**Macdonald F.A., Jones D.S., Schrag D.P. (2009a):** *Stratigraphic and tectonic implications of a newly discovered glacial diamictite-cap carbonate couplet in southwestern Mongolia.* Geology 37, 123-126

**Macdonald F.A., McClelland W.C., Schrag D.P., Macdonald W.P. (2009b):** *Neoproterozoic glaciation on a carbonate platform margin in Arctic Alaska and the origin of the North Slope subterrane.* Geological Society of America Bulletin 121, 448-473

**Machel H.G. (2000):** *Application of cathodoluminescence to carbonate diagenesis.* In: Pagel M., Barbin V., Blanc P., Ohnenstetter D. (eds.): Cathodoluminescence in Geosciences. Springer Berlin Heidelberg, 271-301

**Machel H.G., Burton E.A. (1991):** *Factors governing cathodoluminescence in calcite and dolomite, and their implications for studies of carbonate diagenesis.* In: Luminescence Microscopy and Spectroscopy: Qualitative and Quantitative Applications. SEMP Short Course 25, 37-57

**Marenco P.J., Griffin J.M., Fraiser M.L., Clapham M.E. (2012):** *Paleoecology and geochemistry of Early Triassic (Spathian) microbial mounds and implications for anoxia following the end-Permian mass extinction.* Geology 40, 715-718

**Marfunin A.S. (1979):** *Spectroscopy, luminescence and radiation centres in minerals.* Springer Berlin Heidelberg, 352

**Marshall D.J. (1988):** *Cathodoluminescence of Geological Materials.* Boston, Unwin Hyman.

**Mart Y. (1987):** *Superpositional tectonic patterns along the continental margin of the southeastern Mediterranean: a review.* Tectonophysics 140, 213-232

**Mason R.A., Mariano A.N. (1990):** *Cathodoluminescence activation in manganese-bearing and rare earth-bearing synthetic calcites.* Chemical Geology 88, 191-206

**Meijers M.J.M., Smith B., Kirscher U., Mensink M., Sosson M., Rolland Y., Grigoryan A., Sahakyan L., Avagyan A., Langereis C., Müller C. (2015):** *A paleolatitude reconstruction of the South Armenian Block (Lesser Caucasus) for the Late Cretaceous: Constraints on the Tethyan realm.* Tectonophysics 644-645, 197-219

**Merz M.U. (1992):** *The biology of carbonate precipitation by cyanobacteria.* Facies 26, 81-102

**Monin A.S., Zonenshain L.P. (1987):** *History of the Ocean Tethys.* Moscow Institute of Oceanology (in Russian)

**Monty C.L.V. (1976):** *The origin and development of cryptalgal fabrics.* In: Walter M.R. (ed.): Stromatolites, Developments in Sedimentology 20, 193-249

**Morgan J.P., Reston T.J., Ranero C.R. (2004):** *Contemporaneous mass extinctions, continental flood basalts, and 'impact signals': are mantle plume-induced lithospheric gas explosions the causal link?* Earth and Planetary Science Letters 217, 263-284

**Mu X., Kershaw S., Li Y., Guo L., Qi Y., Reynolds A. (2009):** *High-resolution carbon isotope changes in the Permian-Triassic boundary interval, Chongqing, South China: implications for control and growth of earliest Triassic microbialites.* Journal of Asian Earth Sciences 36, 434-441

**Nalivkin P.V. (1976):** *Geological Map of Caucasus at 1/500 000 scale.* Ministry of Geology, USSR, Cief

## References

**Okay A. I., Tüysüz O. (1999):** *Tethyan sutures of northern Turkey.* In: Durand B., Jolivet L., Horváth F., Séranne M. (eds.): The Mediterranean Basins: Tertiary Extension Within the Alpine Orogen. Geological Society of London, Special Publications 156, 475-515

**O'Leary M.H. (1988):** *Carbon isotopes in photosynthesis.* Bioscience 38 (5), 328-336

**Olivieri N., Brayard A., Fara E., Bylund K.G., Jenks J.F., Vennin E., Stephen D.A., Escarguel G. (2014):** *Smithian shoreline migrations and depositional settings in Timpoweap Canyon (Early Triassic, Utah, USA).* Geological Magazine 151, 938-955

**Paffenholtz K.N. (1959):** *Geological History of the Caucasus.* Academia of Sciences of the Armenian SSR, Yerevan (in Russian)

**Payne J.L., Clapham M.E. (2012):** *End-Permian mass extinction in the oceans: an ancient analog for the twenty-first century?* Annual Review of Earth and Planetary Sciences 40, 89-111

**Payne J.L., Kump L.R. (2007):** *Evidence for recurrent Early Triassic massive volcanism from quantitative interpretation of carbon isotope fluctuations.* Earth and Planetary Science Letters 256, 264-277

**Payne J.L., Lehrmann D.J., Wei J., Orchard M.J., Schrag D.P., Knoll A.H. (2004):** *Large perturbations of the carbon cycle during recovery from the end-Permian extinction.* Science 305, 506-509

**Payne J.L., Turchyn A.V., Paytan A., DePaolo D.J., Lehrmann D.J., Yu M., Wei, J. (2010):** *Calcium isotope constraints on the end-Permian mass extinction.* Proceedings of the National Academy of Sciences 107, 8543-8548

**Pedone V.A., Cercone K.R., Burruss R.C. (1990):** *Activators of photoluminescence in calcite: evidence from high-resolution, laser-excited luminescence spectroscopy.* Chemical Geology 88, 183-190

**Pierson B.K., Bauld J., Castenholz R.W., D'amelio E., Des Marais D.J., Farmer J.D., Grotzinger J.P., Jorgensen B.B., Nelson D.C., Palmisano A.C., Schopf J.W. Summons R.E., Walter M.R., Ward D.M. (1992):** *Modern mat-building microbial communities: a key to the interpretation of Proterozoic stromatolitic communities.* Cambridge University Press, New York

**Planavsky N., Grey K. (2008):** *Stromatolite branching in the Neoproterozoic of the Centralian Superbasin, Australia: an investigation into sedimentary and microbial control of stromatolite morphology.* Geobiology 6, 33-45

**Power I.M., Wilson S.A., Dipple G.M., Southam G. (2011):** *Modern carbonate microbialites from an asbestos open pit pond, Yukon, Canada.* Geobiology 9, 180-195

**Pruss S., Corsetti F.A., Bottjer D.J. (2005):** *The unusual sedimentary rock record of the Early Triassic: a case study from southwestern United States.* Palaeogeography, Palaeoclimatology, Palaeoecology 222, 33-52

**Pruss S.B., Bottjer D.J. (2004):** *Early Triassic trace fossils of the western United States and their implications for prolonged environmental stress from the end-Permian mass extinction.* Palaios 19, 551-564

**Pruss S.B., Bottjer D.J. (2005):** *The reorganization of reef communities following the end-Permian mass extinction.* Comptes Rendus Palevol 4, 553-568

**Pruss S.B., Bottjer D.J., Corsetti F.A., Baud A. (2006):** *A global marine sedimentary response to the end-Permian mass extinction: examples from southern Turkey and the western United States.* Earth-Science Reviews 78, 193-206

**Rampino M.R., Prokoph A., Adler A. (2000):** *Tempo of the end-Permian event: High-resolution cyclostratigraphy at the Permian-Triassic boundary.* Geology 28, 643-646

**Reeder R.J. (1991):** *An overview of zoning in carbonate minerals.* In: Barker C.E., Kopp O.C. (eds.): Luminescence Microscopy and Spectroscopy: Qualitative and Quantitative Applications. SEMP Short Course 25, 77-82

# References

**Reitner J. (1992):** *"Coralline Spongien" – Der Versuch einer phylogenetischen-taxonomischen Analyse.* Berliner Geowissenschaftliche Abhandlungen Reihe E 1, 1-352

**Reitner J., Gautret P. (1996):** *Skeletal formation in the modern but ultraconservative chaetetid sponge Spirastrella (Acanthochaetetes) wellsi (Demospongiae, Porifera).* Facies 34, 193-208

**Rengarten V.P. (1959):** *Stratigraphy of the Cretaceous Deposits of the Lesser Caucasus.* Regional Stratigraphy of USSR. Izdatelstvo of AS of USSR, Moscow (in Russian)

**Renne P.R., Black M.T., Zichao Z., Richards M.A., Basu A.R. (1995):** *Synchrony and causal relations between Permian-Triassic boundary crises and Siberian flood volcanism.* Science 269, 1413-1416

**Richoz S. (2004):** *Stratigraphie et variations isotopiques du carbone dans le Permien supérieur et le Trias inférieur de la Néotéthys (Turquie, Oman et Iran).* PhD Thesis, Université de Lausanne, p. 303

**Richoz S. (2006):** *Stratigraphie et variations isotopiques du carbone dans le Permien supérieur et le Trias inférieur de la Néotéthys (Turquie, Oman et Iran).* Mémoires de Géologie (Lausanne) 46, 1-251

**Richoz S., Krystyn L., Baud A., Brandner R., Horacek M., Mohtat-Aghai M. (2010):** *Permian-Triassic boundary interval in the Middle East (Iran and N. Oman): progressive environmental change from detailed carbonate carbon isotope marine curve and sedimentary evolution.* Journal of Asian Earth Sciences 39, 236-253

**Richter D.K., Götte T., Götze J., Neuser R.D. (2003):** *Progress in application of cathodoluminescence (CL) in sedimentary petrology.* Mineralogy and Petrology 79, 127-166

**Riding R. (1994):** *Evolution of algal and cyanobacterial calcification.* In: Bengtson S. (ed.): Early Life on Earth, Nobel Symposium 84, 426-438, Columbia University Press New York

**Riding R. (2000):** *Microbial carbonates: the geological record of calcified bacterial–algal mats and biofilms.* Sedimentology 47, 179-214

**Riding R. (2005):** *Phanerozoic reefal microbial carbonate abundance: comparisons with metazoan diversity, mass extinction events, and seawater saturation state.* Revista Española de Micropaleontología 37, 23-39

**Rolland Y., Perincek D., Kaymakci N., Sosson M., Barrier E., Avagyan A. (2012):** *Evidence for ~80-75 Ma subduction jump during Anatolide-Tauride-Armenian block accretion and ~48 Ma Arabia-Eurasia collision in Lesser Caucasus-East Anatolia.* Journal of Geodynamics 56-57, 76-85

**Saylor B.Z., Kaufman A.J., Grotzinger J.P., Urban F. (1998):** *A composite reference section for terminal Proterozoic strata of southern Namibia.* Journal of Sedimentary Research 68, 1223-1235

**Schidlowski M. (2000):** *Carbon Isotopes and Microbial Sediments.* In: Riding R.E., Awramik S.M. (eds.): Microbial sediments. Springer Berlin Heidelberg, 84-95

**Schubert J.K., Bottjer D.J. (1992):** *Early Triassic stromatolites as post-mass extinction disaster forms.* Geology 20, 883-886

**Semikatov M.A., Gebelein C.D., Cloud P., Awramik S.M., Benmore W.C. (1979):** *Stromatolite morphogenesis – progress and problems.* Canadian Journal of Earth Sciences 16, 992-1015

**Sepkoski J.J. Jr, Bambach R.K., Droser M.L. (1991):** *Secular changes in Phanerozoic event bedding and the biological overprint.* In: Einsele G., Ricken W., Seilacher A. (eds.): Cycles and events in stratigraphy. Springer Berlin, 298-312

**Seyed-Emami K. (2003):** *Triassic in Iran.* Facies 48, 91-106

**Shapiro R.S. (2000):** *A Comment on the Systematic Confusion of Thrombolites.* Palaios 15 (2), 166-169

**Shapiro R.S., Awramik S.M. (2000):** *Microbialite morphostratigraphy as a tool for correlating Late Cambrian-Early Ordovician sequences.* The Journal of Geology 108, 171-180

**Sokolov S.D. (1977):** *The Olistostromes and Ophiolitic Nappes of the Lesser Caucasus.* Izdatelstvo "Nauka", Moscow (in Russian)

**Song H., Wignall P.B., Tong J., Yin H. (2013):** *Two pulses of extinction during the Permian-Triassic crisis.* Nature Geoscience 6, 52-56

**Sosson M., Rolland Y., Müller C., Danelian T., Melkonyan R., Kekelia S., Adamia S., Babazadeh V., Kangarli T., Avagyan A., Galoyan G., Mosar J. (2010):** *Subductions, obduction and collision in the Lesser Caucasus (Armenia, Azerbaijan, Georgia), new insights.* In: Sosson M., Maymakci N., Stephenson R. A., Bergerat F., Starostenko V. (eds.): Sedimentary Basin Tectonics from the Black Sea and Caucasus to the Arabian Platform. Geological Society of London, Special Publications 340, 329-352

**Stal L.J., (2000):** *Microbial mats and stromatolites.* In: Whitton B.A., Potts M. (eds.): The Ecology of Cyanobacteria. Their Diversity in Time and Space. Kluwer, Dordrecht

**Stampfli G., Marcoux J., Baud A. (1991):** *Tethyan margins in space in time.* Palaeogeography, Palaeoclimatology, Palaeoecology 87, 373-409

**Stampfli G.M. and Borel G.D. (2002):** *A plate tectonic model for the Paleozoic and Mesozoic constrained by dynamic plate boundaries and restored synthetic ocean isochrons.* Earth and Planetary Science Letter 196, 17-33

**Stampfli G.M. and Borel G.D. (2004):** *The TRANSMED transect in space and time: constraints on the paleotectonic evolution of the Mediterranean domain.* In: Cavazza W., Roure F., Spakman W., Stampfli G.M., Ziegler P. (eds.): The TRANSMED Atlas: the Mediterranean Region from Crust to Mantle, Springer Berlin Heidelberg, 53-80

**Stepanov D.L., Golshani F., Stöcklin J. (1969):** *Upper Permian and Permian-Triassic boundary in North Iran.* Geological Survey of Iran 12, 1-72

**Sumner D.Y. (2001):** *Microbial influences on local carbon isotopic ratios and their preservation in carbonate.* Astrobiology 1, 57-70

**Sun Y., Joachimski M.M., Wignall P.B., Yan C., Chen Y., Jiang H., Wang L., Lai, X. (2012):** *Lethally hot temperatures during the Early Triassic greenhouse.* Science 338, 366-370

**Szulc J. (2007):** *Sponge-microbial stromatolites and coral-sponge reef recovery in the Triassic of the western Tethys domain.* In: Lucas S.G., Spielmann J.A. (eds.): The Global Triassic. New Mexico Museum of Natural History and Science Bulletin 41, 402

**Taraz H., Golshani F., Nakazawa K., Shimizu D., Bando Y., Ishii K.I., Murata M., Okimura Y., Sakagami S., Nakamura K., Tukuoka T. (1981).** *The Permian and the Lower Triassic Systems in Abadeh Region, Central Iran.* Memoirs of the Faculty of Science, Kyoto University, Series of Geology and Mineralogy 47, 61-133

**Thompson J.B., Schultze-Lam S., Beveridge T.J. (1997):** *Whiting events: Biogenic origin due to the photosynthetic activity of cyanobacterial picoplankton.* Limnology and Oceanography 42, 133-141

**Tong J., Zuo J., Chen Z.Q. (2007):** *Early Triassic carbon isotope excursions from South China: proxies for devastation and restoration of marine ecosystems following the end-Permian mass extinction.* Geological Journal 42, 371-389

**Torsvik T.H., Van der Voo R., Preeden U., Mac Niocaill C., Steinberger B., Doubrovine P.V., van Hinsbergen D.J.J., Domeier M., Gaina C., Tohver E., Meert J.G., McCausland P.J.A., Cocks L.R.M. (2012):** *Phanerozoic pole wander, palaeogeography and dynamics.* Earth-Science Reviews 114, 325-368

**Valero-Garcés B.L., Delgado-Huertas A., Ratto N., Navas A. (1999**): *Large $^{13}$C enrichment in primary carbonates from Andean Altiplano lakes, northwest Argentina.* Earth and Planetary Science Letters 171, 253-266

# References

**Vennin E., Olivier N., Brayard A., Bour I., Thomazo C., Escarguel G., Fara E., Bylund K.G., Jenks J.F., Stephen D.A., Hofmann R. (2015):** *Microbial deposits in the aftermath of the end-Permian mass extinction: A diverging case from the Mineral Mountains (Utah, USA).* Sedimentology 62, 753-792

**Vieira L.C., Nédélec A., Fabre S., Trindade R.I.F., De Almeida R.P. (2015):** *Aragonite Crystal Fans in Neoproterozoic Cap Carbonates: A Case Study from Brazil and Implications for the Post-Snowball Earth coastal Environment.* Journal of Sedimentary Research 85, 285-300

**Visscher P.T., Beukema J., van Gemerden H. (1991):** *In situ characterization of sediments: Measurements of oxygen and sulfide profiles with a novel combined needle electrode.* Limnology and Oceanography 36, 1476-1480

**Visscher P.T., Reid R.P., Bebout B.M. (2000):** *Microscale observations of sulfate reduction: correlation of microbial activity with lithified micritic laminae in modern marine stromatolites.* Geology 28, 919-922

**Walker G. (1985):** *Mineralogical applications of luminescence techniques.* In: Berry F.J., Vaughan D.J. (eds.): Chemical Bonding and Spectroscopy in Mineral Chemistry. Chapman and Hall, London, 103-140

**Walker G., Abumere O.E., Kamaluddin B. (1989):** *Luminescence spectroscopy of $Mn^{2+}$ centres in rock-forming carbonates.* Mineralogical Magazine 53, 201-211

**Wignall P.B., Hallam A. (1992):** *Anoxia as a cause of the Permian/Triassic mass extinction: facies evidence from northern Italy and the western United States.* Palaeogeography, Palaeoclimatology, Palaeoecology 93, 21-46

**Wignall P.B., Newton R., Brookfield M.E. (2005):** *Pyrite framboid evidence for oxygen-poor deposition during the Permian-Triassic crisis in Kashmir.* Palaeogeography, Palaeoclimatology, Palaeoecology 216, 183-188

**Wignall P.B., Twitchett R.J. (1996):** *Oceanic anoxia and the end Permian mass extinction.* Science 272, 1155-1158

**Wignall P.B., Twitchett R.J. (2002***): Extent, duration, and nature of the Permian-Triassic superanoxic event.* In: Koeberl C., MacLeod K.C. (eds.): Catastrophic events and mass extinctions: impacts and beyond. Special Papers – Geological Society of America 356, 395-413

**Woods A.D. (2005):** *Paleoceanographic and paleoclimatic context of Early Triassic time.* Comptes Rendus Palevol 4, 395-404

**Woods A.D., Bottjer D.J. (2000):** *Distribution of ammonoids in the Lower Triassic Union Wash Formation (eastern California): evidence for paleoceanographic conditions during recovery from the end-Permian mass extinction.* Palaios 15, 535-545

**Woods A.D., Bottjer D.J., Corsetti F.A. (2007):** *Calcium carbonate seafloor precipitates from the outer shelf to slope facies of the Lower Triassic (Smithian-Spathian) Union Wash Formation, California, U.S.A.: sedimentology and palaeobiologic significance.* Palaeogeography, Palaeoclimatology, Palaeoecology 252, 281-290

**Woods A.D., Bottjer D.J., Mutti M., Morrison J. (1999):** *Lower Triassic large sea-floor carbonate cements: their origin and a mechanism for the prolonged biotic recovery from the end-Permian mass extinction.* Geology 27, 645-648

**Wörheide G. (1998):** *The reef cave dwelling ultraconservative coralline demosponge Astrosclera willeyana Lister 1900 from the Indo-Pacific.* Facies 38, 1-88

**Yang H., Chen Z.Q., Wang Y., Tong J., Song H., Chen J. (2011):** *Composition and structure of microbialite ecosystems following the end-Permian mass extinction in South China.* Palaeogeography, Palaeoclimatology, Palaeoecology 308, 111-128

References

**Zakharov Y.D., Biakov A.S., Baud A., Kozur H. (2005):** *Significance of Caucasian Sections for Working out Carbon-Isotope Standard for Upper Permian and Lower Triassic (Induan) and Their Correlation with the Permian of North-Eastern Russia.* Journal of China University of Geosciences 16 (2), 141-151

**Zaninetti L., Brönnimann P., Bozorgnia F., Huber H. (1972):** *Étude lithologique et micropaléontologique de la formation d'Elika dans la coupe d'Aruh, Alborz Central, Iran septentrional.* Archives des Sciences de Génève 25(2), 215-249

**Zhang R., Follows M.J., Grotzinger J.P., Marshall J. (2001):** *Could the Late Permian deep ocean have been anoxic?* Paleoceanography 16, 317-329

**Zuo, J., Tong, J., Qiu, H., & Zhao, L. (2006):** *Carbon isotope composition of the Lower Triassic marine carbonates, Lower Yangtze region, South China.* Science in China Series D Earth Sciences 49, 225-241